Bioactive Materials 37 (2024) 348–377

Contents lists available at ScienceDirect

Bioactive Materials

journal homepage: www.keaipublishing.com/en/journals/bioactive-materials

Review article

4D bioprinting of programmed dynamic tissues

Jiahui Lai [a,b], Yuwei Liu [a,c], Gang Lu [b,d], Patrick Yung [b,e], Xiaoying Wang [f], Rocky S. Tuan [b,d,e,g,**], Zhong Alan Li [a,b,d,h,i,*]

[a] Department of Biomedical Engineering, The Chinese University of Hong Kong, NT, Hong Kong SAR, China
[b] Center for Neuromusculoskeletal Restorative Medicine, Hong Kong Science Park, NT, Hong Kong SAR, China
[c] The First Affiliated Hospital of Shenzhen University, Shenzhen Second People's Hospital, Shenzhen, Guangdong, China
[d] School of Biomedical Sciences, The Chinese University of Hong Kong, NT, Hong Kong SAR, China
[e] Department of Orthopaedics & Traumatology, The Chinese University of Hong Kong, NT, Hong Kong SAR, China
[f] State Key Laboratory of Pulp & Paper Engineering, South China University of Technology, 381 Wushan Road, Tianhe District, Guangzhou, 510640, China
[g] Institute for Tissue Engineering and Regenerative Medicine, The Chinese University of Hong Kong, NT, Hong Kong SAR, China
[h] Key Laboratory of Regenerative Medicine, Ministry of Education, School of Biomedical Sciences, Faculty of Medicine, The Chinese University of Hong Kong, Hong Kong SAR, China
[i] Shenzhen Research Institute, The Chinese University of Hong Kong, Shenzhen, China

ARTICLE INFO

Keywords:
4D bioprinting
Bioprinting technology
Smart material
Smart design
Programmed dynamic tissue

ABSTRACT

Setting time as the fourth dimension, 4D printing allows us to construct dynamic structures that can change their shape, property, or functionality over time under stimuli, leading to a wave of innovations in various fields. Recently, 4D printing of smart biomaterials, biological components, and living cells into dynamic living 3D constructs with 4D effects has led to an exciting field of 4D bioprinting. 4D bioprinting has gained increasing attention and is being applied to create programmed and dynamic cell-laden constructs such as bone, cartilage, and vasculature. This review presents an overview on 4D bioprinting for engineering dynamic tissues and organs, followed by a discussion on the approaches, bioprinting technologies, smart biomaterials and smart design, bioink requirements, and applications. While much progress has been achieved, 4D bioprinting as a complex process is facing challenges that need to be addressed by transdisciplinary strategies to unleash the full potential of this advanced biofabrication technology. Finally, we present future perspectives on the rapidly evolving field of 4D bioprinting, in view of its potential, increasingly important roles in the development of advanced dynamic tissues for basic research, pharmaceutics, and regenerative medicine.

1. Introduction

Printing technologies have a long history and have produced huge impacts on various aspects of human society (Fig. 1a). In the 1980s, additive manufacturing, alias 3D printing, emerged and resulted in rapid development that offers new opportunities for the applications in various areas, such as engineering, biology, and medicine [1–3]. 3D bioprinting emerged about two decades ago, which enables the processing of living cells, biomolecules and biomaterials into 3D living constructs that mimic the native tissues and organs [4]. Today, 3D bioprinting is widely applied to create diverse tissues and organs for basic research, high-throughput drug screening, and tissue regeneration [5,6]. While 3D printed constructs remain static after fabrication, native tissues and organs not only possess complex 3D hierarchical structures, but also exhibit dynamic features, such as conformational changes and functional transformations, to achieve unique functions. For example, the regular contraction of cardiac tissue enables the heart to pump blood throughout the body [7]. As another example, the size of blood vessels can be modulated by many factors such as nitric oxide (causing vasodilation) and caffeine (causing vasoconstriction) [8,9]. As such, in many cases, static products constructed by 3D printing/bioprinting may not meet the high demands of biomedical engineering.

Over the last decade, 4D printing has emerged by incorporating time as the fourth dimension. The concept of 4D printing was first described

Peer review under responsibility of KeAi Communications Co., Ltd.
* Corresponding author. Department of Biomedical Engineering, The Chinese University of Hong Kong, NT, Hong Kong SAR, China.
** Corresponding author. Center for Neuromusculoskeletal Restorative Medicine, Hong Kong Science Park, NT, Hong Kong SAR, China.
E-mail addresses: tuanr@cuhk.edu.hk (R.S. Tuan), alanli@cuhk.edu.hk (Z.A. Li).

https://doi.org/10.1016/j.bioactmat.2024.03.033
Received 22 December 2023; Received in revised form 12 March 2024; Accepted 28 March 2024

in 2013 by Tibbitts of the Self-Assembly Lab at the Massachusetts Institute of Technology (MIT) [10,11]. At that time, 4D printing was simply defined as "3D printing + time" that allowed the fabrication of 4D objects with the ability to change their shape over time. In recent years, 4D printing is defined as a technology to fabricate 3D structures with desirable stimuli-responsive properties in response to external stimuli (i.e., water, heat, pH, light, and electric and magnetic fields) [12]. Smart materials and smart design are two key components for 4D printing to achieve the desirable 4D effect. Smart materials are materials that can change their shape or properties under external stimuli [13]. The aim of smart design is the programmable transformation by fully accounting for any time-dependent transformation of printed objects [14]. With the ability to produce dynamic features, 4D printing has gained increased research attention in recent years (Fig. 1b). As shown in Fig. 1c, the number of publications related to the topic of 4D printing grew rapidly. With dynamic shape, property, or functionality, 4D printed products can better meet the needs for use in medicine. Over the past few years, 4D printing has been increasingly used to fabricate dynamic products for biomedical applications [15,16], and this emerging technology is anticipated to drive the development of next-generation tissue regeneration and medical devices [17].

With the inception of 4D printing in 2013, the development of "4D bioprinting" was very soon perspective in some reviews [18–20], expecting that 4D printing would advance to process biocompatible smart materials, biochemicals, and living cells to generate dynamic 3D living constructs (i.e., 4D bioprinting) [21]. Compared to 3D bioprinting, 4D bioprinting enables the creation of dynamic living constructs, which can accurately recapitulate the intrinsic dynamic and conformation change of native tissues and potentially address the need for dynamic engineered tissues and organs. It should be noted that there is controversy over the concept of 4D printing in tissue engineering. It has been claimed that 3D bioprinting actually is one specific type of 4D printing, as the 3D bioprinted scaffolds are "active" and are often accompanied by dynamic changes over time [22]. It is because that the cells undergo reorganization to produce tissues and the degradable materials would break down over time when implanted *in vivo*. However, in some contexts, degradation is not considered as a 4D effect since the printed products serve as a carrier to account for the desired shape and function, and the degraded product no longer retains the intact construct [15,23]. For the cell-driven post-bioprinting changes, it has been claimed that the maturation of the printed microtissues derived from cell coating, cell organization, and/or matrix deposition belong to 4D bioprinting [22,24]. In such cases, 3D bioprinting is already "4D printing", as the 3D bioprinted scaffolds can develop into functional tissues over time via cell (re)organization and matrix deposition. In response to this controversy, some researchers have re-defined 4D bioprinting as a strategy that combines 3D bioprinting with smart materials to create scaffolds capable of predictable and tunable structural remodeling in response to specific external stimuli [25]. 3D bioprinted products are typically static or undergo natural spontaneous changes without external stimuli. In contrast, 4D bioprinted products are expected to display programmable and controllable dynamic changes triggered by physical, chemical, and biological stimuli. In this review, in order to distinguish 4D bioprinting from 3D bioprinting, 4D bioprinting is defined as a group of technologies that can be used to deposit smart bioink (i.e., smart biocompatible materials, biochemicals, and living cells), in a layer-by-layer manner, based on smart pre-design patterns to create programmed dynamic structures with stimuli-responsive properties.

4D bioprinting has undergone rapid development in recent years, resulting in an increasing number of relevant publications (Fig. 1d). Although a number of recent reviews presented excellent discussions on

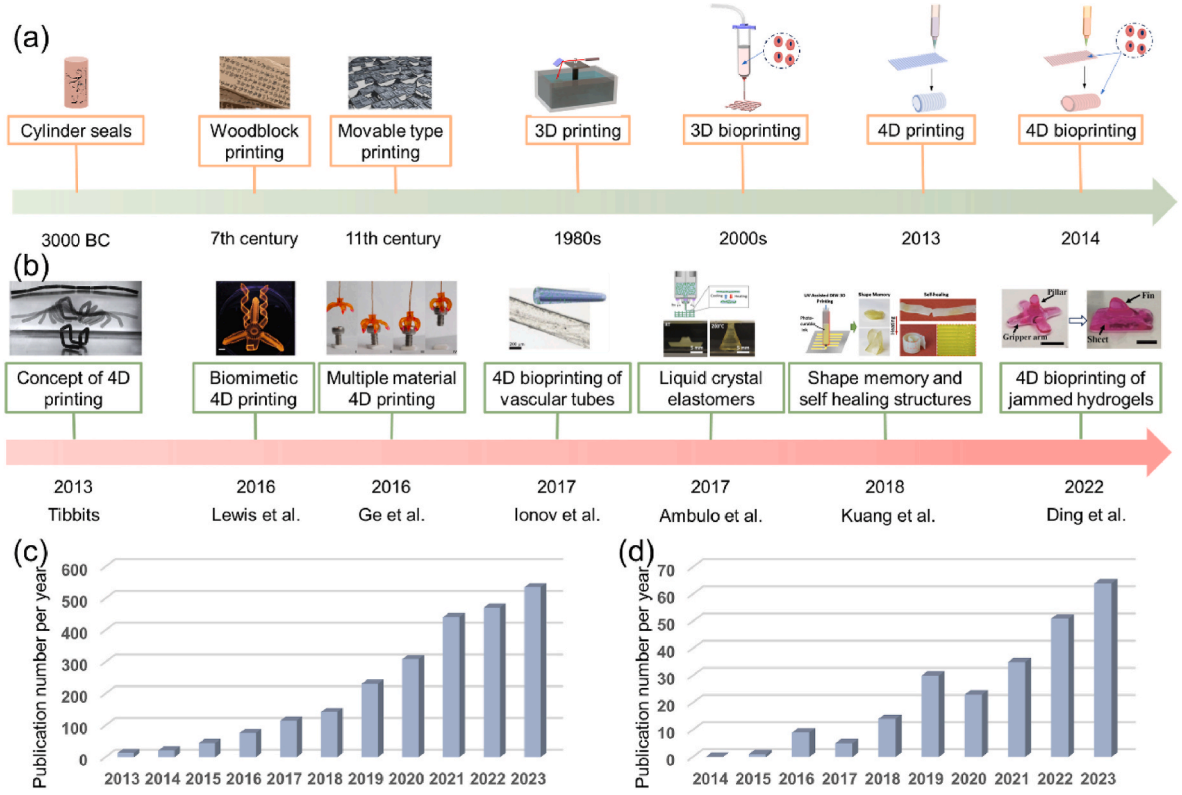

Fig. 1. Development of 4D printing and 4D bioprinting. (a) Evolution of printing technologies. (b) A timeline highlighting key milestones of 4D printing/bioprinting. Figures (from left to right) reproduced with permission from Ref. [11] (Copyright 2014, Wiley-VCH) [35], (Copyright 2016, Springer Nature) [36], (Licensed under a Creative Commons CC BY license) [37], (Copyright 2017, Wiley-VCH) [38], (Copyright 2017, American Chemical Society) [39], (Copyright 2018, American Chemical Society) [40], (Copyright 2022, Wiley-VCH). (c, d) Number of publications related to (c) 4D printing and (d) 4D bioprinting in the past decade. Statistics of the publication data are collected from Web of Science on March 9, 2024.

4D printing and bioprinting [17,25–34], most of them only reviewed 4D bioprinting as a part of a broader topic and lacked an up-to-date and comprehensive presentation of this rapidly developing field. Besides, previously published related reviews rarely discussed the still debatable definition of 4D bioprinting. Thus, we address this issue by providing a historical overview and the conceptualization of 4D bioprinting. Further, this review provides a comprehensive discussion on 4D bioprinting and its recent advances in the biofabrication of dynamic tissues and organs. Firstly, the major approaches of creating dynamic tissue constructs via 4D bioprinting are discussed. The mainstream bioprinting technologies for 4D bioprinting are then presented by highlighting their key features and recent developments. Subsequently, smart materials and smart design for achieving the 4D effects of 4D bioprinted constructs are described, followed by a discussion of the requirements for developing and selecting smart bioinks. Finally, applications of 4D bioprinting in creating dynamic tissues and organs as well as related challenges and perspectives are discussed in depth. The goal of this review is to offer useful insights into the latest development of the 4D bioprinting technology and its wider future biomedical application in basic biomedical research, tissue engineering, and drug screening.

2. Approaches for 4D bioprinting

The two major approaches for 4D bioprinting are shape morphing and functional transformation (Fig. 2). Other approaches that have been proposed include biomimicry, self-assembly, and "*in vivo*" 4D bioprinting [21,41]. For instance, *in vivo* 4D bioprinting refers to the creation and implantation of polymer medical devices that can transform to accommodate tissue or organ growth by responding to the stimuli induced by tissue growth [21]. The two major approaches, shape morphing and functional transformation, will be the focus of this section.

2.1. Shape morphing

The shape morphing approach strictly follows the initial Tibbits's concept of 4D printing and has become the most common approach to achieve 4D bioprinting. For shape-morphing 4D bioprinting, the fabricated cell-laden constructs with living cells or tissue materials can change their shape from a 2D/3D morphology to a desirable 3D configuration (Fig. 2a). The programmed shape-shifting ability of a dynamic object can be achieved by strategically distributing different components within the object. Typically, controlling the distribution of different components (single or multiple materials) across its thickness, plane, or both thickness and plane can lead to different 3D deformations [42–44]. For example, a shape memory polymer with a gradient in the degree of molecular orientation across the thickness can self-fold when it was heated to its transition temperature [44]. Chitosan can be processed into a series of 2D patterns with a gradient in crosslinking degree across the thickness, resulting in different 3D morphologies (e.g., tube, helix, and flower) by responding to pH changes [45].

2.2. Functional transformation

Another approach to introducing dynamic features into 4D bioprinted structures is function transformation (Fig. 2b). As living cells are already encapsulated within 4D bioprinted constructs, the engineered tissue constructs can undergo functional transformation and maturation, representing another dynamic feature of 4D bioprinting. The functionalities of a bioprinted tissue construct should be induced in a programmable and controllable manner under specific stimuli, such as magnetic field, mechanical force, enzymes, and biomolecules. As shown in Fig. 2b (i), the 4D bioprinted tissue constructs with living cells can directly grow into matured constructs during post-bioprinting culture via cell proliferation, differentiation and matrix deposition under appropriate stimuli such as physical factors, drug molecules, and growth factors. Moreover, as shown in Fig. 2b(ii), the cell patterns can be first stimulated to transform into another pattern, which can then change over time to obtain the programmed functions via self-organization and self-development. For instance, magnetic fields can be applied to assemble different cells patterns by labeling the cells with magnetic nanoparticles (e.g., gold/iron oxide nanoparticles, filamentous phages, etc.) [46,47] or by exploiting the innate diamagnetism of cells (i.e., the Magneto-Archimedes effect) [48]. In addition to individual cells, cell

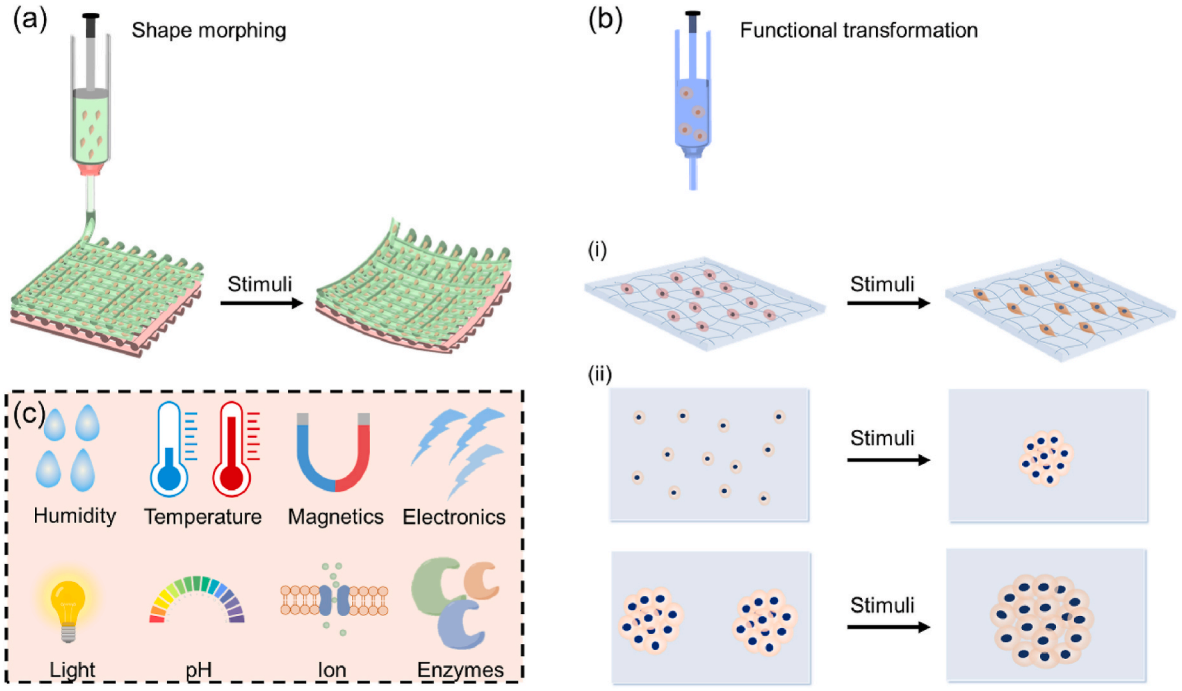

Fig. 2. Approaches to achieving 4D effects.(a) Shape morphing, (b) functional transformation, including (i) tissue maturation and (ii) cell pattern changes. (c) Common external stimuli employed to induce 4D effects in 4D bioprinting. OBB: organ building block.

spheroids or organoids can fuse to generate organ building blocks (OBBs), and the differentiation, maturation, and 3D assembly of these OBBs can lead to the creation of functional organ-specific tissues [49–51]. A deep understanding of multiple disciplines such as cell biology, mechanobiology, and cell biophysics is required to achieve programmable and controllable functional transformation.

3. 4D bioprinting technologies

For 4D bioprinting, mild processing environments are needed to maintain cell viability and functionality. Currently, the main bioprinting technologies for processing living cells and smart biomaterials are micro extrusion-based bioprinting (MEB), inkjet bioprinting, stereolithography (SLA), digital light processing (DLP), and laser-assisted bioprinting (LAB). This section discusses the key features of these 4D bioprinting technologies (Table 1) and recent advances. Detailed descriptions of these bioprinting technologies are presented in several recent outstanding reviews [31,52–55].

3.1. Micro extrusion-based bioprinting

MEB is a commonly used 4D bioprinting technique. For MEB bioprinting, inks with or without cells are loaded into syringes and extruded through a nozzle to form continuous filaments, which are then deposited in a layer-by-layer manner to form a 3D object. As shown in Fig. 3a, the inks/bioinks are extruded via a pneumatic or a mechanical dispensing system (using piston or screw). Pneumatic dispensing systems have a relatively simple air-driven component, while mechanical dispensing systems require more complex components. Mechanical dispensing systems enable more direct control over the materials flow, while there is a volumetric delay of compressed air in pneumatic dispensing systems. MEB is able to process a variety of materials with a wide viscosity range of 1 to $>10^7$ mPa s [56,57]. However, MEB faces challenges when processing low viscosity materials. In recent years, several strategies, such as *in situ* crosslinking [57] and FRESH bioprinting [83], have been developed to improve the capabilities of MEB in processing materials with ultra-low viscosity. Most of the shape memory polymers (SMPs), shape morphing hydrogels (SMHs) and their composites are printable by MEB. Besides, this type of bioprinting technology can be used to process cell spheroids or organoids into constructs with high cell density [49,64,65], which are challenging to achieve using other bioprinting technologies. The printing resolution of MEB is determined in part by the diameter of the used nozzle, where a smaller diameter of nozzle generally leads to higher printing resolution. However, nozzles with a small diameter can cause clogging issues, leading to decreased cell viability as increased shear stress is applied on the cells; cell viability for micro extrusion-bioprinting is also greatly affected by the shear stress exerted on the cells [71,84]. It is believed that cell viability decreases exponentially as shear stress increases, related to increased cell deformation and even significant cell damage/death [85]. In practice, different cell types also show distinct responses towards shear stress, leading to difference in cell viability. Therefore, the shear stress aspect of MEB should be carefully considered and controlled to avoid significant cell damage/death. Shear stress may be controlled by several factors, including material viscosity, pneumatic pressure (or piston/screw speed), and nozzle diameter. Some methods have been developed to improve cell viability of MEB-bioprinted cell-laden constructs. For instance, moderate shear stress before bioprinting was found to enhance the ability of cells to tolerate the bioprinting induced stress and improve their viability post-bioprinting [86]. Li and coworkers used a bioprinting method that applied bioink pairs of alginate/MC and trisodium citrate (or GelMA) and achieved a cell viability of above 93% after bioprinting [87,88]. MEB bioprinting has many advantages, including easy operation, ability to process a wide range of biomaterials, and capability of printing cell aggregates [49,87,89]. However, MEB faces the shortcomings of relatively slow printing speed and low printing resolution in comparison with other bioprinting technologies [2,33]. To improve the printing speed of MEB, a type of multi-material, multi-nozzle, extrusion-based 3D printer (MM3D) has been developed to simultaneously deposit multiple inks to form periodic structures with much higher fabrication speed [90]. However, this MM3D technology encounters several constraints such as limited available materials and fixed nozzle arrays. Besides, the feasibility of MM3D in processing 4D bioinks still needs to be further explored.

3.2. Inkjet bioprinting

Inkjet bioprinting has been one of the most commonly used technology for bioprinting applications [52]. It is a drop-on-demand (DOD) printing technology that ejects droplets only when an ejection signal arrives. Fig. 3b illustrates three mainstream inkjet bioprinting systems: thermal inkjet bioprinting, piezoelectric inkjet bioprinting, and electrostatic inkjet bioprinting. In thermal inkjet bioprinting, a heater is used to heat the surrounding liquid to about 250–350 °C in a very short time (~2 μs), which causes the generation of a bubble. The bubble expands rapidly and produces a driving force to overcome the surface tension of the ink and eject it out of an orifice. In piezoelectric inkjet bioprinting, a piezoelectric actuator can change its shape when

Table 1
Comparison of different 4D bioprinting technologies.

	4D bioprinting technologies				
	MEB	Inkjet	SLA	DLP	LAB
Ink/bioink viscosity	1 to $>10^7$ mPa s [56,57]	3–30 mPa s [52]	3–300 mPa s [58,59]	1–200 mPa s [60,61]	1–300 mPa s [62,63]
Cell density	10^8 cells/ml, cell spheroids, organoids [49,51,64,65]	10^6 cells/ml [66,67]	$>10^6$ cells/ml [68,69]	10^6 to10^8 cells/ml [61,70]	10^8 cells/ml [62]
Cell viability	70–95% [37,71]	>85% [67,72,73]	>75% [68,69]	>75% [74]	>85% [63,75]
Nozzle diameter	200 μm to mm scale	20–150 μm	Nozzle free	Nozzle free	Nozzle free
Resolution	200 μm to mm scale	50–300 μm	20–80 μm	<150 μm	<150 μm
Printing speed	Slow	Fast	Medium to fast	Fast	Slow
Typical materials	Shape memory polymers, hydrogels, and composites (e.g., AlgMA [37,40], MC/alginate [42,76], cellulose nanofiber/NIPAM [35])	Hydrogels (e.g., GelMA [73])	Photopolymers (e.g., soybean oil epoxidized acrylate [77])	Photopolymers (e.g., silk fibroin [70], GelMA/PEGDA [74])	Hydrogels (e.g., collagen [75])
External stimuli	Humidity [37,40], heat [78,79], and light [80,81]	Humidity [82]	Humidity, temperature [77]	Humidity [70,74]	Patterned fibroblasts [75]

Abbreviation: AlgMA, methacrylate alginate; MC, methylcellulose; NIPAM, N-isopropylacrylamide; GelMA, gelatin methacryloyl; PEGDA, poly(ethylene glycol) diacrylate.

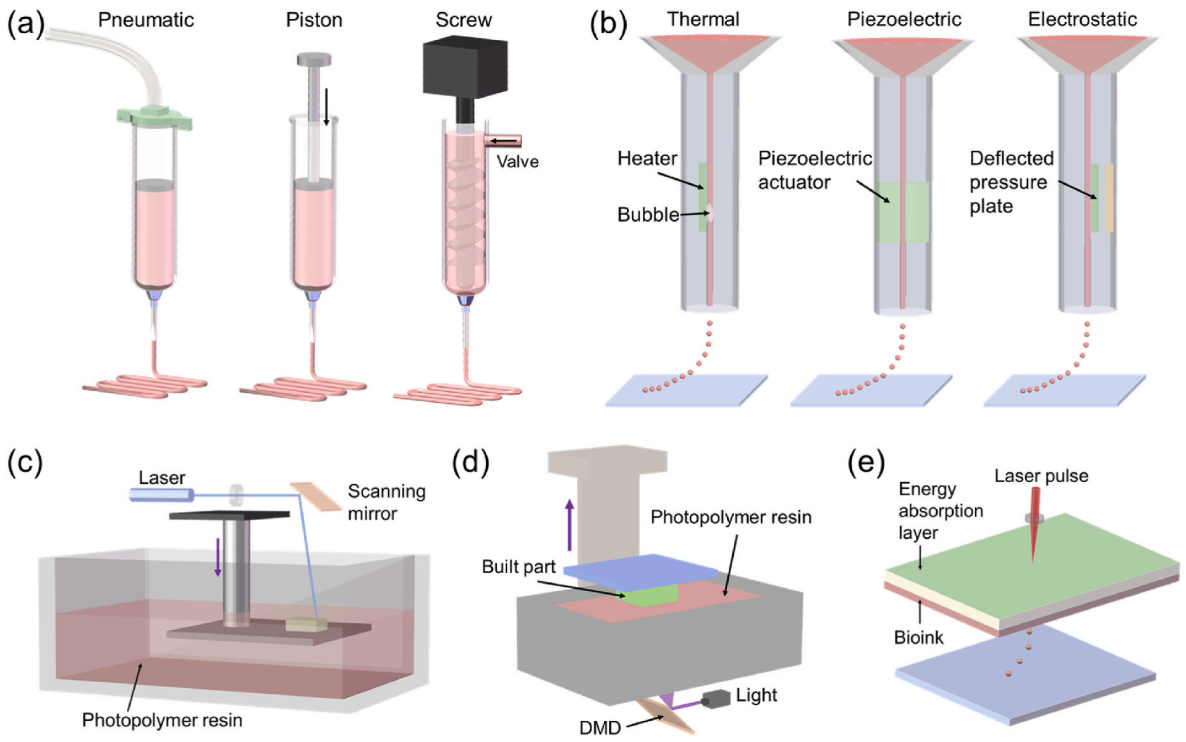

Fig. 3. Schematic illustration of 4D bioprinting technologies. (a) Micro extrusion-based bioprinting using pneumatic, piston, or screw dispensing systems. (b) Inkjet bioprinting using thermal, piezoelectric, or electrostatic ejecting systems. (c) Stereolithography. (d) Digital light processing. (e) Laser-assisted bioprinting.

receiving a voltage pulse, leading to a sudden volumetric change of the ink chamber and hence ejection of a droplet. In electrostatic inkjet bioprinting, a defected pressure plate is attracted to the other plate under the action of static electricity, leading to chamber deformation and hence droplet ejection. The use of inkjet printing for 4D bioprinting has several advantages, including low cost, high printing speed, and high availability. However, inkjet bioprinting also has some shortcomings. Firstly, the materials used for inkjet bioprinting are restricted to a relatively narrow viscosity range of 3–30 mPa s [52]. Secondly, due to the low viscosity, it is hard to maintain the structures of the printed objects before solidification [91,92]. Thirdly, the orifice diameter of inkjet bioprinting is relatively small, which impairs the ability of inkjet bioprinting to process bioinks with high cell density [67,93]. Also, bioinks made of cell spheroids and organoids are not processable for inkjet bioprinting due to the small orifice. Finally, there are concerns over cell viability when inkjet bioprinting is used to process live cells. The transient high temperature for thermal inkjet bioprinting can cause cell death [72,93]; for piezoelectric and electromagnetic inkjet bioprinting, the high frequencies used may disrupt the cell membranes and cause cell lysis [94]. As inkjet bioprinting involves the use of an orifice for ejecting inks, shear stress should be carefully controlled and kept below 10 kPa to avoid significant cell death [84]. Although inkjet bioprinting can cause varying degrees of cell death, most of the cells remain viable after bioprinting. Generally, inkjet bioprinting can achieve a cell viability higher than 85%, which is larger than that of MEB [72,73].

3.3. Stereolithography

Stereolithography (SLA) has emerged for over 30 years since Hull patented the first SLA apparatus in 1986 [1]. As shown in Fig. 3c, SLA is mainly composed of a laser source, an X–Y scanning mirror, a build platform, and a vat containing photopolymer resin. In SLA, a laser is used to selectively cure and solidify the photopolymer resins point-by-point to generate one solidified layer. Afterwards, the build platform moves down one-layer thickness, and one layer of fresh resin is coated on the built part. As such, this process is repeated until the final layer is fabricated. In as early as 2004, SLA was used for fabricating tissue engineered cell-laden constructs by Dhariwala and coworkers [95]. Compared to MEB, SLA bioprinting has the advantages of faster building speed and higher printing resolution (about 20–80 μm). The high printing resolution of SLA is attributed to the small laser spots. Besides, SLA is a nozzle-free fabricating process, which avoids cells being exposed to shear stress that may compromise cell viability. However, there are some drawbacks when using SLA for bioprinting. First, in most cases, SLA bioprinting systems solidify the bioinks using UV-light or near-UV blue light, which may negatively affect cell viability, especially with long light exposure. To fabricate living constructs with improved cell viability and proliferation, visible light has often been used to replace UV light in SLA, thus requiring the development of new photoreactive groups [68]. Secondly, since the resin being polymerized is in direct contact with the air, oxygen-based inhibition occurs easily for SLA and causes incomplete crosslinking and overhanging. Thirdly, the resin-recoating step of SLA is time-consuming and significantly slows down the printing speed. To overcome this limitation, a microfluidic circulation has been used in SLA to achieve continuous replenishment of the liquid resin atop the built part and allow fabrication of multiscale solid hydrogels within minutes [96]. Fourthly, it is difficult to integrate multiple bioinks into one living construct using SLA due to the challenge in switching between different bioinks during the same manufacturing process. However, efforts are being made to address this issue. For example, Miller's group used an automated material selection process and a manual saline rinsing step to achieve multiple-material SLA bioprinting [97].

3.4. Digital light processing

Digital light process (DLP) is a manufacturing process similar to SLA. However, unlike the point-by-point solidification of rein in SLA, DLP can solidify a layer of photopolymer resin at one exposure, resulting in a significant increase in building speed (Fig. 3d). Such a printing speed

improvement in DLP is achieved by using a critical component, digital micromirror device (DMD). DMD is made of an array of micromirrors, which can rotate independently to guide the light to cure one layer of photopolymer resin all at once. In addition, DLP light cures the resin in the bottom of the vat and moves upwards, which avoids oxygen inhibition during printing. Like SLA, DLP is a nozzle-free manufacturing process with fast printing speed, high printing resolution, and good cell viability. Nevertheless, the printing speed of DLP can be further improved by using an O_2-permeable membrane in the bottom of the vat, which induces the formation of a "dead zone" that allows the continuous flow of the liquid resin without a recoating step, hence the name continuous liquid interface production (CLIP) [98]. However, CLIP still faces challenges in processing high viscosity materials. To mitigate this issue, microfluidic channels have been applied in CLIP to positively inject high viscous materials into the built part without interruption [99]. It was reported that as compared to CLIP, the microfluidic channel-integrated CLIP technique could cure resins that are an order of magnitude more viscous and achieve a 5- to 10-fold increase in the printing speed [99]. It is worth noting that DLP faces difficulty in integrating multiple materials into one single object. Several strategies have been developed to address this issue. For example, Han and coworkers developed a dynamic fluidic control unit consisting of a cylindrical printing chamber with integrated microfluidic inlets and outlets, enabling material exchange to achieve multi-material printing of DLP [100]. However, this fluid flow method has drawbacks of small building size, limited available materials, and significant material contamination. To solve these issues, Ge's group proposed a DLP-based centrifugal multimaterial (CM) 3D printing method [101]. In their method, a glass plate was used to support two or more polymer resin containers and could move horizontally to deliver a specific resin for the corresponding slice. During the material switching, a rotating motor was applied to spin the printing platform to remove residual resin on the printed part. As such, the DLP-based CM 3D printing system could print multi-material 3D structures in an area of up to 180 mm × 130 mm without material contamination [101]. SLA, DLP, and CLIP belong to the category of vat polymerization 3D printing technologies. Currently, there are many biocompatible and shape memory polymers or resins (e.g., polyurethane-based polymers and polyester-based polymers), and digital multimaterials (i.e., variable and automatic mixtures of at least two resins) have been developed for these vat polymerization technologies [102]. It is worth paying caution when UV light is used to cure bioinks, as UV exposure can cause damage to cells. Increased UV exposure time has been reported to decrease cell viability [103]. For instance, when the irradiation dose of UV (365 nm) was increased from 1350 mJ cm^{-2} to 5400 mJ cm^{-2} for printing cell-laden GelMA hydrogel, the viability of Hep-G2 cells was significantly reduced from 90% to 56% [104]. Besides, in DLP and SLA, a cell density of higher than 2×10^7 cells/ml causes a light scattering effect, which may reduce the printing resolution and may also affect photopolymerization. To mitigate this scattering-induced decrease in resolution, iodixanol was added to the bioinks as iodixanol could greatly reduce light scattering and achieve a resolution of 50 μm with a bioink of a high cell density of 10^8 cells/ml [61].

3.5. Laser-assisted bioprinting

Laser-assisted bioprinting (LAB) is a nozzle-free manufacturing process that uses a laser pulse to eject the bioink layer to generate droplets containing a specific number of cells (Fig. 3e). Due to the use of laser pulses, LAB can achieve a high printing resolution at microscale (<10 pL droplets). As a nozzle-free approach, living cells processed via LAB is not subjected to shear stress, leading to high cell viability of >85% [63,75]. However, the cell viability of LAB decreases with increasing energy of laser source [63]. LAB is able to process bioinks with a cell density up to 10^8 cells/ml [62]. With high printing resolution, high cell viability and density, LAB has been commonly used for bioprinting to process different biomaterials (e.g., RNA, and protein) and living cells [e.g., human osteosarcoma cells and mesenchymal stem cells (MSCs)] into customized cell patterns [54]. However, the wider bioprinting applications of LAB are limited by several drawbacks. Firstly, the biomaterials that can be printed via LAB are relatively limited. Secondly, the speed of printing (or droplet generation) for LAB is lower than other bioprinting technologies. Thirdly, the high cost of LAB equipment further limits its applications in academic and commercial research.

4. Smart biomaterials and smart designs for 4D bioprinting

Smart biomaterials and designs are two key elements for 4D bioprinting to achieve programmable dynamic behaviors. Smart biomaterials currently used for 4D bioprinting include shape memory polymers, shape morphing hydrogels, and their composites. According to the specific smart design, these smart biomaterials are strategically deposited via 4D bioprinting to generate dynamic structures that can change their shape and functionality by responding to appropriate stimuli.

4.1. Shape memory polymers

Shape memory polymers (SMPs) are smart polymeric materials with the ability to maintain a temporary shape and return to their permanent shape when exposed to external stimuli, such as heat, magnetic field, stress and light (Fig. 2c). SMPs-based structures can retain (or fix) the permanent shape via different programmable (or reshaping) strategies. The most commonly used reshaping strategy for SMPs is heat programming, which is strictly related to their transition temperature (T_t). T_t is the melting temperature (T_m) for a semicrystalline polymer, or the glass transition temperature (T_g) for an amorphous polymer. Typically, an SMP-based structure is deformed to the "permanent" shape at a temperature higher than T_t for a specific time period. The reshaped SMP-based structure is then cooled down below T_t and unloaded to remember the deformed shape. At a temperature below T_t, the SMP-based structure can be arbitrarily deformed to any temporary shape. Upon direct or indirect heating (e.g., photothermal effect and Joule heating) to a temperature above T_t, the SMP-based structure can undergo shape-transition and recover to its permanent shape. For example, poly(D, L-lactide-*co*-trimethylene carbonate) (PDLLA-*co*-TMC) is a temperature-responsive, amorphous SMP, and its T_g is determined by the ratio of DLLA and TMC monomers [105]. The PDLLA-*co*-TMC with a 9:1 ratio of DLLA:TMC exhibits a T_g close to the human body temperature [106]. In a representative application of this SMP, PDLLA-*co*-TMC was initially processed as 2D membranes [78]. The membranes were shaped into a tube structure using a glass rod, followed by incubation in an 80 °C oven to fix the reshaped structure. After cooling down to ~25 °C, the reshaped structure could flatten as a 2D shape (Fig. 4a–c). Upon heating to 37 °C, the temporary 2D shape automatically folded into a permanent tubular shape within 1 min (Fig. 4c–e) [44,78]. However, heat programming faces some limitations such as whole energy waste and local shape programming. Efforts have been made to develop new mechanisms for programming SMPs. For example, Qi's group presented a cold-programming strategy by using the principle that the relaxation of SMP is a function of stress rather than temperature [107]. By using the grayscale-DLP (g-DLP, Fig. 4f) [108], a photocurable resin was 4D printed into multi-material objects with strategically designed hinges, which exhibited different 3D deformations by applying stretching force (Fig. 4g–l). In addition, Ni and coworkers proposed a phase-separation strategy for programming SMPs into specific shape-morphing structures, in which the onset of 3D deformation took place at a natural ambient temperature of 25 °C via internal mass diffusion instead of heat transport, which can be employed to lower the difficulty in deploying medical devices (Fig. 4m–r) [109].

A variety of SMPs have been applied to produce different tissue

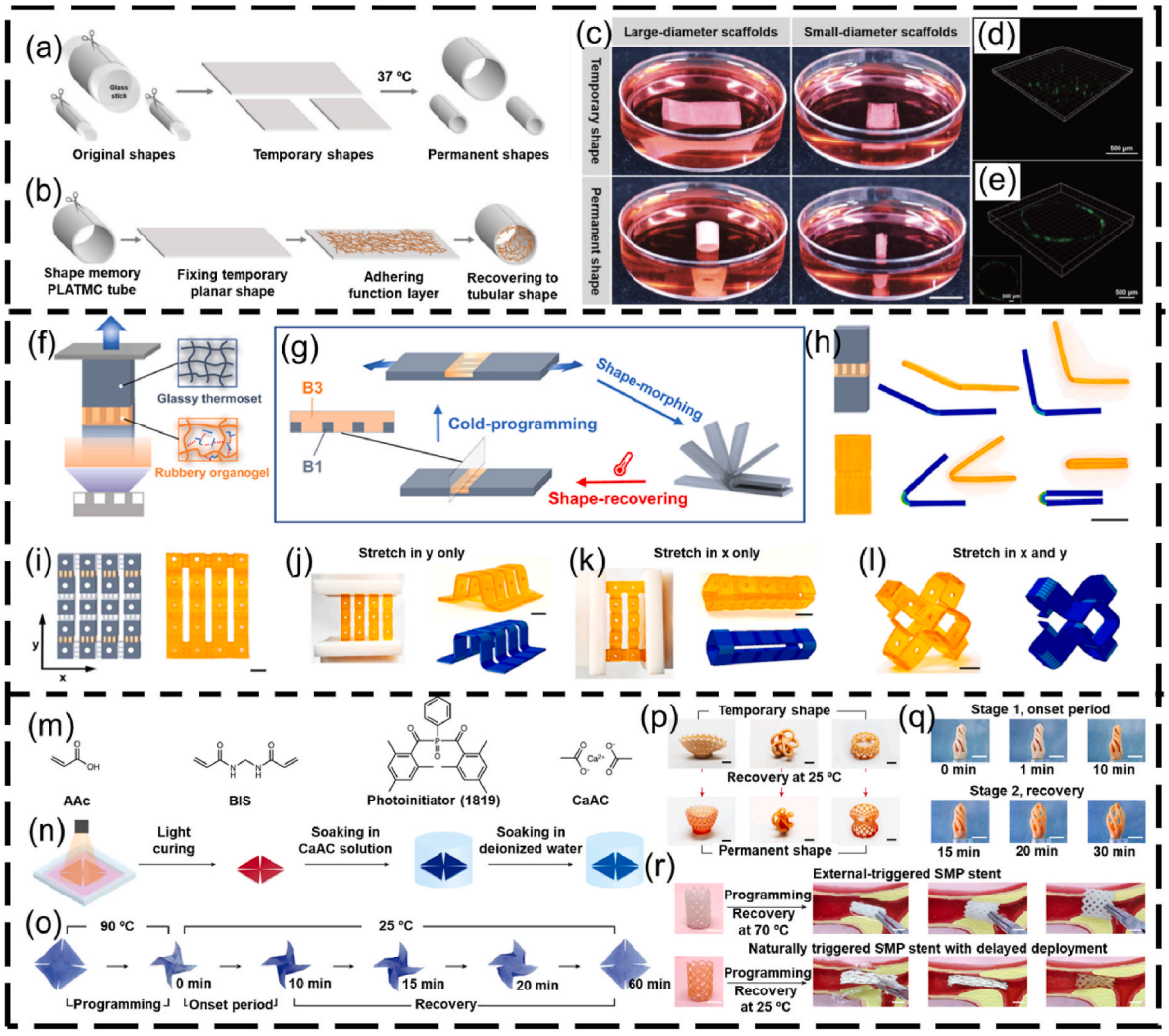

Fig. 4. SMPs reshaping using heat programming, cold programming, and phase separation programming. (a–e) Heat programming of PDLLA-*co*-TMC: (a) reshaping PDLLA-*co*-TMC membranes into tubular structures, (b) attachment of a fibrous membrane with the PDLLA-*co*-TMC to form bilayer scaffolds, (c) photograph showing the self-tubing of bi-layer scaffolds (scale bar = 1 cm), (d, e) confocal images showing the cell distribution (d) before and (e) after deformation. Reproduced with permission [44]. Copyright 2018, Wiley-VCH. (f–l) Cold programming of shape-shifting structures via g-DLP: (f) schematic illustration of g-DLP to create multi-material objects combining B1 glassy thermoset and B3 rubbery organogel (B1 and B3 refer to two different photocuring resins), (g) schematic of the heterogeneous hinge module design and morphing, (h) bending degrees of the hinge under different strain forces, (i) g-DLP 4D-printed structures with the hinges, and (j–l) corresponding different deformed morphologies by applying (j) y-directional force, (k) x-directional force, and (l) dual x-y directional forces (scale bar = 1 cm). Reproduced with permission [107]. Licensed under a Creative Commons CC BY license. (m–r) Programming SMPs via phase separation: (m) monomer precursors of a 4D photocurable ink, (n) DLP-4D printing process of a windmill, (o) a shape-shifting process of the windmill under 25 °C including a programming step of the shape-morphing onset time at 90 °C, an onset period, and a shape recovery period at 25 °C, (p) different shape-morphing structures, (q) shape morphing with a controlled onset of 10 min at the ambient temperature of 25 °C, (r) a comparison of the deployment of SMP stents made of heat programming and phase separation (scale bar = 1 cm). BIS, N,N′-methylenebisacrylamide; AAc, acrylic acid; CaAc, calcium acetate [109]. Reproduced with permission [109]. Copyright 2023, Springer Nature.

engineering products via 4D printing [15,16,110]. The SMPs available for 4D printing of tissue engineering scaffolds are summarized in Table 2. These SMPs exhibit good biocompatibility and shape memory properties, making them appealing for fabricating different 4D structures with programmable shape-morphing behaviors. For instance, Manen and colleagues processed polylactic acid (PLA) into a series of 2D shape-shifting patterns using fused deposition modeling (FDM, a type of extrusion-based 3D printing that melts and extrudes polymer filaments to form 3D structures) [111]. In their method, PLA was melted above its transition temperature and extruded as stretched filaments, which were "memorized" after cooling them down. By strategically designing the porosity and thickness of the structures, the 2D patterns were programmed and could be deformed into a series of simple or complex 3D morphologies upon heating [111]. Using the same principle, Koh and Sutradhar printed a ferromagnetic PLA layer between each PLA patterns, which enabled selectively heating and actuation by microwave radiation (Fig. 5a–d) [112]. Although the biomedical applications of 4D printed PLA structures were not demonstrated in these studies, PLA is biocompatible and has been 4D printed into shape-morphing structures for tissue engineering [79,113]. Miao and coworkers developed a SMP using soybean oil epoxidized acrylate (SOEA), which could be 4D printed into tissue engineering scaffolds with programmable shape-morphing behaviors via SLA [77,114]. As shown in Fig. 5e–h, SOEA incorporated with GO was produced via SLA as dynamic scaffolds, that could self-fold into tubular structures for repairing damaged nerves, demonstrating promising potential for neural regeneration [77]. These SMPs hold significant potential for use in 4D bioprinting to fabricate living constructs with shape memory effects. In addition to these SMPs,

Table 2
SMPs for 4D printing.

SMP	Printer type	External stimuli	Activation temperature	Application	Reference
Polylactic acid (PLA)	FDM	Heat	About 80 °C	_	[111]
PLA and ferromagnetic PLA	FDM	Microwave	28 °C to 130 °C	_	[112]
Soybean oil epoxidized acrylate	SLA	Heat or water	37 °C	Tissue engineering scaffolds	[77,114]
Methacrylated polycaprolactone	SLA	Heat	40 °C to 50 °C	Airway stent	[117]
Black phosphorus nanosheets/TCP/PDLLA-*co*-TMC	MEB	Light	45 °C	Bone tissue engineering scaffolds	[80]
Polycarbonates	SLA	Heat	37 °C	Scaffolds for soft tissue repair	[118]
SMPs combined with two PCL-diacrylates with different molecular weights	_	Heat	30 °C to 55 °C	Bone tissue engineering scaffolds	[119]
MDI/PEG/PU	_	Heat	37 °C	Cartilage tissue engineering scaffolds	[120]
Poly(glycerol dodecanoate) acrylate	MEB	Heat	20 °C to 37 °C	Vascular grafts	[121]
Poly(glycerol sebacate) acrylate-*co*-hydroxyethyl methacrylate	DLP	Heat	37.8 °C	Inferior vena cava filters	[122]

Abbreviation: MDI, andmethylene diphenyl 4,4-diisocyanate; PEG, poly (ethylene glycol); PU, polyurethane.

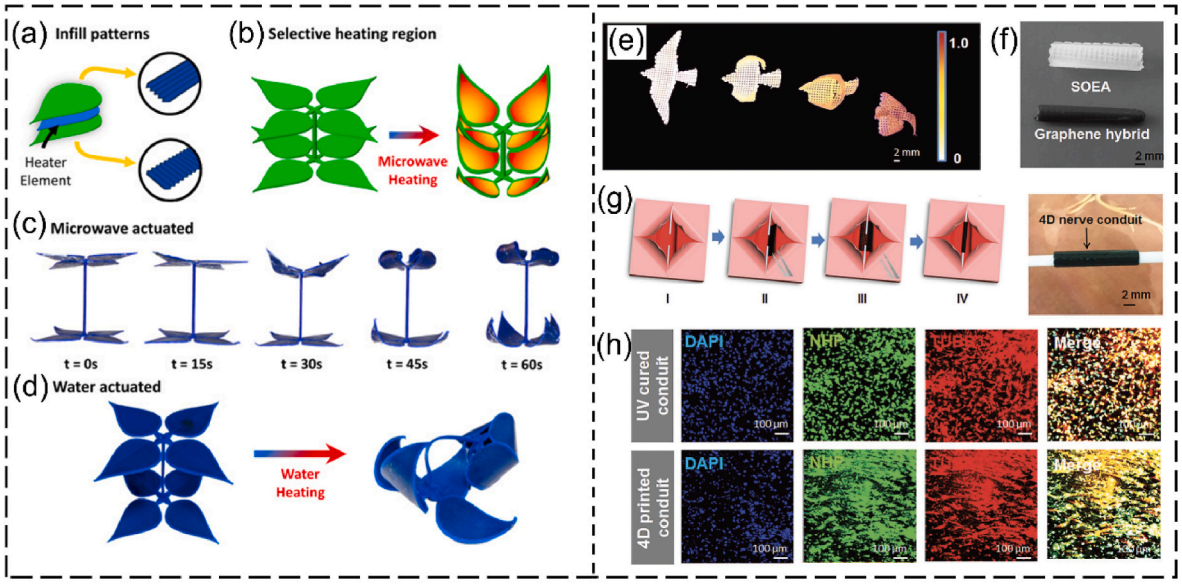

Fig. 5. 4D printing of SMPs. (a–f) 4D printing of PLA-based shape-changing leaves. (a) Schematic tri-layer configuration of a leaf showing two layers of PLA patterns (green) and one layer of ferromagnetic PLA (heater element). (b) Selective heating region of the leaves by microwave heating without heating the PLA stem. (c, d) Comparison of the shape-shifting process of the blooming leaves under (c) microwave selective heating of the leaves and (d) water heating of the whole structure. Reproduced with permission [112]. Copyright 2022, Elsevier B.V. (e–h) 4D printing of graphene/SOEA shape-morphing structures. (e) A series of structures mimicking flying actions of birds fabricated with SOEA with different graphene contents. (f) SLA-manufactured nerve guidance conduits without and with 0.8% GO. (g) A demonstration of the self-folding of a 4D structure to connect the broken nerve. (h) Immunofluorescence images of neurogenic differentiation of MSCs for UV cured conduit and 4D printed conduit. Reproduced with permission [77]. Copyright 2018, Wiley-VCH.

other smart biopolymers, such as polynucleotides (RNA and DNA) and polypeptides, are also promising candidates for 4D bioprinting applications [115,116]. These smart biopolymers are sensitive to several external stimuli like temperature, humidity, and pH. Most importantly, they are derived from living (plant) materials and thus provide excellent biocompatibility and a favorable microenvironment for cell survival and growth during and after bioprinting.

Most SMPs are synthetic, and their printing process often involves hazardous environments involving high temperatures and organic solvents, which can damage cells. As a result, it is often not feasible to directly incorporate living cells within these SMPs during 4D bioprinting. To make these SMPs available for 4D bioprinting, one feasible strategy is to produce cell-laden constructs with multiple layers, as illustrated in Fig. 6. In the multiple-layer configuration, the SMP is printed as the first layer that provides the shape memory behavior. Subsequently, the other bioinks with living cells are bioprinted onto the SMP layer to provide biological functions. By programming the SMPs, these multi-layer cell-laden structures can achieve the desired shape-shifting process in response to external stimuli, enabling the use of

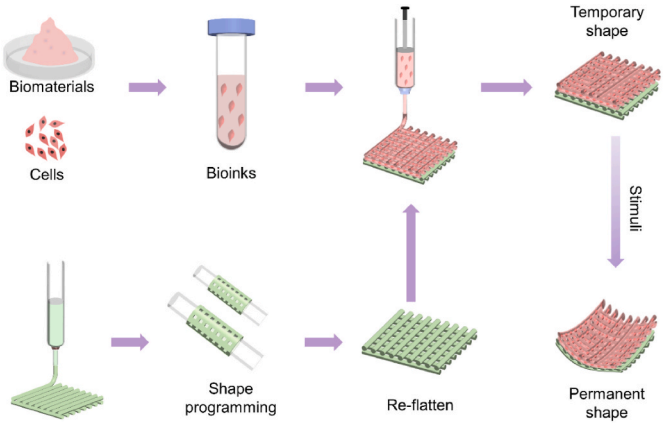

Fig. 6. Schematic illustration of 4D bioprinting for fabricating cell-laden biphasic constructs using SMPs and bioinks.

SMPs in 4D bioprinting. Several points are worth noting for 4D bioprinting of multiple-layer cell-laden dynamic structures using SMPs and bioinks. Firstly, although some SMPs can provide good shape memory behavior, their activation temperature is often much higher than the physiological temperature, potentially compromising cell viability and hampering their use in 4D bioprinting. Secondly, re-flattened 2D SMP membranes often do not have a perfectly flat surface, and deposition of bioinks onto the uneven SMP layer can be very difficult. Some strategies can be applied to address this issue. For MEB and inkjet bioprinting, distance sensing components can be equipped on printheads to enable real-time sensing of the distance between the printhead and printed surface during the printing process. Besides, some researchers have developed adaptive multi-degree-of-freedom bioprinters [123,124], which can achieve stereotactic deposition of bioinks onto skin defects with irregular geometry and satisfy the requirements of depositing bioinks onto an uneven SMP layer. For SLA and DLP, the fabrication of the second layer onto a SMP layer has been achieved, where the flattened SMP layer is placed on the bottom of build platform and coated with the bioink resin. Selective exposure of light on the bioink resin is then performed to generate a cell-laden layer on the SMP layer. Also noteworthy is that the interface between the cell-laden layer and the SMP layer should be tightly bonded to avoid their separation during *in vitro* and *in vivo* development. This 4D bioprinting approach for SMPs has been demonstrated for producing multi-layer shape-morphing living

Table 3
SMHs currently used for 4D bioprinting.

SMH	4D bioprinter	Mechanism for 4D effect	External stimuli	Cells	Cell viability	Structural stability	Application	Reference
AlgMA or HAMA	MEB	Crosslinking degree gradient across the thickness of the hydrogel	Water	Mouse bone marrow stromal cells	>95%	Self-folded tubes remained stable for at least 7 days but showed cracks on the wall of the tubules	Vasculature	[37]
GelMA and Gel–COOH–MA	Inkjet	Swelling difference between GelMA layer and Gel–COOH–MA layer	Water	Human umbilical vein endothelial cells	>90% on day 3	Self-folded microtubes could remain stable while experiencing the contraction force of the cells during 3 days of *in vitro* culture	Vasculature	[73]
Silk	DLP	Crosslinking difference between the first and second layer	Water	Chondrocytes and turbinate-derived mesenchymal stem cells	_	Transformed bending structure kept stable during 4-week *in vitro* culture	Cartilage	[70]
PEGDA	_	Swelling difference between the first and second layer	Water	Fibroblasts	_	Self-folded microtubes maintained their shape for 66 days	Vasculature	[131]
Oxidized AlgMA and GelMA	MEB	Swelling difference between oxidized AlgMA layer and GelMA layer	Water	NIH3T3	_	Bilayer structures with a low cell density ($\leq 5 \times 10^7$ cell/ml) could not keep maximum curved structure over 21 days, while those with a high cell density (1×10^8 cell/ml) showed steady, increased curvature during 21 days of *in vitro* culture	Bone	[132]
Jammed micro flake hydrogel made of oxidized AlgMA	MEB	Crosslinking degree gradient across the thickness of hydrogel	Water or pH	Human MSC	_	Bending structures remained stable during 21 days of *in vitro* culture	Cartilage	[40]
Oxidized AlgMA, GelMA, or 8-arm PEG-acrylate	MEB	Crosslinking degree gradient across the thickness of hydrogel	Water, pH, or chemicals	Human MSC	86%–89% after 3 days of culture	Deformed structures retained similar bending degrees during 21 days of *in vitro* culture	Bone	[133]
Oxidized AlgMA and GelMA	MEB	Swelling difference between oxidized AlgMA layer and GelMA layer	Water	Human MSC	_	Bilayer structures underwent tunable deformation due to unstable structure	Cartilage	[134]
Tyramine-functionalized hyaluronan (HAT) and alginate/HAT	MEB	Swelling difference between the first and second layer	Water	MSC	~75%	Curvature of the bilayer scaffolds gradually decreased during four weeks of *in vitro* culture	Cartilage	[135]
Ferromagnetic NdFeB microparticles, HAMA, and Alg/polyacrylamide	_	Magnetic actuation	Magnetic field	Fibroblasts, epithelial cells	~90% for 3% (w/v) HAMA, and ~70% for 5% (w/v) HAMA	Bilayer constructs retained regular folding under a magnetic field for 2 days with 3 h of stimulation each day	Bronchi	[136]
GelMA, poly-l-lysine (PLL)	MEB	Induction of membrane contraction by immersing anionic GelMA in cationic PLL solution	Opposite charge interactions	MSCs	<40%	Contracted thin membranes remained stable for at least two days	Membranous tissues	[128]
PEGDA/GelMA	DLP	Crosslinking degree gradient across the thickness of hydrogel	Water	NIH3T3	73% on day 1 and 90% on day 4	Folded constructs kept stable for up to 14 days	_	[74]

constructs. For instance, You and colleagues firstly cast out a SMP layer, followed by DLP-curing of a second hydrogel layer onto the SMP layer to form a bilayer scaffold, which could achieve self-bending upon immersion in water and microstructure transformation upon heating, showing potential for bone regeneration [119]. However, in their work, the second hydrogel layer was not laden with cells during the DLP printing. In another study, Luo and coworkers used alginate/polydopamine to form a self-folding layer, while alginate/GelMA was used to encapsulate living cells and bioprinted onto the SMP layer. Such bilayer scaffolds exhibited near-infrared irradiation (NIR)-triggered shape change and high cell viability after 1, 7 and 14 days of culture following NIR irradiation [81]. Wang's group used MEB to deposit a MSC-laden gelatin/GelMA bioink onto a shape-memory, highly stretchable layer of PDLLA-*co*-TMC/poly(lactic acid-*co*-glycolic acid) to obtain bilayer cell-laden scaffolds. The constructs could automatically fold into tubular structures when heated to ~37 °C, showing high potential for regenerating uterine tissues [125].

4.2. Shape morphing hydrogels

Hydrogels are water-containing polymeric networks stabilized via physical or chemical mechanisms. Most hydrogels possess largely reversible volumetric swelling or shrinking properties. Making use of this feature, some schemes have been proposed for developing shape morphing hydrogels (SMHs) by introducing uneven swelling or shrinking into different parts of the hydrogels, leading to nonuniform internal stress and shape-morphing process for the hydrogels. While most SMHs respond to water, however, their shape morphing behavior can also be triggered by other stimuli, such as temperature [126], ions [43,127], pH [45], and charge interactions [128,129]. SMHs are appealing candidates for 4D bioprinting due to their unique advantages, such as excellent biocompatibility, good biodegradability, similarity to extracellular matrix (ECM), ability to support cell survival and growth, and crosslinking ability [20,33,130]. Many SMHs can be directly mixed with living cells to obtain bioinks for 4D bioprinting of dynamic constructs that can change their shape over time. Various SMHs have been used for 4D bioprinting and are summarized in Table 3. Most of these 4D-bioprinted constructs achieved shape morphing (e.g., bending) properties and formed desired architectures, such as tubing and flowers, by responding to water (Fig. 7).

As shown in Table 3, a number of SMHs have been used for 4D bioprinting to produce shape-changing living constructs by strategic allocation of the bioinks. Currently, most of the 4D-bioprinted cell-laden SMHs can change shapes by responding to water. The water-triggered 2D-to-3D or 3D-to-3D shape transformation of 4D bioprinted SMH constructs has been achieved via several strategies, primarily by controlling the crosslinking degree gradient (or swelling ratio gradient) (i) across the thickness of the hydrogels (i.e., out-of-plane), (ii) across the hydrogel plane (i.e., in-plane), or (iii) across both the thickness and plane of the hydrogel (inside-out-plane), as illustrated in Fig. 8.

In the out-of-plane strategy, 4D-bioprinted SMHs exhibit a gradient of swelling ratio along the thickness (i.e., vertical direction) of the hydrogels, resulting in self-bending or folding structures upon immersion on water (Fig. 8a). This strategy has been commonly applied in 4D bioprinting of dynamic cell-laden hydrogels. To achieve the out-of-plane force, one major approach is to use a single SMH to fabricate structures with a gradient in crosslinking degrees from the top to the bottom surface of a hydrogel structure, by modulating the physical or chemical crosslinking process. This results in different contractility and swelling ratio between the upper and lower layers, leading to self-bending or folding of the hydrogel. Fig. 9a–k shows one typical example related to the fabrication of a series of self-folding GelMA micro-tubes [137]. Another major approach is to fabricate bilayer structures using two types of SMHs with different volume expansion properties. For example, bilayer hydrogel scaffolds were fabricated by combining a cell-laden GelMA layer and a cell-laden OMA layer. The differential swelling of

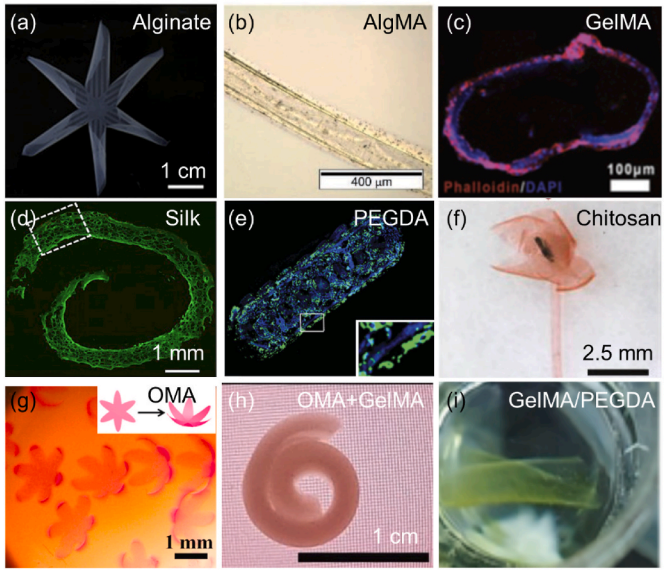

Fig. 7. Shape morphing hydrogels. (a) A 6-petal flower made of alginate. Reproduced with permission [43]. Licensed under a Creative Commons CC BY license. (b) 4D-bioprinted self-folding AlgMA tube. Reproduced with permission [37]. Copyright 2017, Wiley-VCH. (c) Cross section of GelMA tubes seeded with human umbilical vein endothelial cells (HUVECs). Reproduced with permission [137]. Licensed under a Creative Commons CC BY license. (d) PKH dye-labeled cells in 4D-bioprinted silk after two-week culture *in vitro*. Reproduced with permission [70]. Copyright 2020, Elsevier B.V. (e) PEGDA bilayer tubes containing Hoechst-stained fibroblasts (blue) in the inner hydrogel layer and calcein AM-stained fibroblasts (green) in the outer hydrogel layer. Reproduced with permission [131]. Copyright 2013, Wiley-VCH. (f) An artificial flower changed from a chitosan sheet. Reproduced with permission [45]. Licensed under a Creative Commons CC BY license. (g) Human MSC-laden 6-petal blossoms made of oxidase AlgMA (OMA). Reproduced with permission [133]. Licensed under a Creative Commons CC BY license. (h) Cell-laden bilayer tubes composed of an OMA layer and a GelMA layer. Reproduced with permission [132]. Copyright 2021, Wiley-VCH. (i) DLP-produced GelMA/PEGDA self-folding scaffolds containing NIH/3T3 cells. Reproduced with permission [74]. Copyright 2023, American Chemical Society.

the two layers led to the self-folding of the scaffolds in aqueous solution [132].

The in-plane force of 4D-bioprinted SMHs can also lead to the self-bending or folding process in aqueous environment by introducing a swelling ratio gradient across the plane (or in the horizontal direction) of the hydrogels (Fig. 8b). The in-plane SMHs can be fabricated using single materials or multiple materials with different swelling ratios. For example, a single smart hydrogel composed of methylcellulose and alginate has been 4D printed into a series of in-plane 2D patterns, which could transform into different simple or complex 3D morphologies in $CaCl_2$ solution [42]. Wu and coworkers produced a series of hydrogel sheets composed of alternate strips of poly(N-isopropylacrylamide) (PNIPAm) and poly(2-acrylamido-2-methylpropane sulphonic acid) (PAMPS/PNIPAm) (Fig. 9l) [138]. Temperature-responsive structures could be fabricated through using these two hydrogels as they had different swelling ratios under the same temperature in water (Fig. 9m–n).

Although out-of-plane and in-plane SMHs can be used to achieve different 3D shape-morphing processes, in some cases, only out-of-plane or in-plane forces are not sufficient to achieve a desired shape-shifting process. To address this issue, swelling ratio gradients across both the thickness and plane (i.e., inside-out plane) of hydrogels have been developed, which enables the production of structures with improved shape-morphing ability (Fig. 8c). For instance, single out-of-plane GelMA hydrogels could self-fold into microtubes with a diameter ranging from 50 to 500 μm [137], but they do not have sufficient

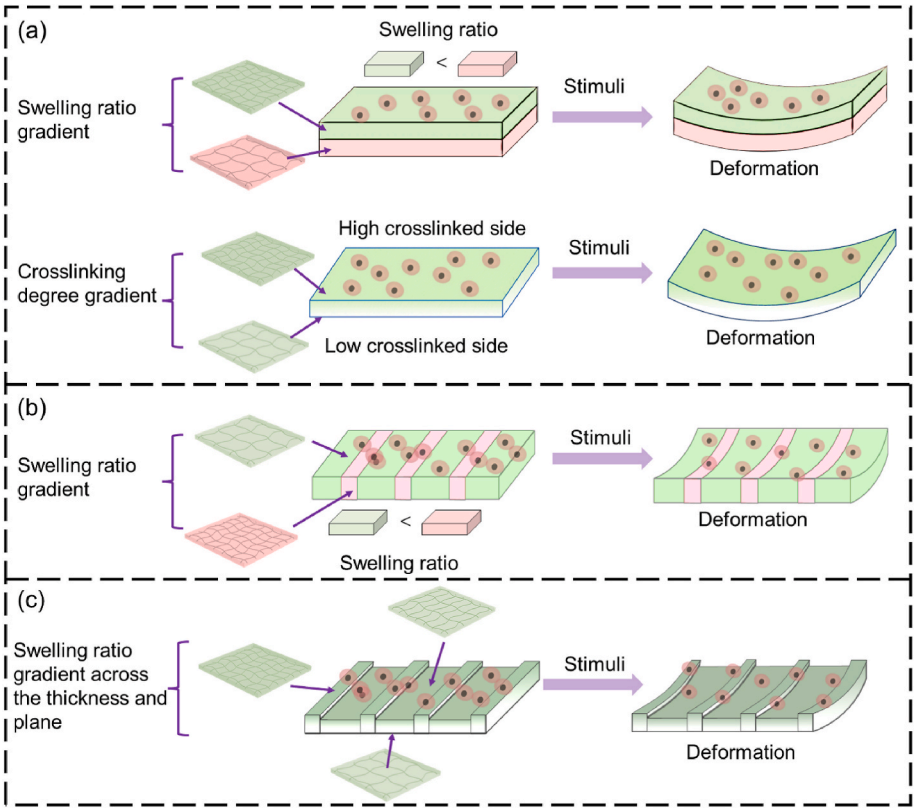

Fig. 8. Strategies for 4D bioprinting of SMHs.(a) Out-of-plane SMHs. (b) In-plane SMHs. (c) Inside-out plane SMHs.

internal force to achieve a large tube with a diameter comparable to that of large blood vessels, such as veins with a diameter of 7–14 mm. Zhao and coworkers introduced a photocrosslinking gradient across the thickness and the plane of GelMA by constructing a second layer of strips onto the first solid membrane [139]. The inside-out GelMA hydrogels could fold into tubes with increased diameters of up to 6 mm. In another study, Du's group developed inside-out reversible alginate hydrogels by introducing different periodic patterns onto a solid membrane layer, leading to various 3D morphologies such as twist, tube, and plant-inspired architectures by responding to Ca^{2+} solution (Fig. 9o–t) [43].

4.3. Smart composite biomaterials

The applications of single SMPs or SMHs in 4D bioprinting are often hampered by their limited shape morphing ability, insufficient mechanical properties, poor printability, and low biocompatibility. To overcome the limitations of a single biomaterial, a typical solution is to develop smart composite biomaterials (SCBs) by incorporating suitable reinforcements (e.g., micro particles, nanofibers, and sheets) into the matrix [140]. Leveraging the advantages of different types of biomaterials, SCBs can achieve properties that cannot be obtained by a single biomaterial. The properties of SCBs can be influenced by the matrix, the reinforcement, and the interface between the matrix and reinforcement.

Various SCBs (Table 4) have been developed for 4D printing (Table 4). The incorporation of reinforcements into the base polymers can improve their performance such as printability, mechanical properties, and shape memory properties [25,141,142]. SMHs often have low printability and weak mechanical properties. This can make it challenging to print them as 2D/3D structures with high precision. Laponite nanoclay, a commonly used rheology modifier, is often added to hydrogel-based bioinks to improve their rheological properties and printability [143–145]. Laponite nanoclay is a sodium lithium magnesium silicate and these nanoscale disks have a thickness of ~1 nm and a diameter of ~25 nm. It can be dispersed in hydrogels and interact with them to form nanoclay/hydrogel composites with improved performances [143]. For instance, in the work by Lewis's group, Laponite nanoclay and nanofibrillated cellulose (NFC) were added to the NIPPAm SMH to form a composite ink, in which nanoclay offered good extrudability and printability and NFC was aligned during extrusion to induce the in-plane force (i.e., anisotropic swelling ratio) [35]. This composite ink was 4D printed into different accurate, complex plant-inspired architectures that could undergo 3D deformation upon immersion in water (Fig. 10a–e). In another study by Guo and colleagues, Laponite nanoclay was incorporated into agarose and polyacrylamide (PAM) hydrogels to enhance their shear viscosity and extrudability. This allowed the composite to be 4D printed into temperature-responsive dynamic structures resembling fish and whales, as depicted in Fig. 10f [146]. In addition to nanoclay, magnetic nanoparticles have been incorporated into SMPs or SMHs to endow them with remote and/or cyclic actuation capability in response to magnetic fields [142,147]. For example, Fe_3O_4 nanoparticles incorporated in SMPs can be heated by alternating magnetic fields and hence allow us to trigger shape-shifting of SMPs remotely [148–150]. Fe_3O_4/PLA composites have been 4D printed to generate different magnetic field-responsive structures including line- and flower-like shapes and vascular stents (Fig. 10g) [148]. Other reinforcements have also been applied for developing SMP or SMH-based composites. For instance, hydroxyapatite, a bioactive ceramic, was incorporated into collagen to improve the osteogenic activities of 4D-printed bone scaffolds [151]. In another study, Wang and coworkers developed a SCB by combining black phosphorus nanosheets (BPN), tricalcium phosphate (TCP), and PDLLA-*co*-TMC, in which PDLLA-*co*-TMC provided shape memory property, TCP enhanced the bone regeneration efficacy, and BPN could be heated by NIR to drive the shape-morphing process of the 4D-printed scaffolds [80].

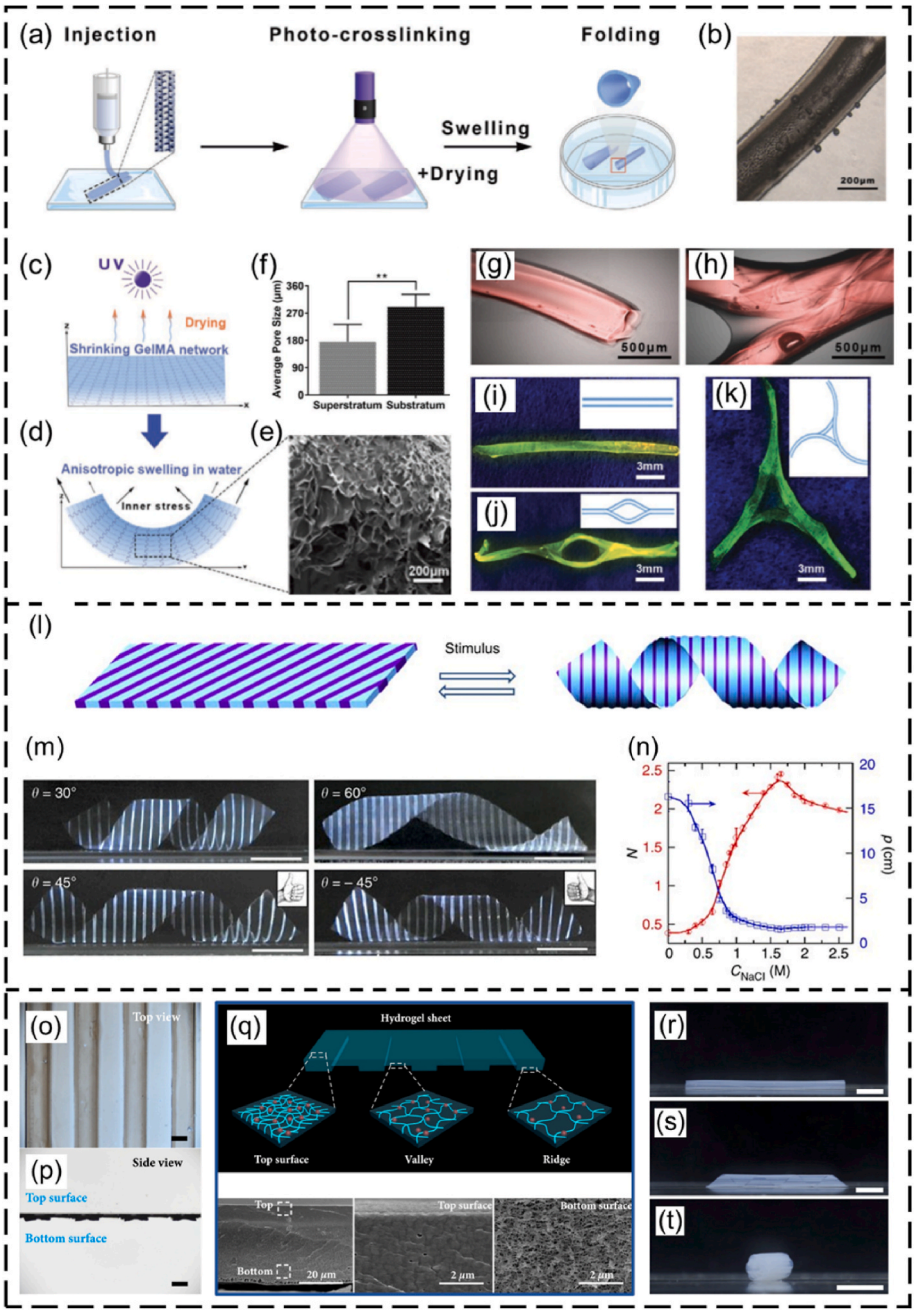

Fig. 9. SMHs engineered using different strategies. (a–k) Self-forming GelMA tubes with crosslinking gradient across the thickness: (a) the 4D printing process, (b) optical image of a GelMA tube, (c, d) schematic illustration of the difference in crosslinking degree between the upper and lower layers and (e) corresponding SEM image and (f) pore sizes, (g–k) different GelMA microtubes fabricated by 4D printing. Reproduced with permission [137]. Licensed under a Creative Commons CC BY license. (l–n) In-plane force triggered helical structures formation: (l) planar sheet of the composite gel patterned with PNIPAm strips (dark blue) and PAMPS/P-NIPAm strips (light blue), (m) different helical structures governed by the patterned angles (θ) (scale bar: 1 cm); (n) variation in the pitch (p) and number of turns (N) of the left-handed helix ($\theta = 45$ °C), plotted as a function of the concentration of NaCl solution. Reproduced with permission [138]. Copyright 2013, Springer Nature. (o–t) Inside-out shape-morphing alginate: (o, p) top view and side view of an alginate pattern, (q) illustration of the hydrogel pattern with different crosslinking gradient across the thickness and plane of alginate (upper image) and SEM images of top and bottom parts of the alginate pattern (bottom images). (r–t) Tube formation (r), twisting (s), and curving (t) of the inside-out alginate after immersing it in Ca^{2+} solution (scale bar: 0.5 cm). Reproduced with permission [43]. Licensed under a Creative Commons CC BY license.

4.4. Smart design

While smart materials are a key element for the shape and functional transformation of dynamic structures, smart design is also essential in regulating these changes in a controllable manner. The smart design of 4D bioprinted structures should be conducted by taking into account the anticipated time-dependent transformation of objects [14]. A successful 4D bioprinting design requires a holistic consideration of shape memory property and mechanisms of the smart materials, patterns of the smart materials, type of 4D printer, and target tissues. Different smart materials exhibit distinct shape memory mechanisms and thus should be programmed using different 4D strategies to achieve controllable shape change. The properties of printed patterns of the smart materials are significantly influenced by the printing parameters (e.g., angle, position,

Table 4
Smart composite biomaterials for 4D printing.

Composite	Printer type	Mechanism for 4D effect	External stimuli	Application	Reference
NIPPAm + Laponite nanoclay + NFC + glucose + glucose oxidase	MEB	In-plane force induced by the alignment of NFC	Water or heat	Biomimetic structures	[35]
Agarose + polyacrylamide + Laponite nanoclay	MEB	Sol-gel transition of agarose	Temperature	Tissue engineering	[146]
Fe_3O_4 + PLA	MEB	Shape memory effect of PLA	Magnetic field	Vascular stents	[113, 148]
Fe_3O_4 + PLA + thermoplastic polyurethane (TPU)	FDM	Shape memory polymers	Magnetic field	Biomimetic structures	[150]
Poly-hydroxybutyrate/PCL + Fe_3O_4 + cellulose nanofiber	FDM	Shape memory polymer	Magnetic field	_	[149]
Black phosphorus nanosheets/TCP/PDLLA-*co*-TMC	MEB	Shape memory polymer	NIR-irradiation	Bone tissue engineering	[80]
Hydroxyapatite + collagen	MEB	Leaching of the constituent components from printed structs to form fibrous bindles	Solvent leaching	Bone tissue engineering	[151]

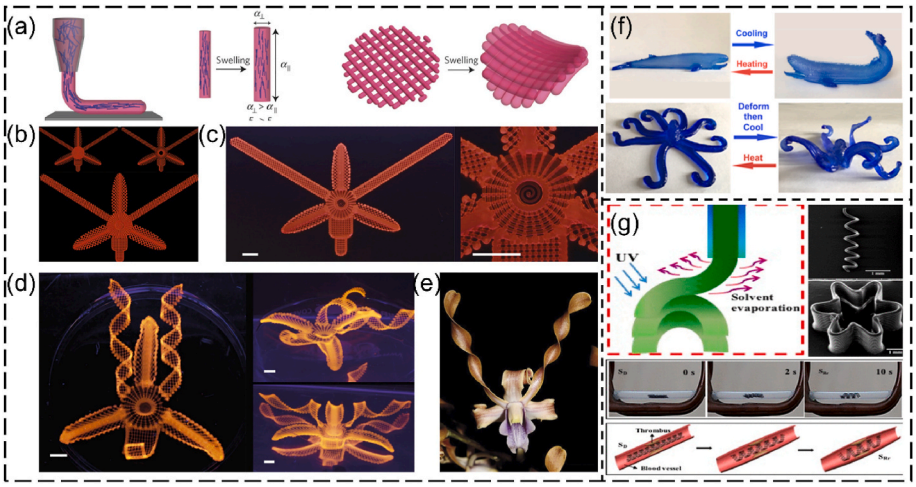

Fig. 10. 4D printing of SCBs. (a–e) 4D printing of Laponite/NFC/NIPPAm: (a) schematic illustration of the shear-induced alignment of cellulose fibrils during extrusion and subsequent effects on anisotropic stiffness E and swelling strain α, (b) printing path of an orchid, (c) printed structure, (d) shape-morphing orchid from different views, (e) a native orchid (scale bar: 5 mm). Reproduced with permission [35]. Copyright 2016, Springer Nature. (f) Temperature-triggered shape change of 4D printed whale-like and octopus-like structures made of Laponite/agarose/PAM. Reproduced with permission [146]. Copyright 2018, American Chemical Society. (g) 4D printing of shape memory structures (line, flower, vascular stents) using Fe_3O_4/PLA. Reproduced with permission [148]. Copyright 2017, American Chemical Society.

and layer thickness), which affect the shape-morphing behavior (e.g., orientation, bending degree, and spiral angle) and thus should be controlled carefully. Based on the designed printing path, the 4D printer type should be carefully selected as certain printing technologies may not be able to achieve the desired smart design. For example, inkjet bioprinting or LAB may struggle to process smart designs for building complex 3D constructs with high precision. The target tissues also need to be considered when designing the dynamic scaffolds. For instance, to (re)generate vasculature requires structures with good self-folding capabilities to conform to the native tubular shape of vessels, while bone regeneration requires structures with good shape transformation abilities to fit irregular bone defects.

The complexity of intended shape-shifting behavior greatly affects the smart design procedure. Smart design for simple 2D-to-3D deformations, such as bending, twisting, and forming tubular structures, is relatively straightforward. For instance, self-folding can be achieved in SMHs by designing a 2D rectangular membrane with different cross-linking degrees between the upper and lower surfaces. As the complexity of 3D deformation increases, the design process becomes more complicated and challenging. For intricate 3D deformation, such as plant-inspired architectures and 3D-to-3D shape transformation, a holistic consideration of many factors is necessary during the smart design process, such as the spatial distribution of different components, the integration of multiple simple 3D deformations, the connection of distinct shape-morphing components, and the properties of connection points.

To assist the design of shape transformations, mathematical models and simulations have been developed to investigate the shape memory or shape morphing behaviors of smart materials. These models and simulations can enhance the users' understanding of shape-shifting mechanisms, thereby facilitating the improvement and optimization of 4D bioprinting paths. SMPs are primarily mathematically modeled based on the standard linear viscoelasticity approach or the thermodynamics behavior approach [152]. The former models SMP by combining elastic and viscous units with temperature-dependent parameters, while the latter models SMP as a mixture of active and frozen phases, in which the conversion of the active phase to the frozen phase causes the shape recovery behavior of SMPs. Many mathematical models have been developed for SMPs based on these two approaches [152–154]. The shape-morphing behavior of SMHs can be modeled based on the Timoshenko bimetal model [35,155]. The Timoshenko bimetal model was initially used for bi-layer metallic thermostat, and has been used, with or without modification, to describe and predict the deformation (or curvature) of SMHs based on the printing path [35,73]. Besides, finite element analysis (FEA) has been commonly used to simulate the shape transformation process of 4D bioprinted structures. The FEA can be performed using commercially available software (e.g., Abaqus) by modeling the 4D structure and selecting/designing a suitable

constitutive model. This allows us to explore the influence of structural, chemical, or environmental factors on shape transformations, which in turn helps users optimize their smart design and 4D systems. Furthermore, machine learning (ML), a subset of artificial intelligence (AI), and neural network algorithms are developing rapidly in recent years and provide a highly efficient tool for optimizing the smart design of 4D bioprinted dynamic constructs through combining with the mathematic models [156,157]. For example, Qi's group developed an AI-strategy for 4D printing by combining FEA, ML, and EA (an AI algorithm inspired by biological evolution) [158–161]. As shown in Fig. 11, two shape memory materials were encoded as "0" and "1" and their distribution in the structures was optimized using the ML-EA approach (Fig. 11a and b). After optimization, the material distribution was converted to grayscale slices, which were then transferred to a DLP printer for processing the two active materials into 4D structures (Fig. 11c). The 4D active composite structures could undergo 3D deformation upon swelling to

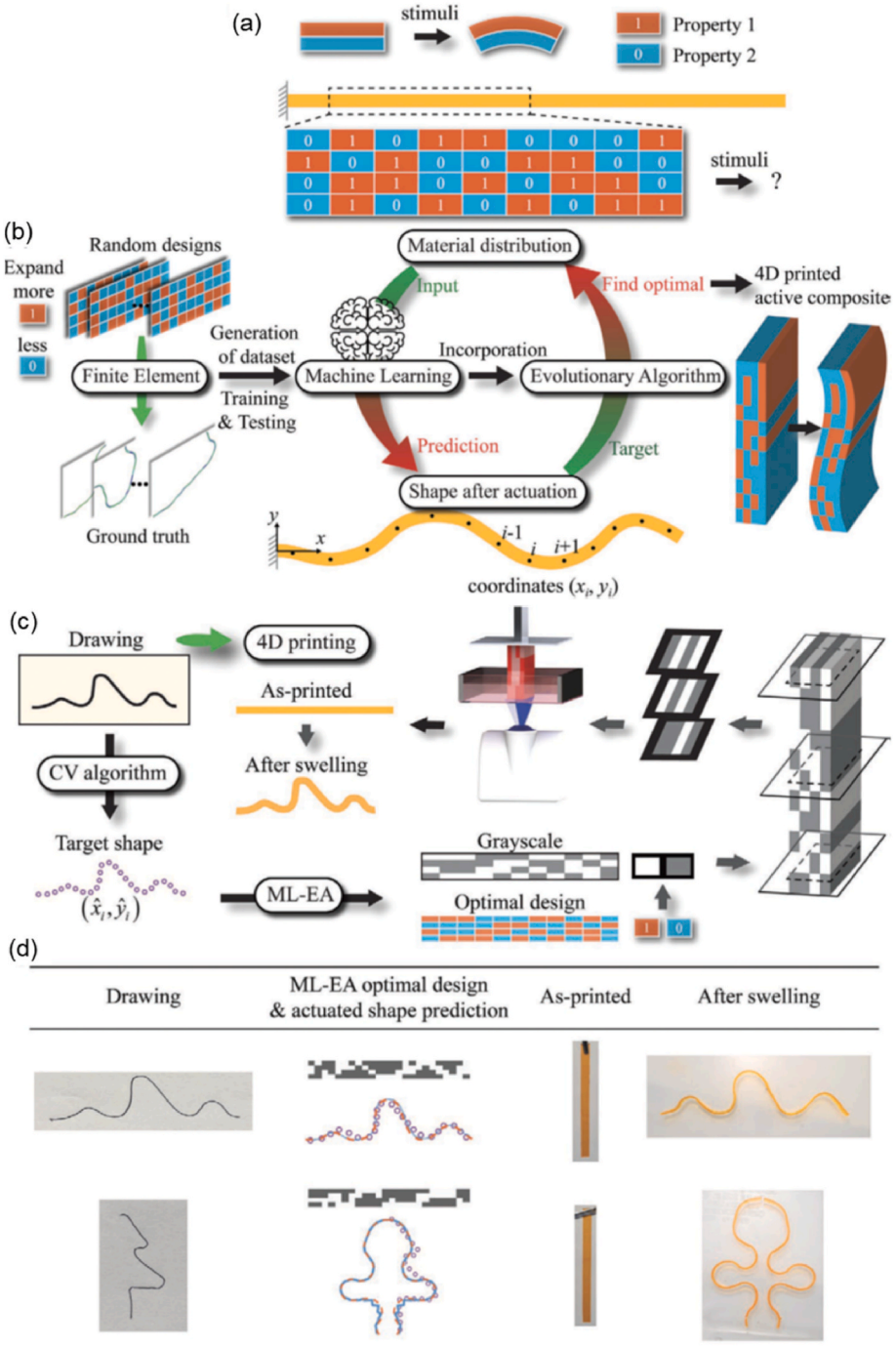

Fig. 11. A machine learning-evolutionary algorithm (ML-EA) to assist the design of 4D printed active composites with desired shape transformation. (a) Property mismatch-induced actuation and distribution of two materials with different shape memory properties (property "1" and property "2" are encoded as "1" and "0" for the algorithm, respectively). (b) A complete design for designing and optimizing the 4D printing path, including generation of the dataset by FEA simulations of random designs, prediction of shape changes by ML, optimization of material distribution by EA, and 4D printing of active composite using the optimized design. (c) 4D printing process based on the ML-EA design, including identification of drawn profiles as target shapes, ML-EA design, conversion of the obtained optimal design to the grayscale slices, 4D printing by DLP, and actuation of the printed structure. (d) Experimental results showing DLP-produced structures with target shape transformation to mimic drawn profiles. Reproduced with permission [159]. Copyright 2021, Wiley-VCH.

achieve the target shapes of drawn profiles (Fig. 11d) [159].

5. Requirements for bioinks in 4D bioprinting

Smart bioinks for 4D bioprinting can be made of cell-laden smart biomaterials or solely living cells. As 4D bioprinting is still in its early development stage, limited smart biomaterials are available for 4D bioprinting. Currently, one of the major challenges for 4D bioprinting is to develop suitable smart biomaterials that not only have excellent printability and biological functionalities, but also robust responsiveness to stimuli. The fundamental bioink traits in 4D bioprinting include printability, biocompatibility, stimuli-responsiveness, biodegradability, mechanical properties, and cells (Table 5). Except for stimuli-responsiveness, the other traits are also vital for 3D bioprinting and have been discussed in several well-written reviews [2,22,162,163]. However, compared to 3D bioprinting, 4D bioprinting poses more stringent requirements on these features, which will be discussed in this section.

5.1. Printability

Printability is the foremost requisite for bioinks in 4D bioprinting. A bioink with good printability enables the accurate deposition of the materials, enabling the precise fabrication of intricate 4D structures with specific component distributions for achieving desired shape/function transformations. The specific requirements on the printability of bioink materials vary depending on the type of bioprinting technology utilized. For MEB, the bioink materials should have good rheological properties, including a high viscosity, shear thinning behavior, and thixotropic property. The printability of a material for MEB is affected by many parameters such as nozzle size, printing speed, and layer thickness. Some mathematical models have been used to describe the ink flow behavior in MEB [164–166]. Based on these models, a number of approaches have been developed to evaluate the printability of a material for MEB according to the extruded filament size, the printed grid circularity, and the obtained stackability [56,144,167]. As inkjet bioprinting and LAB are DOD-based bioprinting technologies, the printability of a bioink material is mainly affected by its physical parameters such as viscosity, density, and surface tension, which determine the formation and size of a droplet [168]. Besides, fast crosslinking is required for DOD bioprinting as rapid stabilization of the deposited low-viscosity droplets can avoid collapse. SLA and DLP require a bioink material to be photocrosslinkable and have suitable viscosity, thus permitting fresh bioink to flow and re-coat the construct after one layer is printed. The processing parameters should also be optimized to obtain a precise 3D structure with good shape fidelity, such as light intensity, scanning speed, and light exposure time [53].

Table 5
Desired properties for smart bioinks for 4D bioprinting.

Properties	Requirements
Printability	Processable and compatible with different types of bioprinting technologies Production of dynamic constructs with accurate patterns according to the smart design
Biocompatibility and bioactivity	Supporting cell growth and functionality during *in vitro* and *in vivo* development Absence of side effects in the host Facilitating desirable host responses after *in vivo* deployment
Stimuli-responsiveness	Robust stimuli-responsiveness Enabling fabrication of dynamic constructs with preprogrammed changes in shape, property, and function under stimuli Multiple stimuli-responsive, reversible shape changes, remote and cyclic actuation Enabling multi-step 3D deformation Adaptation to the complex human physiological environments
Biodegradability	Achieving a preprogrammed multi-step shape-shifting process by controlling the degradation rates Matching the growth of neo-tissues after deployment *in vivo* by designing appropriate degradation kinetics
Mechanical properties	Supporting structural integrity and shape transformation during evolvement of the 4D bioprinted constructs Matching the mechanical properties of target tissues
Cells	Cell sources with high availability High cell viability Comparable cell density to native tissues Excellent cellular functionalities (e.g., proliferation and differentiation) Generation of cell traction force to induce the shape transformation of microstructures

5.2. Biocompatibility

Biocompatibility refers to the ability of a material to accommodate and permit appropriate biological response in a specific biological application [169,170]. Therefore, a biocompatible material not only can co-exist with the host without producing side effects or toxicity, but also is expected to produce positive responses to and by the host. Like 3D bioprinting, 4D bioprinted constructs involve living components and undergo a broad range of biological interactions with a living system. As a result, a bioink material for 4D bioprinting must be biocompatible to support the in vitro and in vivo development of the fabricated constructs. A material with excellent biocompatibility can support cell growth, maintain high cell viability, facilitate the transfer of molecular or mechanical signals, and interact positively with both endogenous tissues and the immune system, all of which are essential for successful transplantation and function. The SMPs and SMHs listed in section 4 are representative biocompatible materials for 4D bioprinting, and most SMHs are natural polymers and thus provide a comfortable microenvironment for cell survival and growth.

5.3. Stimuli-responsiveness

Robust stimuli-responsiveness is critical for 4D bioprinted constructs as they need to change their shape and/or functionality in response to appropriate stimuli. The human body has intricate microenvironments which are maintained by multiple mechanisms, such as humoral, ionic, and neural regulation. To accommodate such complex conditions, an ideal responsive material should have the capability to self-transform in response to multiple physiological signals, rather than being limited to a single type of stimulus. Currently, stimuli-responsive materials that can be 4D bioprinted are primarily SMPs or SMHs. However, most of them respond to only a single stimulus, such as temperature or humidity. Additionally, it is necessary for stimuli-responsive materials to maintain their shape fidelity and functional stability, even when exposed to disturbance. In certain applications (e.g., recapitulating the regular contraction of native tissues), reversible shape transformation and cyclic reversible shape transformation are needed for 4D bioprinted dynamic structures. In such cases, the 4D bioprinted structure should exhibit robust shape memory behavior with minimal decline in its performance at increased cycles [39,44].

5.4. Biodegradability

Biodegradation is a common property for most biomaterials and scaffolds *in vitro* and *in vivo*. It should be noted that the degradation process *per se* is not generally regarded as a 4D effect for 4D bioprinting [15,23]. However, in some cases, degradation rate is programmed to trigger the specific deformation at specific time point during *in vitro* incubation. For example, Alsberg's group produced shape-morphing trilayer hydrogels composed of two layers of different OMA hydrogels and one layer of GelMA hydrogel [171]. Due to the swelling and

degradation discrepancies of these layers, the trilayer hydrogels underwent multiple-shape (five-phase) transformations during *in vitro* culture [171]. In tissue regeneration, the scaffolds gradually degrade while the embedded cells produce new ECM to replace the degraded materials, ultimately forming new tissues [172]. As such, it is ideal that a material's degradation rate matches the rate of new tissue growth. However, it is still challenging since the new tissue growth rate is dynamic and difficult to control. Besides, the degradation byproducts should be biocompatible (i.e., producing no side effects in the host). The degradation products should also be able to be cleared from the human body via cell metabolism or the urinary system. Most SMPs are synthetic polymers and thus generally exhibit a slower degradation rate compared to SMHs. The degradation rate of SMHs depends on various factors, such as hydrogel type, crosslinking degree, concentration, temperature, and *in vitro* and *in vivo* conditions.

5.5. Mechanical properties

Mechanical properties of a material are a key consideration for bioinks in 4D bioprinting. Firstly, sufficient mechanical strength is needed to support the structural integrity and prevent the bioprinted structures from collapsing during and after bioprinting. Secondly, a 4D bioprinted structure with good mechanical strength and structural stability can effectively support 2D-to-3D and 3D-to-3D shape transformation. Currently used SMHs are mostly natural hydrogels with relatively low mechanical strength. Thus, it is often challenging to print stable structures with designed structural anisotropy, making it difficult to achieve effective 3D shape transformation for biocompatible hydrogels laden with cells [40]. Although a number of studies have reported that simple self-bended and cell-laden hydrogel structures could remain stable over several days of *in vitro* culture [40,70,133], the structural stability of 4D bioprinted constructs still faces many crucial issues. For example, it is often observed that self-tubed cell-laden constructs form loose or leaky tubular structures and cracks on the tubule wall, which are undesirable when using the constructs for vascular regeneration [37,125]. In some studies, the bending degree of self-folded scaffolds would gradually change during days or weeks of *in vitro* incubation [132,135], which may be caused by the structures' degradation and unstable swelling ratio of upper and bottom layers. In addition, cell-laden 4D constructs, especially for micro-constructs, experience cell contraction forces during incubation, which may lead to undesired deformation for the already shape-morphing constructs [73]. In such cases, smart biomaterials must have sufficient mechanical strength to prevent the undesired deformation caused by the cell contraction force. Thirdly, although native tissues and organs show diverse mechanical properties, the implanted constructs should ideally have mechanical properties comparable to those of the target native tissues to avoid mechanical mismatches or transplant failure. At the early stage of tissue regeneration, cells embedded in the hydrogels do not produce sufficient new ECM to support themselves. Therefore, the bioprinted structures should have a certain mechanical strength to support cell growth and functions until the cells are capable of secreting enough of their own ECM.

5.6. Cells

As living cells are utilized in 4D bioprinting, the properties of the embedded cells (e.g., cell source, density, viability, proliferation, and function) need to be taken into account. The cell source for bioprinting can be autologous or exogenous. Autologous cells are free from immune rejection but may be limited by their availability or genetic or metabolic disease states; exogenous cells represent alternative cell sources with higher availability for bioprinting, but may cause rejection by the host immune system [173]. Both somatic and stem cells have been used in 4D bioprinting. Somatic cells are fully differentiated cells that make up the majority of cell populations in tissues and are a suitable choice for bioprinting specific tissues. However, these cells often have limited expansion capabilities, making it difficult to obtain a sufficient number of cells required for bioprinting large tissues or organs. Stem cells are a promising choice for bioprinting due to their high proliferation potential and differentiation capability. Stem cells such as adult tissue-derived MSCs [70,133] and induced pluripotent stem cells (iPSCs) [51,79,174] have been widely used in bioprinting. However, safety concerns, such as potential carcinogenesis, remain in the clinical use of stem cells, especially iPSCs [175].

The cell density in the bioink matrix is a critical issue for bioprinting. The cell density in the bioink should be determined by several factors, such as hydrogel type, bioprinter type, and target applications. A low cell density is relatively easy to process via different types of bioprinting systems, but may not provide sufficient biological functions. A high cell density usually can better support biological functions, but may impact the printability of the bioink and cause issues such as nozzle clogging in MEB and light scattering in DLP. Currently, it is still challenging to process bioinks with very high cell densities (e.g., $> 10^9$ cells/ml) into designed structures [51,61]. In addition, the density of cells encapsulated within the hydrogels may also influence shape transformation. For instance, during 21 days of *in vitro* culture, OMA/GelMA bilayer structures with a low density of NIH3T3 cells ($\leq 5 \times 10^7$ cell/ml) exhibited a decreased bending degree from maximum curvature, while those with a high cell density (1×10^8 cell/ml) showed a gradually increased bending degree [132].

Maintenance of cell viability is crucial during the bioprinting process and post-bioprinting culture. During bioprinting, the viability of cells is affected by various factors such as hydrogel properties, bioprinter type, processing parameters, and bioprinting time. Hydrogel properties, such as viscosity, greatly affect cell viability during bioprinting. For MEB, it was reported that 2% (w/v) partially crosslinked alginate led to much higher cell viability (>90%) than 6% (w/v) partially crosslinked alginate (about 61.5%) immediately after bioprinting, which was mainly due to a significantly increased viscosity of the 6% (w/v) alginate hydrogels [176]. As mentioned in section 3, different types of bioprinters result in varying cell viability when used to process the bioinks. Also, appropriate processing parameters are very important for maintaining high cell viability. For example, UV irradiation dosage, one of the vital parameters for curing UV-reactive bioinks, can greatly affect cell viability and cause significant cell death when the dosage exceeds a threshold [177,178]. As the living cells in the bioink must have sufficient nutrients and oxygen for survival, the bioprinting time should not last too long, otherwise the bioprinting process may cause major cell death.

For the post-bioprinting period, the viability of cells in the hydrogels could be affected by the hydrogel type, crosslinking density, and structural configurations (e.g., porosity). Hydrogel type can significantly influence the cell viability during *in vitro* culture. It was reported that after 7 days of *in vitro* culture, BMSCs encapsulated in 2% (w/v) alginate and Matrigel showed a viability of ~90%, while the viability of those in 1% (w/v) agarose decreased to ~70% and no cell survived in 25% (w/v) Pluronic F-127 [179]. Crosslinking density can also affect cell viability during post-bioprinting incubation period. The crosslinking density of GelMA, a widely used hydrogel in 3D and 4D printing, is dependent on several factors, such as GelMA concentrations and methacrylate degree, where a higher crosslinking density leads to a less porous structure with higher stiffness [139,180–182]. Stevens's group encapsulated astrocytes in GelMA hydrogels with concentrations ranging from 2.5% (w/v) to 10% (w/v) [183]. They found that astrocytes exhibited significant higher viability and more elongated behavior in soft GelMA hydrogels with low-concentrations (2.5% w/v and 3% w/v) than those in stiffer GelMA hydrogels with concentrations higher than 5% (w/v) [183]. Structural configuration is also a key factor affecting cell viability and should be carefully considered. For example, hydrogel pairs with opposite charges can form complex polymer coacervates and thus induce hydrogel shrinking accompanied by decreased mesh size. This strategy has been used to scale down the cell-laden hydrogels

post-bioprinting, but it was found that such processes decrease cell viability, possibly due to the toxicity of the shrinking agents used in the immersion process and increased mechanical stress exerted on the cells during the shrinking process [128,129].

Finally, appropriate cell proliferation and function are required to facilitate the maturation of bioprinted tissue constructs. At the initial development stage after bioprinting, fast cellular proliferation is often required to quickly populate the bioprinted constructs to achieve a physiological cellular level; at the subsequent stage when the bioprinted constructs become mature, a certain level of cell proliferation may be needed to maintain tissue homeostasis [162]. Besides cell proliferation, cells should maintain their functions during the bioprinting process as well as during *in vitro* and *in vivo* development to achieve desired functionalities of the maturated constructs.

Besides using smart materials to induce the shape-morphing of 4D bioprinted structures, living cells can also be utilized as active folding elements to trigger the transformation of temporary microstructures into designed shapes [184]. The driving force is mainly the cell traction force (CTF) attributed to actomyosin interactions and actin polymerization [185]. Making use of the CTF, shape-morphing microstructures were produced by depositing living NIH/3T3 cells on the designed micropatterns composed of parylene (poly(*p*-xylylene) polymer) film coated with fibronectin. Driven by the CTF, these cell-laden micropatterns could automatically transform into a regular dodecahedron and cylindrical tube (Fig. 12) [186]. CTF thus provides another mechanism for 4D bioprinting to produce cell-laden and shape-morphing microstructures.

6. Applications of 4D bioprinting in engineering dynamic tissues

The emergence of 4D bioprinting has opened an exciting avenue for engineering dynamic living constructs that functionally mimic native tissues and organs. The last few years have witnessed the increasing application of 4D bioprinting in producing dynamic tissues and organs, including skin, bone, cartilage, and others. This section presents current applications of 4D bioprinting in engineering different dynamic tissues and organs (Table 6).

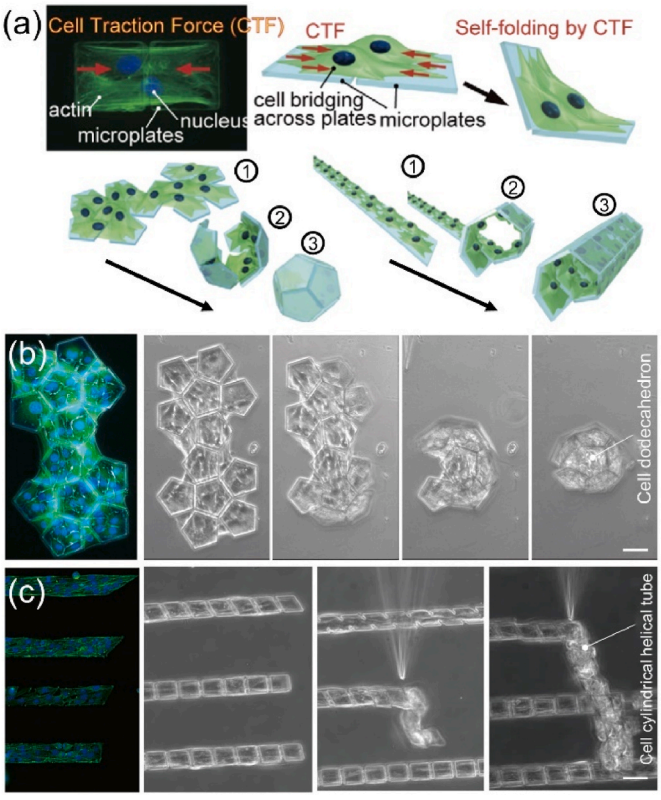

Fig. 12. Cell origami forms cell-laden 3D microstructures.(a) Schematic illustration of CTF and the self-bending and deformation processes. (b, c) Corresponding shape-shifting process of (b) regular dodecahedron and (c) cylindrical tube (scale bar: 50 μm). Reproduced with permission [186]. Licensed under a Creative Commons CC BY license.

6.1. Skin

Skin is arguably the largest human organ and serves many important functions, such as providing a barrier against pathogens, temperature regulation, and control of water evaporation. Skin wounds resulting from diabetes, venous or pressure ulcers, and burns significantly impact thousands of patients each year. Current methods for repairing skin wounds include transplantation of autologous skin, artificial and/or cell engineered skin grafts, and 3D bioprinting. 3D bioprinted cell-laden skin substitutes have been found to accelerate skin regeneration [187]. However, 3D bioprinted skin tissues are static and may have geometric mismatch with complex or irregular skin wounds, which may cause undesirable features at the interacting surface and slow down skin regeneration [188]. To overcome this issue, *in situ* bioprinting has been applied for skin repair and demonstrated encouraging outcomes in animal models [66,188]. 4D bioprinting demonstrates the capability of fabrication of dynamic skin substitutes, which provides a promising approach to skin regeneration. 4D printed skin grafts can change their shape to match the geometry of the skin wounds with better integration and lead to accelerated recovery of wounded skin. Additionally, 4D bioprinting enables the fabrication of dynamic skin tissue models to investigate the dynamic interactions between skin cells and ECM. LAB of (myo)fibroblast was carried out onto collagen matrix to generate an *in vitro* 4D skin models that replicated dynamic features of fibroblast (Fig. 13a–c) [75]. After 5 days of *in vitro* culture, the patterned fibroblasts and myofibroblasts were matured and reorganized into dispersed and aggregated cells, respectively (Fig. 13d). As the collagen was detached from the substrate, the traction force of these two cell patterns would cause different levels of collagen contraction and differentially orient global matrix remodeling (Fig. 13e–h). In addition, the displacement pattern of fluorescent microbeads embedded in collagen 6 h post-printing indicated that fibroblast maturation could also result in anisotropic reorganization of collagen at the microscale [75]. This study showed that the 4D bioprinted dynamic living constructs provide a promising tool to understand the dynamic features of skin and its repair process.

6.2. Bone

Engineering bone tissues is among the common applications of 4D bioprinting, as reviewed previously [23]. 4D bioprinting of bone typically involves the use of SMHs and SMPs and is followed by maturation of the engineered bone scaffolds. For SMHs, the first strategy is to inject the cell-laden SMH ink into the bone defects, where it gels under body temperature. A number of injectable temperature-responsive hydrogels such as PNIPAm [189,190], gelatin [191], collagen [192,193], and chitosan/silk [194], have been used for bone regeneration. Additionally, other responsive hydrogels, such as those responding to NIR or magnetic stimuli, have also been developed for osteoregeneration [195–197]. The second strategy for using SMHs in 4D bioprinting involves directly fabricating dynamic cell-laden bone-like tissues by controlling the gradient of crosslinking within the hydrogel. Fig. 14 shows an example for creating self-folding and cell-laden hydrogels for bone tissue engineering. By controlling the photocrosslinking gradient throughout the thickness of hydrogels, three types of photocrosslinked SMHs exhibited distinct degrees of bending in response to water (Fig. 14a–e). Human MSC-laden OMA formed stable bent structures (Fig. 14f) and maintained high cell viability and proliferation (Fig. 14g and h) during a four-week *in vitro* culture. When cultured in osteogenic medium, the MSCs showed

Table 6
Applications of 4D bioprinting in fabricating different dynamic tissues.

Tissues	4D Bioprinting technologies	Smart material types	Cells	Benefits from 4D bioprinting	Reference
Skin	MEB, LAJ	SMHs	Fibroblast, keratinocytes, HUVECs	Investigating the dynamic interactions between fibroblasts and ECM; shape-changing ability to seamlessly match the complex skin wounds	[75,205]
Bone	MEB, inkjet bioprinting	SMPs, SMHs and SCBs	MSCs, osteoblasts	Shape transformation to improve the integration between the scaffold and the irregular bone defect; contribution to the maturation of neo-bone formation	[80,133, 195–197, 206]
Cartilage	MEB, SLA, DLP	SMHs	MSCs, chondrocytes	Shape changes during *in vitro* culture to form structures recreating the curved and multi-layered structures of native cartilage	[40,70,134, 135]
Vasculature	MEB, SLA, inkjet bioprinting	SMHs	HUVECs, MSCs	Vascular structures with precise control over their diameter and architecture	[37,73,131, 199,207]
Muscle	MEB, MEW	SMPS, SMHs	Myoblasts	Multi-layered and self-scrolling scaffolds with ability to guild the orientation of cells to mimic native muscle tissues	[201,202]
Thin membrane tissues (e.g., cornea, epidermis)	MEB	SMHs	MSCs	Thin membranes with thickness comparable to that of native thin membranous tissue	[128]
Cardiac	MEB, DLP	SMHs, SMPs and SCBs	MSCs, cardiomyocytes	Enabling the production of shape-morphing cardiac patches that match well with the curved topology of the heart; production of dynamic ventricles recapitulating the dynamic motion of native counterparts	[79,203,204]

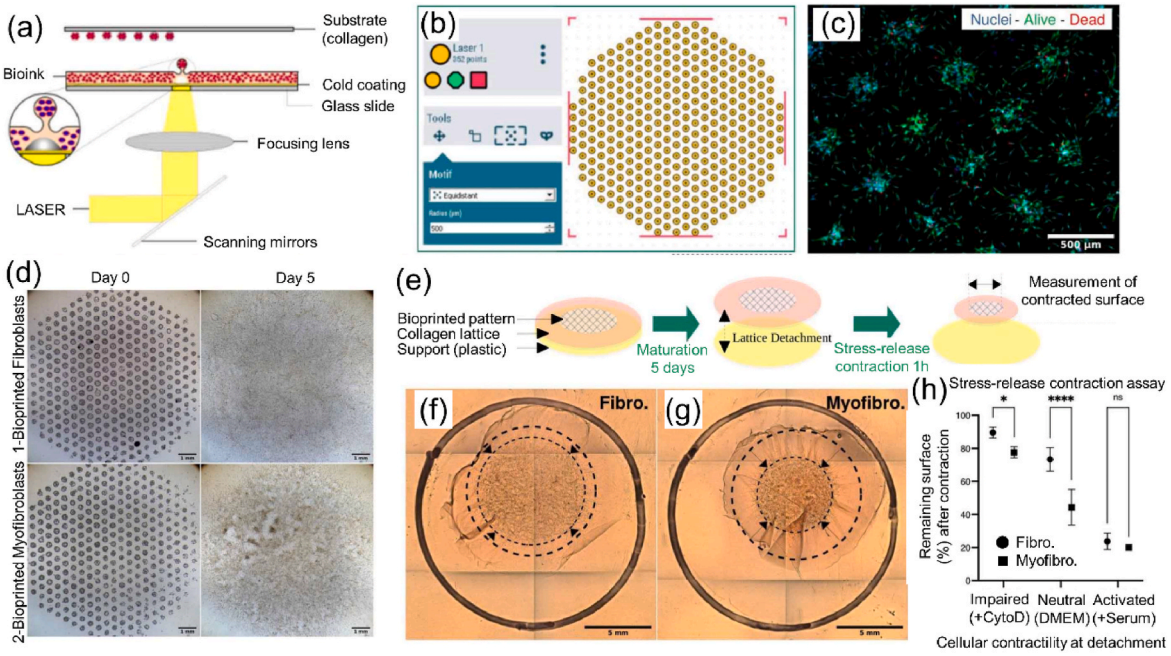

Fig. 13. 4D bioprinting of a dynamic skin tissue model via LAB.(a) Set-up of LAB bioprinter. (b) Cell pattern design using Poietis dedicated software. (c) Live/Dead image of LAB-bioprinted fibroblasts after 2 days on collagen. (d) Maturation of LAB patterns from day 0 to day 5: fibroblasts formed cell layers and myofibroblasts gathered in clusters. (e) Schematic illustration of collagen matrix remodeling or contraction process by the bioprinted (myo)fibroblasts under the cell-induced shear stress. (f, g) Contracted collagen with the bioprinted (f) fibroblasts and (g) myofibroblasts (outer and inner dotted lines indicate the change in collagen lattice size during the contraction process). (h) Contracted surface area as a percentage of original bioprinted surface under different conditions (cytochalasin D (CytoD) used for inhibiting cellular contractility, and DMEM alone or DMEM with 10% serum used for promoting cellular contractility). Reproduced with permission [75]. Copyright 2022, IOP Publishing Ltd.

robust osteogenic differentiation and mineral deposition in the OMA scaffolds (Fig. 14i–k), indicating high potential for bone regeneration applications [133].

For SMPs, they can be 4D printed as shape memory scaffolds that can change their shape to match the irregular bone defects with improved integration, leading to enhanced bone regeneration. For example, Wang's group applied cryogenic 4D printing to process BPN/TCP/PDLLA-*co*-TMC composites into dynamic bone scaffolds. The scaffolds produced could change their shape under NIR radiation to achieve compact integration of the scaffolds in rat cranial bone defects, which speeded up new bone formation [80]. It should be pointed out that these shape memory cell-scaffolds were generated via a post-printing cell seeding strategy. Although the post-printing cell seeding strategy is commonly used and easy to operate, it is a 2D cell seeding technique and often causes non-uniform cell distribution on the scaffolds [177]. In this sense, bioprinting is advantageous in fabricating cell-laden scaffolds with a homogenous distribution of living cells in 3D space. In the near future, cell-encapsulated SMPs are expected to be 4D-bioprinted into cell-laden bone scaffolds to further enhance their bone regeneration capability. For the maturation of 4D bioprinted bone-like constructs, the functional transformation can be affected by several factors. Native bone tissues possess complex hierarchical structures with anisotropic mechanical and electromechanical properties. Therefore, a biomimetic bony microenvironment can be established to promote the biological

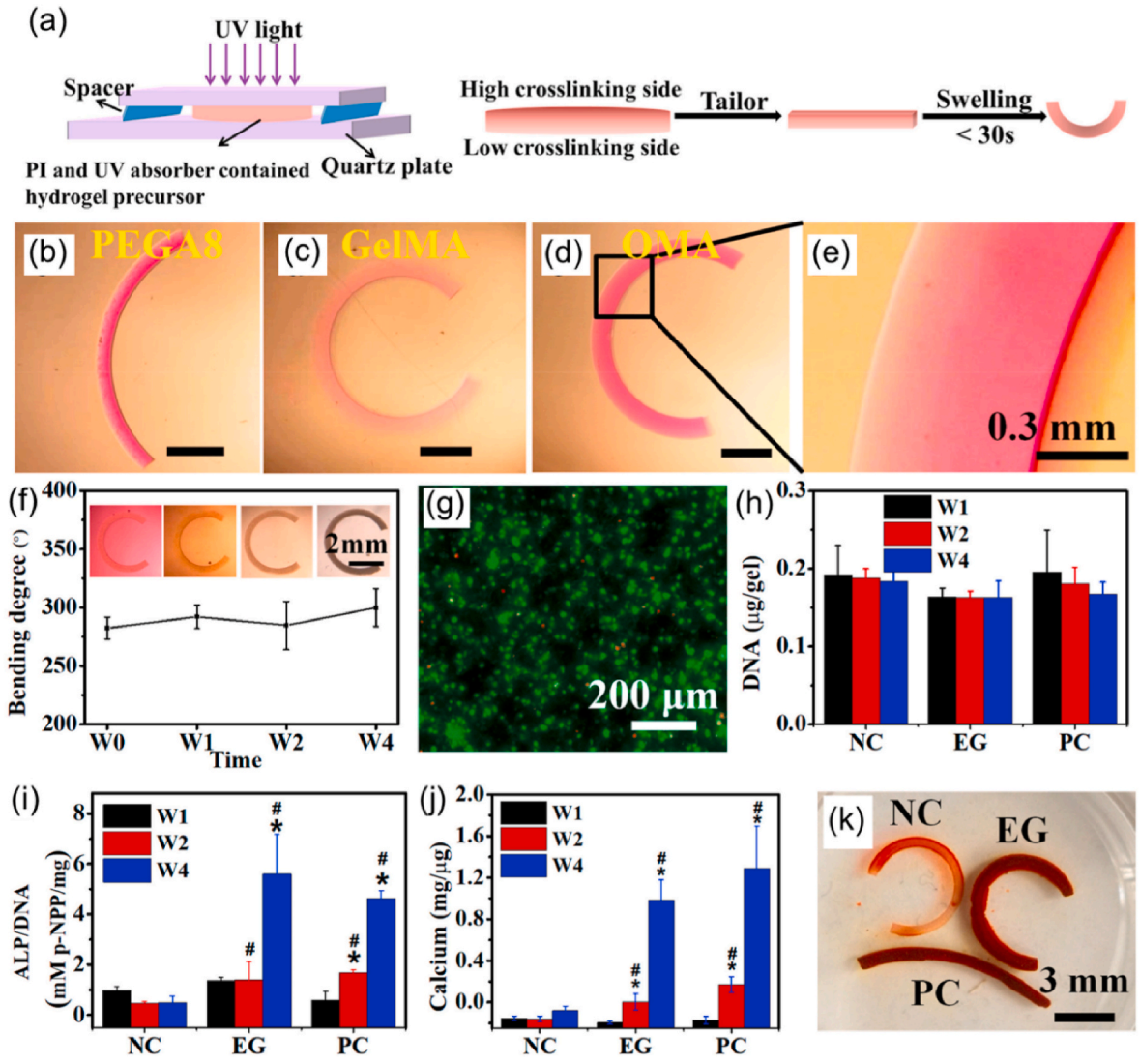

Fig. 14. 4D biofabrication of a crosslinking gradient in cell-laden bone-like tissues. (a) Schematic illustration of the 4D biofabrication process to form structures with different crosslinking degrees on the upper and lower sides: hydrogel precursor containing photocurable polymer, photoinitiator (PI), and UV absorber was placed between two quartz plates, followed by UV irradiation to obtain hydrogels with crosslinking gradient and hence self-bending ability by responding to water. (b–e) Photographs showing bending structures fabricated with different SMHs. (f) Bending degree of the cell-laden OMA structures during 4 weeks of *in vitro* culture in osteogenic medium. (g) An image of Live/Dead staining showing the cell viability after 4-week *in vitro* culture. (h–j) Quantification of (h) DNA content, (i) ALP activity normalized to DNA content, and (j) calcium content normalized to DNA content in the cell-laden hydrogels at varying time points. (k) Alizarin red stained scaffolds after 4-week *in vitro* culture. NC (negative control): cell-laden hydrogels obtained in the presence of a UV absorber and cultured in cell growth medium, EG (experimental group): cell-laden hydrogels obtained in the presence of a UV absorber and cultured in osteogenic medium, PC (positive control): cell-laden hydrogels obtained in the absence of a UV absorber and cultured in osteogenic medium. Reproduced with permission [133]. Licensed under a Creative Commons CC BY license.

functionality of 4D-bioprinted constructs. Moreover, bioactive (e.g., osteogenic growth factors and small molecules) and minerals can be added to enhance cell growth, differentiation, and function and hence facilitate the functional maturation of the neo-bone tissues.

6.3. Cartilage

Several studies have reported the use of 4D bioprinting in fabricating dynamic cartilage tissues. These studies focused on 4D bioprinting of cell-laden scaffolds with self-bending ability, which could improve the integration between the scaffold and native cartilage with curvature and multi-layers, leading to improved cartilage regeneration. In the work by Kim and coworkers, cell-laden scaffolds with self-folding ability were fabricated via DLP, as shown in Fig. 15a [70]. The scaffold was designed as a bilayer configuration with a base layer containing turbinate-derived MSCs (TBMSCs) and a patterned layer containing chondrocytes. UV crosslinking gradient was introduced to these two layers during DLP bioprinting process. Responding to water, the bilayer hydrogel patterns could fold into a tubular structure (Fig. 15b). The 4D bioprinted scaffold was implanted into a damaged trachea of rabbit (Fig. 15c), and the implant well integrated with the host trachea and contributed to the formation of new epithelium and cartilage [70]. In another study, Díaz-Payno and coworkers produced bilayer self-bending, cell-laden scaffolds via extrusion of two inks: tyramine-functionalized hyaluronan (HAT, with a high swelling ratio) and alginate with HAT (AHAT, with a low swelling ratio) containing human MSCs (Fig. 15d) [135]. The dynamic cell-laden scaffolds demonstrated good water-responsive self-bending capabilities, maintained high cell viability, and produced cartilage-like matrix during 28 days of *in vitro* culture in chondrogenic medium (Fig. 15e–g). Alsberg's group carried out two studies on 4D

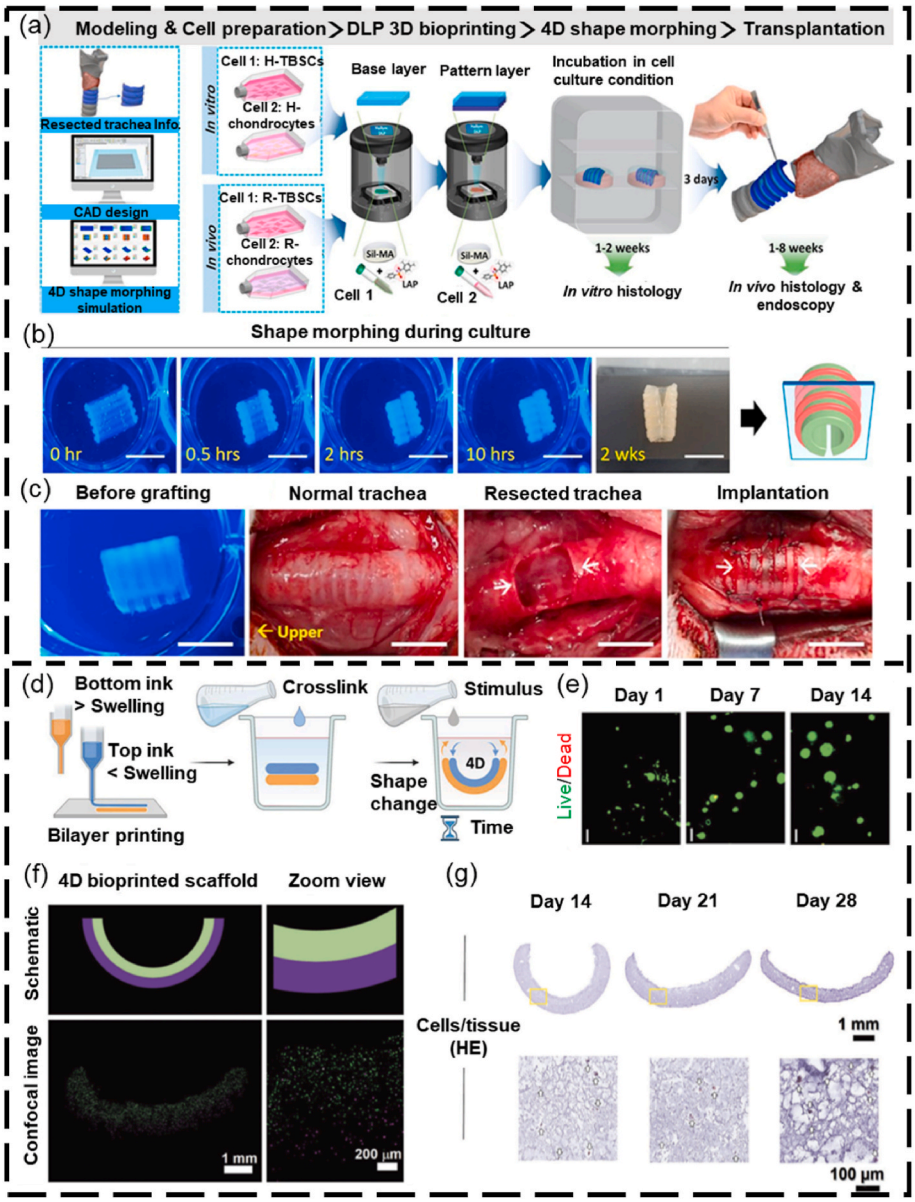

Fig. 15. 4D bioprinting of cartilage tissues.(a–d) DLP of silk-based bilayer bending scaffolds: (a) schematic illustration of the DLP 4D bioprinting process, (b) self-folding process during *in vitro* culture (scale bars = 1 mm), (c) implantation of the 4D bioprinted cell-laden scaffolds for repairing resected trachea. Reproduced with permission [70]. Copyright 2020, Elsevier B.V. (d–g) 4D bioprinting of bilayer cell-laden scaffolds containing a HAT layer and a AHAT layer: (d) schematic of the 4D bioprinting process using these two inks, (e) Live/Dead images of the cell-laden scaffolds at different time points, (f) schematic and confocal images of the bent cell-laden scaffolds, wherein cells in the top AHAT layer were labeled green and those in the bottom AHAT layer labeled purple, (g) representative hematoxylin-eosin staining images of the scaffolds at different time points during culture. Reproduced with permission [135]. Licensed under a Creative Commons CC BY license.

bioprinting of cartilage-like tissues [40,134]. In one study, jammed micro-flake hydrogels of OMA containing hMSCs were printed as different shape-changing scaffolds with vertical crosslinking gradient via MEB. Responding to water, these scaffolds could transform into different 3D morphologies. hMSCs in these printed constructs were differentiated into chondrocytes via *in vitro* culture in chondrogenic medium [40]. In another study, self-bending and cell-laden bilayer structures were fabricated by depositing an OMA/GelMA layer and a hMSCs/OMA microgel layer via MEB to create a crosslinking gradient [134]. The bi-layer scaffolds could change into a "C" shape in the culture medium and the cells underwent condensation and chondrogenic differentiation to form a cartilage-like tissue when the microgels degraded during *in vitro* culture in chondrogenic medium. With degradation of microgel degradation, the deformed cell condensate was released from the shape-morphing layer and became scaffold-free structures [134].

6.4. Vasculature

A variety of vascularized structures have been fabricated via different 3D bioprinting strategies, including scaffold-free cell assembly method, bioprinting constructs with growth factors delivery, direct printing of interconnected channels, indirect printing using sacrificed materials, and co-axial nozzle-assisted bioprinting of vascular tubular structures [198]. Although 3D bioprinting of vasculature has been well-established, it lacks the precision and flexibility for accurate printing of small-diameter and complex vascular structures (e.g., capillary networks) in a controlled manner. 4D bioprinting is a uniquely advantageous technique for creating tubular structures for vasculature, and has been employed to produce a variety of tubular structures with precise control over their diameter and architecture. Ionov's group used MEB to extrude AlgMA or HAMA (AA-MA or HA-MA, respectively, in

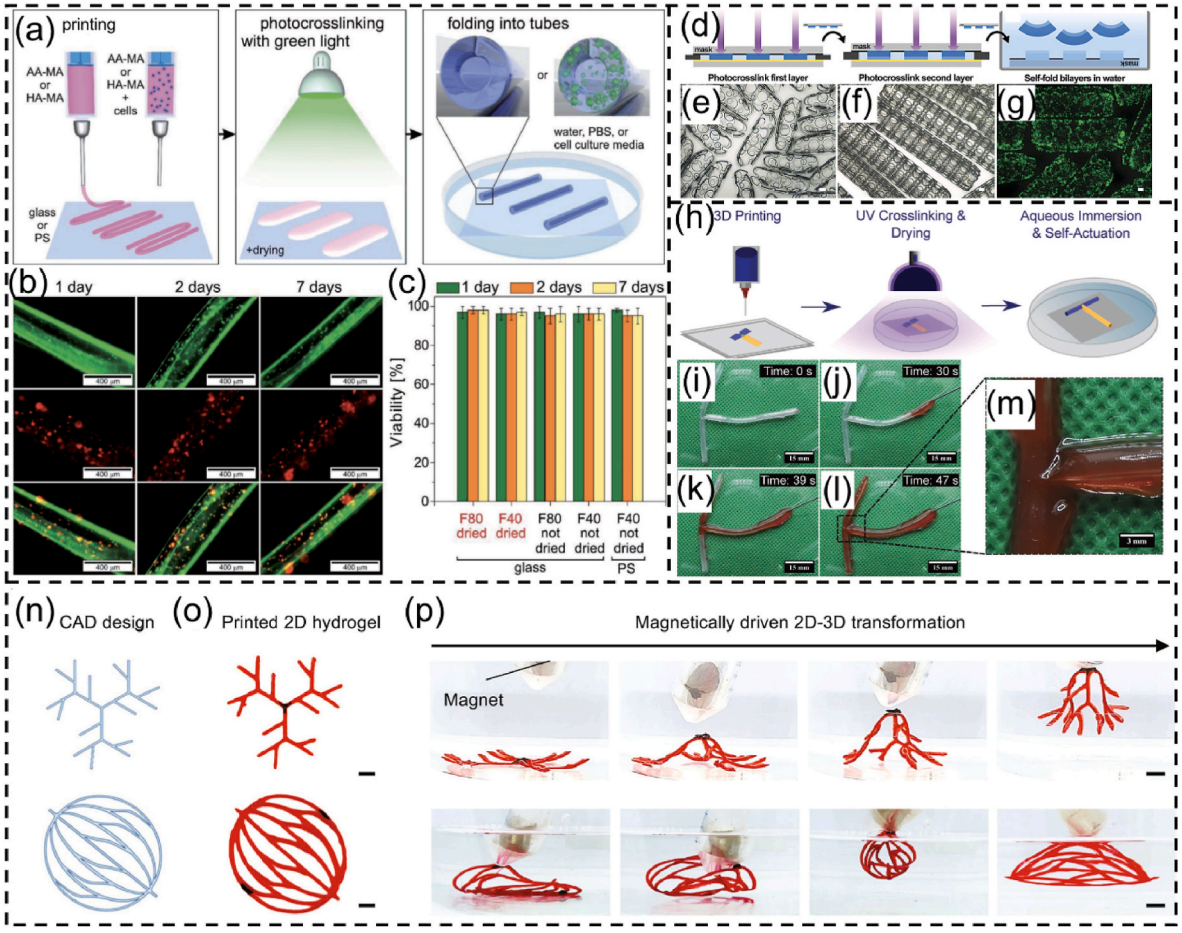

Fig. 16. 4D bioprinting of vascular structures. (a–c) 4D bioprinting of self-folding and cell-laden AlgMA or HAMA: (a) schematic illustration of the printing process, (b) Live/Dead staining images of the cell-laden AlgMA tubes during *in vitro* culture, (c) corresponding quantitative analysis of cell viability. Reproduced with permission [37]. Copyright 2017, Wiley-VCH. (d–g) Self-folding PEGDA bilayer structures: (d) fabrication of the bilayer scaffolds using PEG with different swelling ratio, (e, f) photographs showing the self-folding structures with different micropatterns, (g) cell-laden scaffolds (scale bar: 200 μm). Reproduced with permission [131]. Copyright 2013, Wiley-VCH. (h–m) 4D biofabrication of T-shaped vascular structures: (h) 4D biofabrication process based on a CAD design, (i–m) perfusion of red aqueous solution to the self-tubing T-structure, which showed no signs of leakage. Reproduced with permission [199]. Licensed under a Creative Commons CC BY license. (n–p) 4D printing of branching vascular systems: (n) CAD design, (o) 3D printing based on the design using three kinds of inks, (p) 2D-to-3D transformation to form branching vascular structures driven by magnetic field (scale bar: 1 cm). Reproduced with permission [200]. Licensed under a Creative Commons CC BY license.

Fig. 16a–c) to form 2D membranes with a gradient in crosslinking degree across the thickness of hydrogel sheets (Fig. 16a–c). The 4D bioprinted films could fold into small tubes with internal diameters as low as 20 μm, a dimension comparable to the smallest blood vessels in the human body. The cells exhibited high viability during a one-week *in vitro* culture period [37]. In the study by Gracias's group, self-tubing scaffolds with different microstructures were developed by designing a bilayer structure consisting of two types of PEGDA with different molecular weights (Fig. 16d–g) [131]. After UV crosslinking, the PEGDA bilayer structures possessed different swelling ratios across the thickness direction and could fold into microtubes with different microstructures by responding to water [131]. Despite the advancement in 4D bioprinting of hydrogel-based tubular structures, there are still challenges such as leakage and cracking along the tube walls, a lack of integrity, and difficulties in fabricating tubular branching networks [137,139,199]. One way to mitigate the leakage issue of simple tubular structures is to produce self-folding structures with overlapping areas [139]. For vascular bifurcations, complex CAD models need to be carefully designed to avoid leakage. For example, in the work by Ionov's group, alginate di-aldehyde (ADA) was printed as a 2D pattern based on a complex CAD model [199]. This 2D pattern could fold into a T-shape vascular tube with sealed junctions by responding to water. By visualizing red aqueous solution injected into the T-tubes, little leakage was observed at a maximum flow velocity of 0.11 m s^{-1} (Fig. 16h– m). HUVECs perfused into the tubes showed good attachment and growth, showing high potential for the production of self-tubing vascular bifurcations [199]. Furthermore, Stevens's group developed a magnetic-driven 4D printing strategy to achieve complex branching 3D vascular structures [200]. In their strategy (Fig. 16n–p), the designed 2D patterns were fabricated via MEB using three kinds of inks: 1) an ink composed of gelatin as the main scaffold material, 2) a magnetic ink composed of iron oxide particles and gelatin, and 3) a gravity ink composed of calcium carbonate and gelatin. After printing, the 2D patterns were immersed in a matrix bath and were transformed into 3D branching vascular structures when a magnetic field was applied. The 3D deformed structures could be maintained under the combined buoyancy, gravity, and magnetic forces until the matrix material was fully crosslinked and solidified. Finally, the transformed gelatin-based vasculature could be removed to obtain a hollow vasculature network within a matrix material [200].

6.5. Other tissues

4D bioprinting provides a promising and powerful technique to construct a variety of other tissues and organs, such as muscle, and heart. For instance, Ionov's group produced multilayer self-scroll

structures incorporated with myoblasts through combining MEB and melt-electrowriting (MEW) (Fig. 17a–c) [201,202]. A photo-crosslinkbale hydrogel (AlgMA or HAMA) was first extruded to form the solid hydrogel film, which was followed by MEW of a synthetic polymer (PCL or PCL/PU) fiber pattern onto the hydrogel film. These bilayer structures could scroll upon exposure to water. Myoblasts cultured inside the scrolled scaffolds showed high viability and a high degree of cell orientation along the polymer fibers, showing great potential for muscle

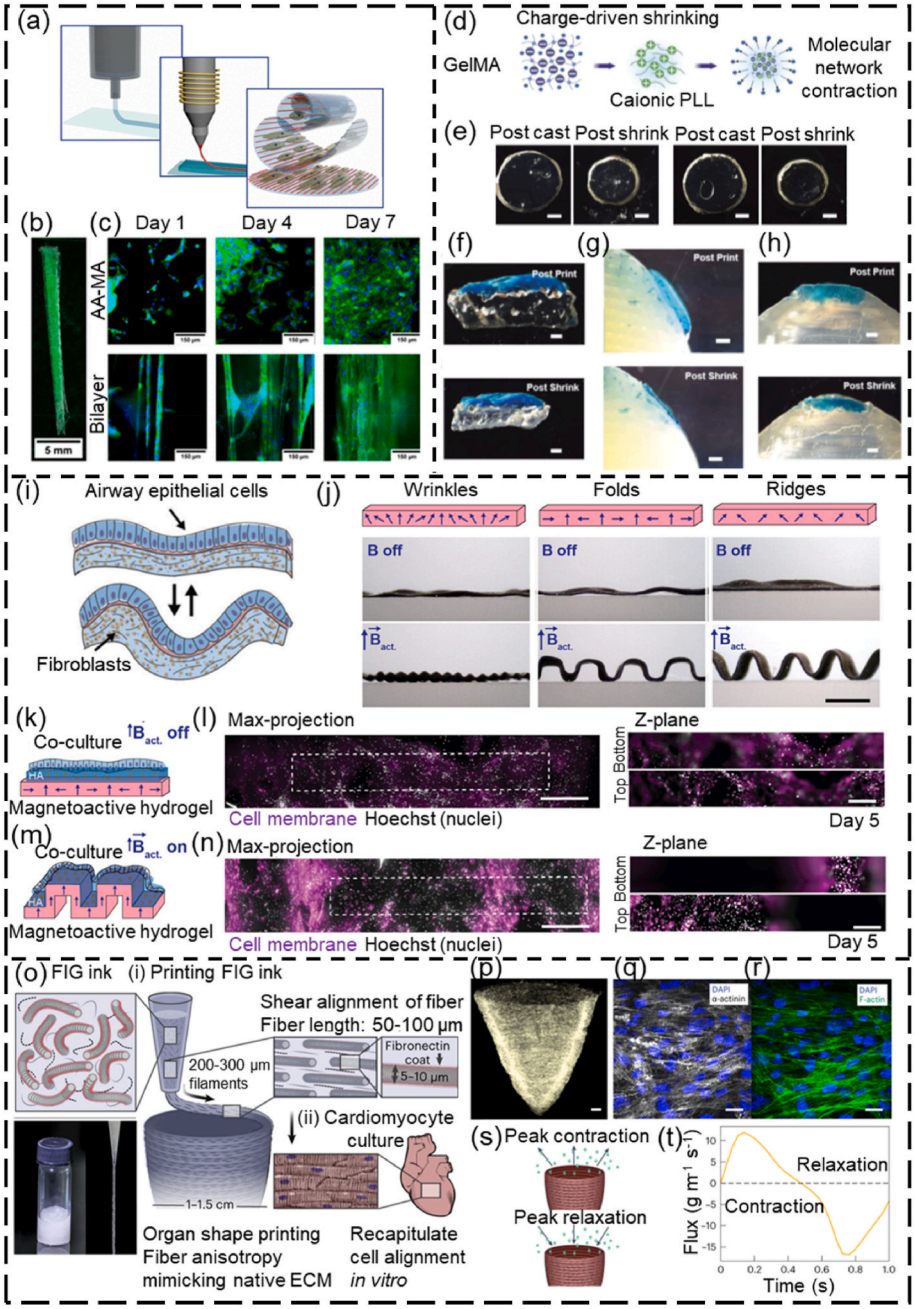

Fig. 17. 4D biofabrication of other tissues. (a–c) Self-scrolled muscle scaffolds: (a) schematic of the fabrication process combining MEB and MEW, (b) a self-folded tube with cells (green) stained with calcein, (c) actin (green) and nuclei (blue) staining for AA-MA (AlgMA) hydrogels and printed bilayer scaffolds (Bilayer). Reproduced with permission [201]. Copyright 2021, American Chemical Society. (d–h) Self-shrinking thin membranes fabrication for regeneration of thin membranous tissues: (d) schematic depicting the shrinking process induced by charge attraction of negatively charged GelMA and positively charged PLL, (e) photographs showing the shrinking behavior of cast GelMA hydrogels before and after shrinking by immersion in different PLL solutions, (f–h) post-printing and post-shrinking morphology of GelMA on the surface of (f) 4% gelatin/1% alginate, (g) PCL and (h) 10% GelMA. (Scale bar = 1 mm). Reproduced with permission [128]. Copyright 2023, Wiley-VCH. (i–n) 4D biofabrication of magnetic field-driven folding structures mimicking the native tissue folding: (i) schematic illustration of the change of the airway epithelium cells and fibroblasts in relaxed and constricted states (j) different folding patterns (i.e., wrinkles, folds, and ridges), of the bilayer hydrogels by applying a magnetic field, (k) schematic and (l) fluorescent images of cell-laden hydrogels in static mode after 5 days of co-culture, (m) schematic and (n) fluorescent images of cell-laden hydrogels in actuation mode after 5 days co-culture (scale bar = 200 μm). Reproduced with permission [136]. Licensed under a Creative Commons CC BY license. (o–t) 4D printing of fiber-infused ventricles with cyclic contractility: (o) schematic illustration of 4D printing of ventricles using the FIG ink, (p) microcomputed tomography image of a printed ventricle (scale bar = 1 mm), (q, r) immunostaining images showing alignment of the cardiomyocytes (scale bar = 20 μm), (s) schematic illustration of microparticles flowing in and out of ventricle models at the peak contraction and peak relaxion, (t) a representative cycle of contraction and relaxation. Reproduced with permission [204]. Copyright 2023, Springer Nature.

tissue regeneration [201,202]. McLoughlin and colleagues used 4D bioprinting to fabricate thin membranes using anionic GelMA and cationic poly-L-lysine (PLL) (Fig. 17d–h) [128]. After bioprinting, the charge attraction between the GelMA and PLL caused the microscale network to collapse and the macroscale hydrogel to shrink. This resulted in the formation of extremely thin membranes with a thickness as low as 65 μm, showing great potential for regenerating thin membranous tissues such as the cornea, epidermis, and periosteum [128]. Roy and coworkers developed cell-laden bilayer folding hydrogels with a HAMA layer atop an alginate/polyacrylamide double-network (DN) hydrogel layer (Fig. 17i–n) [136]. Fibroblasts, embedded in the HAMA hydrogel, were observed to facilitate the formation of a folded pseudostratified monolayer of human bronchial epithelial cells seeded on the HAMA surface. Using NdFeB magnetic microparticles, the bilayer hydrogels showed reversible and cyclical folding motions upon the application of a magnetic field (Fig. 17j), which mimicked the regular relaxation and contraction of native tissues and provided a promising dynamic system in investigating the effect of biomimicking dynamic folding on the cellular functions *in vitro* (Fig. 17k–n) [136]. Zhang's group applied 4D printing technologies to process different SMPs [i.e., graphene/bisphenol A diglycidyl ether (GRA/BADE) or PLA] into cardiac patches that could change their shape to closely match the curvature structures of native heart [79,203]. GRA/BADE cardiac patches were fabricated via a DLP-printed PEGDA mold and could change their curvature remotely under NIR-light stimulus [203]. PLA cardiac scaffolds were printed via FDM and exhibited shape transformation at a temperature close to the physiological temperature [79]. Human-iPSCs-derived cardiomyocytes were seeded to these SMPs scaffolds and showed excellent myocardial maturation, indicating promising potential applications of these scaffolds in myocardial regeneration [79,203]. Choi and coworkers developed fiber-infused gel (FIG) inks composed of gelatin fibers, gelatin, and alginate, which were then extruded to generate ventricles via MEB (Fig. 17o, p) [204]. The shear stress exerted on the fibers during extrusion resulted in their alignment along the printing direction, providing microscale geometric cues that promoted the self-alignment of seeded human cardiomyocytes into anisotropic muscular tissues *in vitro* (Fig. 17q, r). Such anisotropic ventricles produced cellular contraction forces that led to the spontaneous cyclic contraction of the

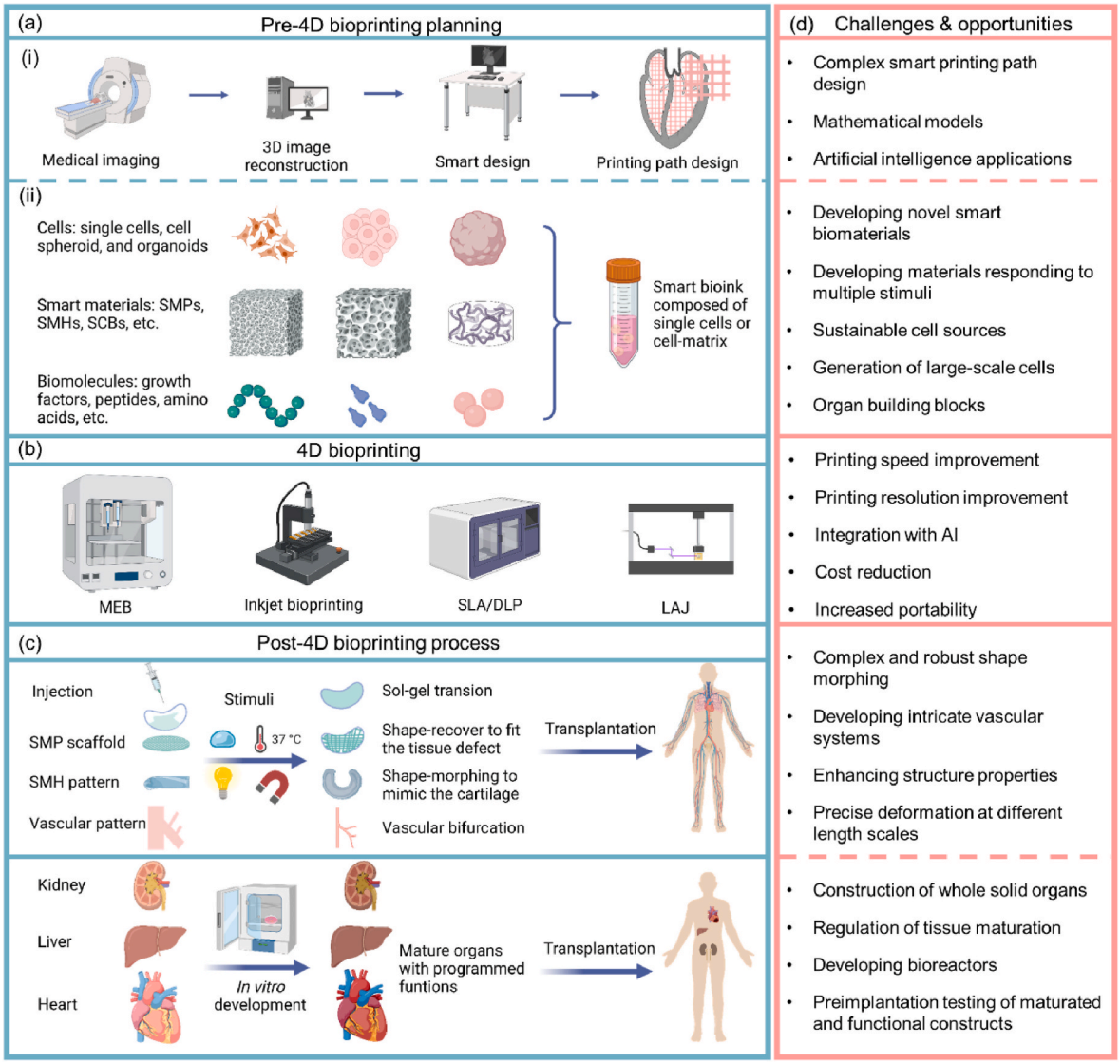

Fig. 18. Challenges and opportunities in the development of 4D bioprinted dynamic tissues and organs. (a) (i) Smart path design based on medical imaging, 3D reconstruction, and CAD design, (ii) smart bioink preparation based on the target tissues/organs, involving cell selection, material selection, and biomolecules. (b) 4D bioprinting process using different bioprinting technologies, carried out based on smart design and bioink. (c) Post-4D bioprinting process, including the shape-morphing process under suitable stimuli, *in vitro* development for tissue maturation, and the transplantation of tissues and organs into patients with tissue/organ dysfunction and failure. (d) Challenges and opportunities in the future development of 4D bioprinting.

printed ventricles (Fig. 17s, t), mimicking the contraction of native cardiac tissues [204]. While the above studies showed encouraging achievements of 4D bioprinting in creating artificial tissues and organs, it is still challenging to produce a whole solid organ (e.g., liver, kidney, and heart) due to issues such as complicated architectures, multiple cellular types, and complex vascular networks.

7. Challenges and outlook

As an emerging biofabrication technique, 4D bioprinting can produce dynamic, living constructs with unprecedented precision and control and is poised to significantly advance our capability to create dynamic tissues that closely mimic native tissues and organs. Fig. 18 illustrates the practical steps for 4D bioprinting of tissues and organs and the relevant areas for improvement. 4D bioprinting typically includes three principal steps: (1) pre-4D bioprinting design, including the 4D bioprinting path design and smart bioink preparation/development; (2) 4D biofabrication of the designed constructs by using a proper bioprinter; and (3) post-4D bioprinting processing, including stimuli-induced shape change and maturation of the tissues and organs. Ultimately, 4D bioprinting will have the capability to generate functional constructs suitable for transplantation into patients, with the aim of regenerating damaged or failing tissues and organs and addressing the pressing issue of organ shortage. Although 4D bioprinting has been used to successfully create a variety of simple dynamic living constructs, this biotechnology is still in its infancy and faces significant challenges before its full potential can be realized. Most of the challenges facing the 4D bioprinting field are related to smart designs, smart bioinks, bioprinting technologies, and post-4D bioprinting processes, which are further elaborated as follows. We also discuss highly promising future applications of 4D bioprinting.

Smart design. Designing printing paths for 4D bioprinting is more complex than for 3D bioprinting due to the inclusion of dynamic features. In 3D bioprinting, the printing path can be designed based on medical imaging, image reconstruction, CAD design, and data slicing. In 4D bioprinting, the inclusion of dynamic features requires a holistic consideration of time-dependent changes and influences of cells on shape, properties, and function after deployment, which greatly complicates the path design. To date, many mathematical models and FEA have been used to successfully predict the shape transformation of 4D bioprinted constructs based on bioink properties and printing path. However, it is more difficult and challenging to design printing paths based on the final desired shape, which lags far behind. Nevertheless, several mathematical models have been applied to guide printing path design for programming shape-shifting processes. Humidity-triggered shape-morphing behaviors of SMHs can be predicted using the mathematic models derived from the Timoshenko bimetal model based on the material properties and printing path [155], as mentioned in section 4.4. On the other hand, these Timoshenko-based models can also be used to design or find the printing path for the target 3D shape. For example, Gladman and coworkers generalized and applied the classical Timoshenko equation to translate the complex target 3D structure into a bilayer printing path for MEB by using the parameters of the local curvatures, swelling ratio, elastic constants, and height and size of the structure [35]. In another study, Cui and co-workers modified and simplified the Timoshenko bending model to make it suitable for inkjet 4D bioprinting [73]. This model could provide droplet distribution of a two-layered printing path by giving the parameters of bending diameter, thickness of the bilayer structures, as well as swelling ratios and Young's moduli of two materials that are ejected to form the first and second layer [73]. However, Timoshenko-based bending models are limited to two-layered printing path design of humidity-responsive materials and unsuitable for guiding the path design for other stimuli-responsive materials and more complex constructs. To improve the applicability and efficiency of mathematical models in inverse printing path design, some optimization algorithms such as topology optimization and evaluation algorithms have recently been integrated with the forward predictive models (e.g., FEA) for designing specific shape deformation. For example, Qi's group combined FEA and evaluation algorithms to solve the voxel-based inverse printing path design problem for specific shape-morphing behaviors [158,208]. The generated and optimized voxel-based material distribution could be converted to grayscale slices for DLP 4D printing. However, the FEA-combined evaluation algorithm is computationally time-consuming and could not process highly complex final desired shapes. To overcome these issues, Qi and colleagues integrated an FEA-trained machine learning model with evaluation algorithms to improve the printing path design capability and optimization efficiency of the targe shape change, as detailed in Fig. 11 [159]. However, the FEA-combined evaluation algorithm only succeeded in designing the smart material beams with two smart materials, and its applications in designing shape-morphing material beams with more than two material phases and in designing more complex 3D deformation structures still need further exploration. Nevertheless, AI is undergoing rapid development and is expected to greatly improve our ability to design 4D printing paths for complex targe shape changes in the near future.

Smart bioinks. The preparation and development of smart bioinks is of crucial importance in 4D bioprinting. Bioinks generally are composed of smart biomaterials, living cells, and/or biomolecules. However, current smart biomaterials with good shape-morphing ability and sufficient biocompatibility are limited to some natural SMHs. Moreover, most of the current smart materials are only responsive to a single or two stimuli, which may be insufficient to meet the requirements of complex environments in the human body. Therefore, it is urgent to develop new smart biomaterials with improved performance for 4D bioprinting. Several solutions can be adopted to quickly expand the smart biomaterials pool for 4D bioprinting. First, suitable biomaterials can be selected from the existing materials pool of 3D bioprinting and modified to extend their use to 4D bioprinting. A large number of biomaterials have been developed for 3D bioprinting and some can be adapted for 4D bioprinting by introducing stimuli-responsive features via different strategies, such as incorporating magnetic nanoparticles or combining them with stimuli-responsive materials. For example, decellularized extracellular matrix (dECM) derived from native tissues generally has high biocompatibility and is commonly used in 3D bioprinting [5, 209–214]. However, these materials' stimuli-responsive features are not yet well defined and their applications in 4D bioprinting require further exploration. The second solution is to improve the performance of currently available smart biomaterials, such as alginate, GelMA, silk, and HAMA, via physical, chemical, and biological modifications or compositing with inorganic materials to make them wider applications for 4D bioprinting. The third solution is to develop new smart biomaterials according to the bioink requirements in 4D bioprinting with a guiding strategy, such as biomimicry, to produce materials with appropriate stimuli-responsiveness and biological activity.

Besides smart biomaterials, living cells are another key component in the preparation of smart bioinks. As mentioned earlier, cell viability, density, cell-cell interactions, and cell-matrix interactions are key issues that must be comprehensively considered for successful 4D bioprinting. The cell density in previously bioprinted living constructs was not comparable to that of native tissues and organs, and using a higher density of living cells to create a solid organ on a physiologically relevant scale is still very challenging. The influence of living cells on the transformation of shape, property, and function of 4D bioprinted should also be noted and carefully considered. OBBs made of multicellular spheroids and organoids have emerged as appealing candidates for engineering functional human tissues, but their limitations include poor printability and structural integrity when used in bioprinting.

Bioprinting technologies. With more than two decades of development, bioprinting technologies are capable of fabricating relatively simple or small-scale complex 3D living constructs with controlled geometry and satisfactory precision. However, further advancement,

particularly in printing speed and resolution, is necessary to extend the applications of these printing technologies. Currently, it still takes hours to fabricate relatively small and simple 3D constructs by bioprinting technologies, which does not meet the demand of fabricating clinically relevant tissues and organs in a shorter time. The printing speed of additive manufacturing is generally limited to its inherent layer-by-layer manufacturing process. Many strategies have been developed to improve the printing speed of different printing technologies. For example, by solidifying multiple layers via the use of several light-sources to create the intersecting points within the liquid, volumetric printing has been developed, which allows us to complete a centimeter-scale object within a few minutes [215,216]. While this volumetric printing has been successfully applied in 3D bioprinting [217,218], its feasibility in 4D printing/bioprinting still needs investigation.

A sufficient printing resolution is required for building accurate structures for achieving programmable shape/functional transformations at different scale levels. Also, high printing resolution is critical because the architectures of native tissues vary widely, ranging from millimeter to nanometer scales. However, there is usually a trade-off between printing resolution and printing speed: an increase in printing speed often decreases the printing resolution. Therefore, these two parameters must be balanced based on the prepared bioink, bioprinter type, and target biomedical applications. With the rapid development of AI, it is exciting and promising to continue exploring the integration of AI into current bioprinting technologies [219–224]. Future AI-integrated 4D bioprinting holds promise in greatly improving the printing efficiency and product quality. Moreover, combining bioprinting technologies with other manufacturing technologies (e.g., electrospinning) should be further explored to fabricate high-quality hybrid structures with desired 4D effects [202,225,226].

Finally, future development in 4D bioprinting technology should also address challenges such as the difficulty in bioprinting cell aggregates, the high equipment cost, and the need for improved portability.

Post-4D bioprinting process. Post-4D bioprinting process involves programed shape-transformation and/or maturation of the bioprinted tissues and organs. Although 4D bioprinting has been used to fabricate various 4D constructs, most of the constructs display simple geometry with low precision. Such simple geometries are insufficient to replicate the highly irregular structure of tissue defects, and the low precision cannot ensure accurate 3D deformation of the 4D constructs during the post-4D bioprinting development. As a result, these 4D bioprinted constructs with simple shape-morphing behavior struggle to achieve complicated 3D deformation needed to mimic the irregular geometry of native tissues. For example, single tubular structures or branching tubular structures have been achieved, but dynamic structures that can change their shape to resemble native complex vascular networks are difficult to create. Besides, 4D bioprinting of dynamic constructs that imitate the regular and cyclic motion (e.g., relaxation and contraction) of native tissues is still challenging. In many cases, the mechanical properties of 4D bioprinted scaffolds still don't match those of native tissues and organs. For example, while researchers have generated self-bending, cartilage-mimicking living constructs [134,135], the mechanical properties of these dynamic scaffolds are not comparable to those of native cartilage. Some shape memory scaffolds exhibited sufficient mechanical properties for cartilage regeneration [120,227], but they cannot directly load living cells during manufacturing process due to some reasons such as hazardous printing environment and post-printing shape programming process. The maturation of engineered tissues and organs can be facilitated by regulating factors such as cell patterning, gene expression, and matrix deposition. Advances in cellular engineering, gene therapy, and cell therapy will contribute to the development of more specific and/or complex programmable biological functions. While bioprinting has been employed to create organs such as kidney, liver, and heart [65,228–231], bioprinting of whole solid organs, especially those with programmable motions and functions, remains a significant challenge [232]. Such endeavors face many obstacles, such as the integration of a complete vascular network, the inclusion of large cell populations, and the creation of structures that accurately mimic the organ's architecture at the macro-, micro-, and nano-scale. Therefore, there is still a long way to go before the clinical applications of 4D dynamic tissues and organs become a practical reality.

Perspectives on future applications. The development of 4D bioprinting continues to broaden the applications of this cutting-edge technology in basic research, pharmaceutics, tissue engineering, and precision medicine (Fig. 19) [24,28,75]. For basic research, 4D bioprinted constructs provide a new, versatile tool for investigating the dynamic interplay between cells, cell aggregates, and the extracellular matrix, the role of these interactions in tissue development, repair and regeneration, and the relevant roles of dynamic features of cellular growth and functions. With the incorporation of dynamic features, 4D bioprinted tissue models can more accurately replicate native cellular environments, leading to enhanced predictive power of engineered tissue/organ models, such as organoids and organs-on-chips, in preclinical drug development and thereby increasing the success rate in clinical trials [233–236]. In addition, 4D bioprinted drug delivery systems can release drugs at target tissue sites in a more controllable and precise manner in response to external stimuli, resulting in improved therapeutic outcomes [126,237]. Moving towards next-stage applications in tissue engineering, *in situ* 4D bioprinting will be used more widely to directly deposit smart bioinks into the sites of damaged tissues to improve implant integration and tissue repair [238]. While previous studies mostly focus on scaffold-based 4D bioprinting, scaffold-free 4D bioprinting has rarely been reported and warrants further exploration. Finally, 4D bioprinting is believed to fuel the development of precision medicine. 4D bioprinting is a versatile tool for fabricating personalized, dynamic constructs that incorporate patient-specific (autologous) cells. Such engineered tissues/organs can be employed to investigate pathological mechanisms specific to individual patients/patient populations, evaluate the safety and efficacy of pharmaceutics in an individualized manner, and ultimately restore functions of diseased body parts via patient-tailored regenerative strategies.

8. Conclusions

This review presents an overview of 4D bioprinting and its application in constructing different dynamic tissues. As an innovative and versatile fabrication technique that integrates 3D bioprinting with time as the fourth dimension, 4D bioprinting enables the creation of programmed dynamic living constructs. Previous studies have demonstrated various 4D effects achieved via shape transformation or stimuli-guided functional maturation of the bioprinted constructs manufactured using extrusion-based bioprinting, inkjet bioprinting, SLA, DLP, and LAB. Promising smart materials for 4D bioprinting include SMPs, SMHs, and their composites. Smart design is another crucial component of 4D bioprinting, allowing strategic allocation of smart materials to program the shape and/or functionality of dynamic constructs in a controlled manner. 4D bioprinting has been successfully applied to create various dynamic tissues and organs, such as skin, bone, cartilage, vasculature, and muscle. Despite being in its early stages and facing significant challenges, 4D bioprinting holds great promise for opening new avenues for biofabrication, tissue engineering, regenerative medicine, drug delivery, and personalized medicine.

Ethics approval and consent to participate

The manuscript is a review article. The authors declare that no experimentation on human or animals was conducted.

CRediT authorship contribution statement

Jiahui Lai: Writing – original draft, Investigation, Conceptualization, Writing – review & editing. **Yuwei Liu:** Funding acquisition,

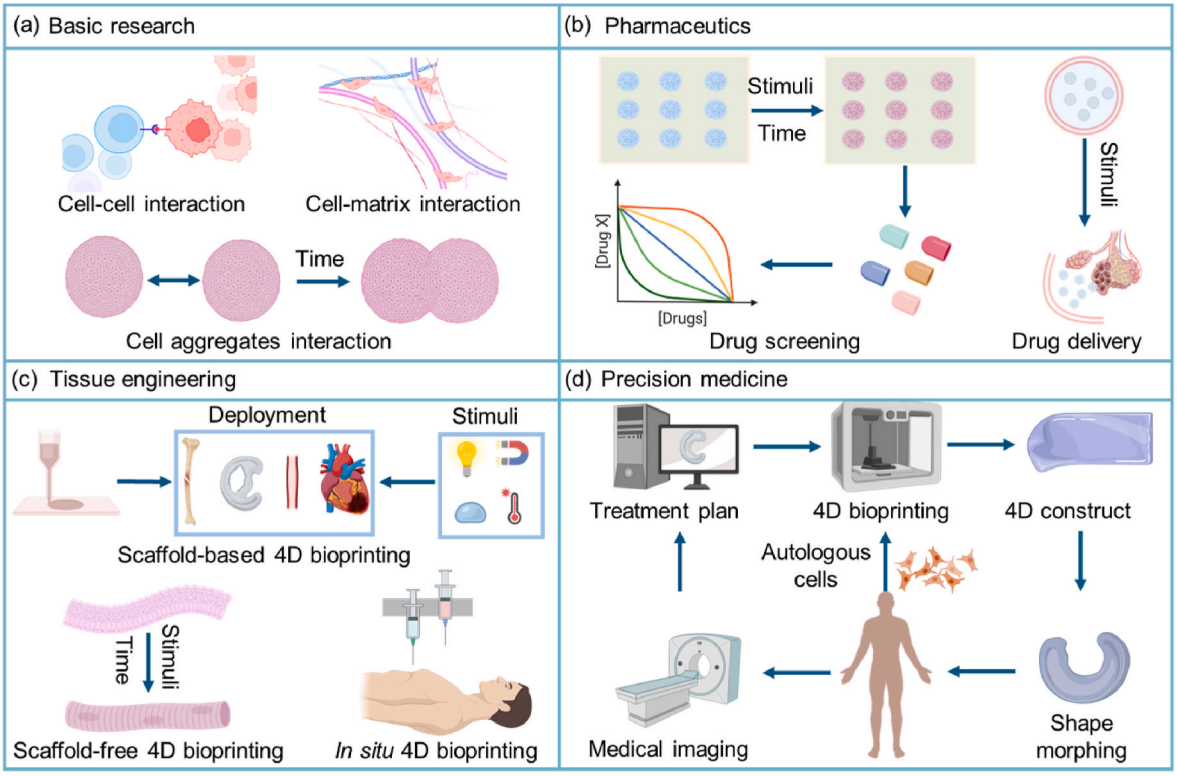

Fig. 19. Emerging applications of 4D bioprinting in different fields These fields include (a) basic research, (b) pharmaceutics, (c) tissue engineering, and (d) precision medicine.

Writing – review & editing. **Gang Lu:** Funding acquisition, Writing – review & editing. **Patrick Yung:** Funding acquisition, Writing – review & editing. **Xiaoying Wang:** Writing – review & editing. **Rocky S. Tuan:** Writing – review & editing, Supervision, Investigation, Funding acquisition. **Zhong Alan Li:** Writing – review & editing, Supervision, Investigation, Funding acquisition.

Declaration of Competing interest

There is no conflict of interest to declare.

Acknowledgements

ZAL acknowledges the support from CUHK's Vice-Chancellor Early Career Professorship Scheme and CUHK Research Committee (via Direct Grant for Research 2022/2023, 4055182). RST is supported by the Lee Quo Wei and Lee Yik Hoi Lun Professorship in Tissue Engineering and Regenerative Medicine of CUHK. This work was supported by the Center for Neuromusculoskeletal Restorative Medicine (to RST, ZAL, GL, and PSY), under the Health@InnoHK program launched by the Innovation and Technology Commission, the Government of the Hong Kong SAR of the People's Republic of China, the National Natural Science Foundation of China (to ZAL, 82302753), the Research Grants Council of Hong Kong SAR of the People's Republic of China (to ZAL, 24203523). YL received funding support from the Shenzhen Science and Technology Project (JCYJ20210324102815040).

References

[1] C.W. Hull, Apparatus for Production of Three-Dimensional Objects by Stereolithography, US, 1986.
[2] J. Lai, C. Wang, M. Wang, 3D printing in biomedical engineering: processes, materials, and applications, Appl. Phys. Rev. 8 (2) (2021) 021322.
[3] T.D. Ngo, A. Kashani, G. Imbalzano, K.T.Q. Nguyen, D. Hui, Additive manufacturing (3D printing): a review of materials, methods, applications and challenges, Compos. B Eng. 143 (2018) 172–196.
[4] A. Atala, Introduction: 3D printing for biomaterials, Chem. Rev. 120 (19) (2020) 10545–10546.
[5] B.S. Kim, S. Das, J. Jang, D.W. Cho, Decellularized extracellular matrix-based bioinks for engineering tissue- and organ-specific microenvironments, Chem. Rev. 120 (19) (2020) 10608–10661.
[6] C. Mota, S. Camarero-Espinosa, M.B. Baker, P. Wieringa, L. Moroni, Bioprinting: from tissue and organ development to in vitro models, Chem. Rev. 120 (19) (2020) 10547–10607.
[7] R. Gordan, J.K. Gwathmey, L.H. Xie, Autonomic and endocrine control of cardiovascular function, World J. Cardiol. 7 (4) (2015) 204–214.
[8] D. Echeverri, F.R. Montes, M. Cabrera, A. Galán, A. Prieto, Caffeine's vascular mechanisms of action, Int. J. Vasc. Med. 2010 (2010) 834060.
[9] A. Ahmad, S.K. Dempsey, Z. Daneva, M. Azam, N. Li, P.L. Li, J.K. Ritter, Role of nitric oxide in the cardiovascular and Renal systems, Int. J. Mol. Sci. 19 (9) (2018) 2605.
[10] S. Tibbits, The emergence of "4D printing". TED Conference, 2013.
[11] S. Tibbits, 4D printing: multi-material shape change, Architect. Des 84 (1) (2014) 116–121.
[12] X. Kuang, D.J. Roach, J. Wu, C.M. Hamel, Z. Ding, T. Wang, M.L. Dunn, H.J. Qi, Advances in 4D Printing: materials and applications, Adv. Funct. Mater. 29 (2) (2019) 1805290.
[13] Z.X. Khoo, J.E.M. Teoh, Y. Liu, C.K. Chua, S. Yang, J. An, K.F. Leong, W.Y. Yeong, 3D printing of smart materials: a review on recent progresses in 4D printing, Virtual Phys. Prototyp. 10 (3) (2015) 103–122.
[14] J. Choi, O.C. Kwon, W. Jo, H.J. Lee, M.W. Moon, 4D printing technology: a review, 3D Print. Addit. Manuf. 2 (4) (2015) 159–167.
[15] S. Miao, N. Castro, M. Nowicki, L. Xia, H. Cui, X. Zhou, W. Zhu, S.j. Lee, K. Sarkar, G. Vozzi, Y. Tabata, J. Fisher, L.G. Zhang, 4D printing of polymeric materials for tissue and organ regeneration, Mater. Today 20 (10) (2017) 577–591.
[16] W. Zhao, C. Yue, L. Liu, Y. Liu, J. Leng, Research progress of shape memory polymer and 4D printing in biomedical application, Adv. Healthc. Mater. 12 (16) (2023) 2201975.
[17] Y. Wang, H. Cui, T. Esworthy, D. Mei, Y. Wang, L.G. Zhang, Emerging 4D printing strategies for next-generation tissue regeneration and medical devices, Adv. Mater. 34 (20) (2022) 2109198.
[18] A.B. Dababneh, I.T. Ozbolat, Bioprinting technology: a current state-of-the-art review, J. Manuf. Sci. Eng. 136 (6) (2014) 061016.
[19] V. Mironov, 4D Bioprinting: biofabrication of rod-like and tubular tissue engineered constructs using programmable self-folding bioprinted biomaterials, International Bioprinting Congress (2014) 24–25.
[20] S. Wang, J.M. Lee, W.Y. Yeong, Smart hydrogels for 3D bioprinting, Int. J. Bioprinting 1 (1) (2015).
[21] J. An, C.K. Chua, V. Mironov, A perspective on 4D bioprinting, Int. J. Bioprinting 2 (1) (2016).

[22] S.V. Murphy, P. De Coppi, A. Atala, Opportunities and challenges of translational 3D bioprinting, Nat. Biomed. Eng. (2019) 370–380.
[23] Z. Wan, P. Zhang, Y. Liu, L. Lv, Y. Zhou, Four-dimensional bioprinting: current developments and applications in bone tissue engineering, Acta Biomater. 101 (2019) 26–42.
[24] B. Gao, Q. Yang, X. Zhao, G. Jin, Y. Ma, F. Xu, 4D bioprinting for biomedical applications, Trends Biotechnol. 34 (9) (2016) 746–756.
[25] M.L. Bedell, A.M. Navara, Y. Du, S. Zhang, A.G. Mikos, Polymeric systems for bioprinting, Chem. Rev. 120 (19) (2020) 10744–10792.
[26] P. Fu, H. Li, J. Gong, Z. Fan, A.T. Smith, K. Shen, T.O. Khalfalla, H. Huang, X. Qian, J.R. McCutcheon, L. Sun, 4D printing of polymers: Techniques, materials, and prospects, Prog. Polym. Sci. 126 (2022) 101506.
[27] M. Chen, M. Gao, L. Bai, H. Zheng, H.J. Qi, K. Zhou, Recent advances in 4D printing of liquid Crystal Elastomers, Adv. Mater. 35 (23) (2023) 2209566.
[28] F. Mota, L. Braga, L. Rocha, B. Cabral, 3D and 4D bioprinted human model patenting and the future of drug development, Nat. Biotechnol. 38 (6) (2020) 689–694.
[29] A. Chen, W. Wang, Z. Mao, Y. He, S. Chen, G. Liu, J. Su, P. Feng, Y. Shi, C. Yan, J. Lu, Multi-material 3D and 4D bioprinting of heterogeneous constructs for tissue engineering, Adv. Mater. (2023) 2307686.
[30] Z. Wang, X. Liang, G. Wang, X. Wang, Y. Chen, Emerging bioprinting for wound healing, Adv. Mater. (2023) 2304738.
[31] J. Lai, M. Wang, Developments of additive manufacturing and 5D printing in tissue engineering, J. Mater. Res. 38 (21) (2023) 4692–4725.
[32] B. Jian, H. Li, X. He, R. Wang, H.Y. Yang, Q. Ge, Two-photon polymerization-based 4D printing and its applications, Int. J. Extrem. Manuf. 6 (1) (2024) 012001.
[33] A. Mandal, K. Chatterjee, Emerging trends in humidity-responsive 4D bioprinting, Chem. Eng. J. 455 (2023) 140550.
[34] X. Han, Q. Saiding, X. Cai, Y. Xiao, P. Wang, Z. Cai, X. Gong, W. Gong, X. Zhang, W. Cui, Intelligent vascularized 3D/4D/5D/6D-printed tissue scaffolds, Nano-Micro Lett. 15 (1) (2023) 239.
[35] A.S. Gladman, E.A. Matsumoto, R.G. Nuzzo, L. Mahadevan, J.A. Lewis, Biomimetic 4D printing, Nat. Mater. 15 (4) (2016) 413.
[36] Q. Ge, A.H. Sakhaei, H. Lee, C.K. Dunn, N.X. Fang, M.L. Dunn, Multimaterial 4D printing with tailorable shape memory polymers, Sci. Rep. 6 (1) (2016) 1–11.
[37] A. Kirillova, R. Maxson, G. Stoychev, C.T. Gomillion, L. Ionov, 4D biofabrication using shape-morphing hydrogels, Adv. Mater. 29 (46) (2017) 1703443.
[38] C.P. Ambulo, J.J. Burroughs, J.M. Boothby, H. Kim, M.R. Shankar, T.H. Ware, Four-dimensional printing of liquid Crystal Elastomers, ACS Appl. Mater. Interfaces 9 (42) (2017) 37332–37339.
[39] X. Kuang, K. Chen, C.K. Dunn, J. Wu, V.C.F. Li, H.J. Qi, 3D printing of highly stretchable, shape-memory, and self-healing Elastomer toward novel 4D printing, ACS Appl. Mater. Interfaces 10 (8) (2018) 7381–7388.
[40] A. Ding, O. Jeon, D. Cleveland, K. Gasvoda, D. Wells, S.J. Lee, E. Alsberg, Jammed micro-flake hydrogel for 4D living cell bioprinting, Adv. Mater. 34 (15) (2022) 2109394.
[41] S. Amukarimi, M. Mozafari, 4D bioprinting of tissues and organs, Bioprinting 23 (2021) e00161.
[42] J. Lai, X. Ye, J. Liu, C. Wang, J. Li, X. Wang, M. Ma, M. Wang, 4D printing of highly printable and shape morphing hydrogels composed of alginate and methylcellulose, Mater. Des. 205 (2021) 109699.
[43] X. Du, H. Cui, Q. Zhao, J. Wang, H. Chen, Y. Wang, Inside-out 3D Reversible Ion-Triggered Shape-Morphing Hydrogels, 2019. Research 2019.
[44] Q. Zhao, J. Wang, H. Cui, H. Chen, Y. Wang, X. Du, Programmed shape-morphing scaffolds enabling facile 3D Endothelialization, Adv. Funct. Mater. 28 (29) (2018) 1801027.
[45] H. Hu, C. Huang, M. Galluzzi, Q. Ye, R. Xiao, X. Yu, X. Du, Editing the Shape Morphing of Monocomponent Natural Polysaccharide Hydrogel Films, Research 2021, 2021.
[46] G.R. Souza, J.R. Molina, R.M. Raphael, M.G. Ozawa, D.J. Stark, C.S. Levin, L. F. Bronk, J.S. Ananta, J. Mandelin, M.-M. Georgescu, J.A. Bankson, J.G. Gelovani, T.C. Killian, W. Arap, R. Pasqualini, Three-dimensional tissue culture based on magnetic cell levitation, Nat. Nanotechnol. 5 (4) (2010) 291–296.
[47] V. Du, N. Luciani, S. Richard, G. Mary, C. Gay, F. Mazuel, M. Reffay, P. Menasché, O. Agbulut, C. Wilhelm, A 3D magnetic tissue stretcher for remote mechanical control of embryonic stem cell differentiation, Nat. Commun. 8 (1) (2017) 400.
[48] T. Ren, M. Maitusong, X. Zhou, X. Hong, S. Cheng, Y. Lin, J. Xue, D. Xu, J. Chen, Y. Qian, Y. Lu, X. Liu, Y. Zhu, J.a. Wang, Programing cell assembly via ink-free, label-free magneto-Archimedes based strategy, ACS Nano 17 (13) (2023) 12072–12086.
[49] A.C. Daly, M.D. Davidson, J.A. Burdick, 3D bioprinting of high cell-density heterogeneous tissue models through spheroid fusion within self-healing hydrogels, Nat. Commun. 12 (1) (2021) 753.
[50] K.J. Wolf, J.D. Weiss, S.G.M. Uzel, M.A. Skylar-Scott, J.A. Lewis, Biomanufacturing human tissues via organ building blocks, Cell Stem Cell 29 (5) (2022) 667–677.
[51] M.A. Skylar-Scott, S.G. Uzel, L.L. Nam, J.H. Ahrens, R.L. Truby, S. Damaraju, J. A. Lewis, Biomanufacturing of organ-specific tissues with high cellular density and embedded vascular channels, Sci. Adv. 5 (9) (2019) eaaw2459.
[52] X. Li, B. Liu, B. Pei, J. Chen, D. Zhou, J. Peng, X. Zhang, W. Jia, T. Xu, Inkjet bioprinting of biomaterials, Chem. Rev. 120 (19) (2020) 10793–10833.
[53] K.S. Lim, J.H. Galarraga, X. Cui, G.C. Lindberg, J.A. Burdick, T.B. Woodfield, Fundamentals and applications of Photo-cross-linking in bioprinting, Chem. Rev. 120 (19) (2020) 10662–10694.
[54] C. Dou, V. Perez, J. Qu, A. Tsin, B. Xu, J. Li, A state-of-the-art review of laser-assisted bioprinting and its future research trends, ChemBioEng Rev. 8 (5) (2021) 517–534.
[55] T. Jiang, J.G. Munguia-Lopez, S. Flores-Torres, J. Kort-Mascort, J.M. Kinsella, Extrusion bioprinting of soft materials: an emerging technique for biological model fabrication, Appl. Phys. Rev. 6 (1) (2019) 011310.
[56] K. Markstedt, A. Mantas, I. Tournier, H.C. Martínez Ávila, D. Hägg, P. Gatenholm, 3D bioprinting human chondrocytes with nanocellulose–alginate bioink for cartilage tissue engineering applications, Biomacromolecules 16 (5) (2015) 1489–1496.
[57] L. Ouyang, C.B. Highley, W. Sun, J.A. Burdick, A generalizable strategy for the 3D bioprinting of hydrogels from Nonviscous Photo-crosslinkable inks, Adv. Mater. 29 (8) (2017) 1604983.
[58] A. Thomas, I. Orellano, T. Lam, B. Noichl, M.-A. Geiger, A.K. Amler, A.E. Kreuder, C. Palmer, G. Duda, R. Lauster, L. Kloke, Vascular bioprinting with enzymatically degradable bioinks via multi-material projection-based stereolithography, Acta Biomater. 117 (2020) 121–132.
[59] R. Hossain Rakin, H. Kumar, A. Rajeev, G. Natale, F. Menard, I.T.S. Li, K. Kim, Tunable metacrylated hyaluronic acid-based hybrid bioinks for stereolithography 3D bioprinting, Biofabrication 13 (4) (2021) 044109.
[60] Z. Wu, J. Liu, J. Lin, L. Lu, J. Tian, L. Li, C. Zhou, Novel digital light processing printing strategy using a collagen-based bioink with Prospective cross-Linker Procyanidins, Biomacromolecules 23 (1) (2022) 240–252.
[61] S. You, Y. Xiang, H.H. Hwang, D.B. Berry, W. Kiratitanaporn, J. Guan, E. Yao, M. Tang, Z. Zhong, X. Ma, D. Wangpraseurt, Y. Sun, T.Y. Lu, S. Chen, High cell density and high-resolution 3D bioprinting for fabricating vascularized tissues, Sci. Adv. 9 (8) (2023) eade7923.
[62] B. Guillotin, A. Souquet, S. Catros, M. Duocastella, B. Pippenger, S. Bellance, R. Bareille, M. Rémy, L. Bordenave, J. Amédée, F. Guillemot, Laser assisted bioprinting of engineered tissue with high cell density and microscale organization, Biomaterials 31 (28) (2010) 7250–7256.
[63] K. Roversi, H. Ebrahimi Orimi, M. Falchetti, E. Lummertz da Rocha, S. Talbot, C. Boutopoulos, Bioprinting of adult Dorsal Root Ganglion (DRG) Neurons using laser-induced side transfer (LIST), Micromachines 12 (8) (2021) 865.
[64] J.A. Brassard, M. Nikolaev, T. Hübscher, M. Hofer, M.P. Lutolf, Recapitulating macro-scale tissue self-organization through organoid bioprinting, Nat. Mater. 20 (1) (2020) 22–29.
[65] K.T. Lawlor, J.M. Vanslambrouck, J.W. Higgins, A. Chambon, K. Bishard, D. Arndt, P.X. Er, S.B. Wilson, S.E. Howden, K.S. Tan, F. Li, L.J. Hale, B. Shepherd, S. Pentoney, S.C. Presnell, A.E. Chen, M.H. Little, Cellular extrusion bioprinting improves kidney organoid reproducibility and conformation, Nat. Mater. 20 (2) (2020) 260–271.
[66] M. Albanna, K.W. Binder, S.V. Murphy, J. Kim, S.A. Qasem, W. Zhao, J. Tan, I. B. El-Amin, D.D. Dice, J. Marco, J. Green, T. Xu, A. Skardal, J.H. Holmes, J. D. Jackson, A. Atala, J.J. Yoo, In situ bioprinting of autologous skin cells accelerates wound healing of Extensive Excisional full-thickness wounds, Sci. Rep. 9 (1) (2019) 1856.
[67] D. Takagi, W. Lin, T. Matsumoto, H. Yaginuma, N. Hemmi, S. Hatada, M. Seo, High-precision three-dimensional inkjet technology for live cell bioprinting, Int. J. bioprinting 5 (2) (2019) 208.
[68] Z. Wang, H. Kumar, Z. Tian, X. Jin, J.F. Holzman, F. Menard, K. Kim, Visible light photoinitiation of cell-adhesive gelatin methacryloyl hydrogels for stereolithography 3D bioprinting, ACS Appl. Mater. Interfaces 10 (32) (2018) 26859–26869.
[69] W. Zhu, H. Cui, B. Boualam, F. Masood, E. Flynn, R.D. Rao, Z.Y. Zhang, L. G. Zhang, 3D bioprinting mesenchymal stem cell-laden construct with core–shell nanospheres for cartilage tissue engineering, Nanotechnology 29 (18) (2018) 185101.
[70] S.H. Kim, Y.B. Seo, Y.K. Yeon, Y.J. Lee, H.S. Park, M.T. Sultan, J.M. Lee, J.S. Lee, O.J. Lee, H. Hong, H. Lee, O. Ajiteru, Y.J. Suh, S.H. Song, K.H. Lee, C.H. Park, 4D-bioprinted silk hydrogels for tissue engineering, Biomaterials 260 (2020) 120281.
[71] C. Gong, Z. Kong, X. Wang, The effect of agarose on 3D bioprinting, Polymers 13 (22) (2021) 4028.
[72] X. Cui, D. Dean, Z.M. Ruggeri, T. Boland, Cell damage evaluation of thermal inkjet printed Chinese hamster ovary cells, Biotechnol. Bioeng. 106 (6) (2010) 963–969.
[73] C. Cui, D.O. Kim, M.Y. Pack, B. Han, L. Han, Y. Sun, L.H. Han, 4D printing of self-folding and cell-encapsulating 3D microstructures as scaffolds for tissue-engineering applications, Biofabrication 12 (4) (2020) 045018.
[74] S.B. Gugulothu, K. Chatterjee, Visible light-based 4D-bioprinted tissue scaffold, ACS Macro Lett. 12 (4) (2023) 494–502.
[75] C. Douillet, M. Nicodeme, L. Hermant, V. Bergeron, F. Guillemot, J.C. Fricain, H. Oliveira, M. Garcia, From local to global matrix organization by fibroblasts: a 4D laser-assisted bioprinting approach, Biofabrication 14 (2) (2022) 025006.
[76] A. Joshi, S. Choudhury, V.S. Baghel, S. Ghosh, S. Gupta, D. Lahiri, G. K. Ananthasuresh, K. Chatterjee, 4D printed programmable shape-morphing hydrogels as intraoperative self-folding nerve conduits for Sutureless Neurorrhaphy, Adv. Healthc. Mater. 12 (24) (2023) 2300701.
[77] S. Miao, H. Cui, M. Nowicki, L. Xia, X. Zhou, S.J. Lee, W. Zhu, K. Sarkar, Z. Zhang, L.G. Zhang, Stereolithographic 4D bioprinting of multiresponsive architectures for neural engineering, Adv. Biosyst. 2 (9) (2018) 1800101.
[78] J. Lai, J. Li, M. Wang, 3D Printed porous tissue engineering scaffolds with the self-folding ability and controlled release of growth factor, MRS Commun. 10 (4) (2020) 579–586.

[79] S.Y. Hann, H. Cui, T. Esworthy, L.G. Zhang, 4D Thermo-responsive smart hiPSC-CM cardiac construct for myocardial cell therapy, Int. J. Nanomed. 18 (2023) 1809–1821.
[80] C. Wang, H. Yue, J. Liu, Q. Zhao, Z. He, K. Li, B. Lu, W. Huang, Y. Wei, Y. Tang, M. Wang, Advanced reconfigurable scaffolds fabricated by 4D printing for treating critical-size bone defects of irregular shapes, Biofabrication 12 (4) (2020) 045025.
[81] Y. Luo, X. Lin, B. Chen, X. Wei, Cell-laden four-dimensional bioprinting using near-infrared-triggered shape-morphing alginate/polydopamine bioinks, Biofabrication 11 (4) (2019) 045019.
[82] G. Villar, A.D. Graham, H. Bayley, A tissue-like printed material, Science 340 (6128) (2013) 48–52.
[83] D.J. Shiwarski, A.R. Hudson, J.W. Tashman, A.W. Feinberg, Emergence of FRESH 3D printing as a platform for advanced tissue biofabrication, APL Bioeng. 5 (1) (2021) 010904.
[84] A. Blaeser, D.F. Duarte Campos, U. Puster, W. Richtering, M.M. Stevens, H. Fischer, Controlling shear stress in 3D bioprinting is a key factor to balance printing resolution and stem cell integrity, Adv. Healthc. Mater. 5 (3) (2016) 326–333.
[85] S. Boularaoui, G. Al Hussein, K.A. Khan, N. Christoforou, C. Stefanini, An overview of extrusion-based bioprinting with a focus on induced shear stress and its effect on cell viability, Bioprinting 20 (2020) e00093.
[86] S. Boularaoui, A. Shanti, K.A. Khan, S. Iacoponi, N. Christoforou, C. Stefanini, Harnessing shear stress preconditioning to improve cell viability in 3D post-printed biostructures using extrusion bioprinting, Bioprinting 25 (2022) e00184.
[87] H. Li, Y.J. Tan, K.F. Leong, L. Li, 3D bioprinting of highly thixotropic alginate/methylcellulose hydrogel with Strong interface bonding ACS Appl. Mater. Interfaces 9 (23) (2017) 20086.
[88] H. Li, Y.J. Tan, R. Kiran, S.B. Tor, K. Zhou, Submerged and non-submerged 3D bioprinting approaches for the fabrication of complex structures with the hydrogel pair GelMA and alginate/methylcellulose, Addit. Manuf. 37 (2021) 101640.
[89] E. Goulart, L.C. de Caires-Junior, K.A. Telles-Silva, B.H.S. Araujo, S.A. Rocco, M. Sforca, I.L. de Sousa, G.S. Kobayashi, C.M. Musso, A.F. Assoni, D. Oliveira, E. Caldini, S. Raia, P.I. Lelkes, M. Zatz, 3D bioprinting of liver spheroids derived from human induced pluripotent stem cells sustain liver function and viability in vitro, Biofabrication 12 (1) (2020) 015010.
[90] M.A. Skylar-Scott, J. Mueller, C.W. Visser, J.A. Lewis, Voxelated soft matter via multimaterial multinozzle 3D printing, Nature 575 (7782) (2019) 330–335.
[91] B. Derby, Inkjet printing of functional and structural materials: fluid property requirements, feature stability, and resolution, Annu. Rev. Mater. Res. 40 (1) (2010) 395–414.
[92] J. Lai, M. Wang, Microvalve jetting of biomaterials, in: R.J. Narayan (Ed.), Additive Manufacturing in Biomedical Applications, ASM International, 2022.
[93] X. Cui, T. Boland, D. D.D'Lima, M.K. Lotz, Thermal inkjet printing in tissue engineering and regenerative medicine, Recent Pat. Drug Deliv. Formulation 6 (2) (2012) 149–155.
[94] R. Seetharam, S.K. Sharma, Purification and Analysis of Recombinant Proteins, CRC Press, 1991.
[95] D. Busaina, E. Hunt, T. Boland, Rapid Prototyping of tissue-engineering constructs, using Photopolymerizable hydrogels and stereolithography, Tissue Eng. 10 (9–10) (2004) 1316–1322.
[96] N. Anandakrishnan, H. Ye, Z. Guo, Z. Chen, K.I. Mentkowski, J.K. Lang, N. Rajabian, S.T. Andreadis, Z. Ma, J.A. Spernyak, J.F. Lovell, D. Wang, J. Xia, C. Zhou, R. Zhao, Fast stereolithography printing of large-scale biocompatible hydrogel models, Adv. Healthc. Mater. 10 (10) (2021) 2002103.
[97] B. Grigoryan, D.W. Sazer, A. Avila, J.L. Albritton, A. Padhye, A.H. Ta, P. T. Greenfield, D.L. Gibbons, J.S. Miller, Development, characterization, and applications of multi-material stereolithography bioprinting, Sci. Rep. 11 (1) (2021) 3171.
[98] J.R. Tumbleston, D. Shirvanyants, N. Ermoshkin, R. Janusziewicz, A.R. Johnson, D. Kelly, K. Chen, R. Pinschmidt, J.P. Rolland, A. Ermoshkin, E.T. Samulski, J. M. DeSimone, Continuous liquid interface production of 3D objects, Science 347 (6228) (2015) 1349–1352.
[99] G. Lipkowitz, T. Samuelsen, K. Hsiao, B. Lee, M.T. Dulay, I. Coates, H. Lin, W. Pan, G. Toth, L. Tate, E.S.G. Shaqfeh, J.M. DeSimone, Injection continuous liquid interface production of 3D objects, Sci. Adv. 8 (39) (2022) eabq3917.
[100] D. Han, C. Yang, N.X. Fang, H. Lee, Rapid multi-material 3D printing with projection micro-stereolithography using dynamic fluidic control, Addit. Manuf. 27 (2019) 606–615.
[101] J. Cheng, R. Wang, Z. Sun, Q. Liu, X. He, H. Li, H. Ye, X. Yang, X. Wei, Z. Li, B. Jian, W. Deng, Q. Ge, Centrifugal multimaterial 3D printing of multifunctional heterogeneous objects, Nat. Commun. 13 (1) (2022) 7931.
[102] L.J. Tan, W. Zhu, K. Zhou, Recent progress on polymer materials for additive manufacturing, Adv. Funct. Mater. 30 (43) (2020) 2003062.
[103] C. Colosi, S.R. Shin, V. Manoharan, S. Massa, M. Costantini, A. Barbetta, M. R. Dokmeci, M. Dentini, A. Khademhosseini, Microfluidic bioprinting of heterogeneous 3D tissue constructs using low-viscosity bioink, Adv. Mater. 28 (4) (2016) 677–684.
[104] T. Billiet, E. Gevaert, T. De Schryver, M. Cornelissen, P. Dubruel, The 3D printing of gelatin methacrylamide cell-laden tissue-engineered constructs with high cell viability, Biomaterials 35 (1) (2014) 49–62.
[105] M. Bao, X. Lou, Q. Zhou, W. Dong, H. Yuan, Y. Zhang, Electrospun biomimetic fibrous scaffold from shape memory polymer of PDLLA-co-TMC for bone tissue engineering, ACS Appl. Mater. Inter. 6 (4) (2014) 2611–2621.
[106] C. Wang, Y. Zhou, M. Wang, In situ delivery of rhBMP-2 in surface porous shape memory scaffolds developed through cryogenic 3D plotting, Mater. Lett. 189 (2017) 140–143.
[107] L. Yue, X. Sun, L. Yu, M. Li, S.M. Montgomery, Y. Song, T. Nomura, M. Tanaka, H. J. Qi, Cold-programmed shape-morphing structures based on grayscale digital light processing 4D printing, Nat. Commun. 14 (1) (2023) 5519.
[108] X. Kuang, J. Wu, K. Chen, Z. Zhao, Z. Ding, F. Hu, D. Fang, H.J. Qi, Grayscale digital light processing 3D printing for highly functionally graded materials, Sci. Adv. 5 (5) (2019) eaav5790.
[109] C. Ni, D. Chen, Y. Yin, X. Wen, X. Chen, C. Yang, G. Chen, Z. Sun, J. Wen, Y. Jiao, C. Wang, N. Wang, X. Kong, S. Deng, Y. Shen, R. Xiao, X. Jin, J. Li, X. Kong, Q. Zhao, T. Xie, Shape memory polymer with programmable recovery onset, Nature 622 (7984) (2023) 748–753.
[110] C.A. Spiegel, M. Hackner, V.P. Bothe, J.P. Spatz, E. Blasco, 4D printing of shape memory polymers: from macro to micro, Adv. Funct. Mater. 32 (51) (2022) 2110580.
[111] T. van Manen, S. Janbaz, A.A. Zadpoor, Programming 2D/3D shape-shifting with hobbyist 3D printers, Mater. Horiz. 4 (6) (2017) 1064–1069.
[112] T.Y. Koh, A. Sutradhar, Untethered selectively actuated microwave 4D printing through ferromagnetic PLA, Addit. Manuf. 56 (2022) 102866.
[113] F. Zhang, N. Wen, L. Wang, Y. Bai, J. Leng, Design of 4D printed shape-changing tracheal stent and remote controlling actuation, Int. J. Smart Nano Mater. 12 (4) (2021) 375–389.
[114] S. Miao, W. Zhu, N.J. Castro, M. Nowicki, X. Zhou, H. Cui, J.P. Fisher, L.G. Zhang, 4D printing smart biomedical scaffolds with novel soybean oil epoxidized acrylate, Sci. Rep. 6 (2016) 27226.
[115] N.A. Pattanashetti, G.B. Heggannavar, M.Y. Kariduraganavar, Smart biopolymers and their biomedical applications, Procedia Manuf. 12 (2017) 263–279.
[116] A. Lendlein, M. Balk, N.A. Tarazona, O.E.C. Gould, Bioperspectives for shape-memory polymers as shape programmable, active materials, Biomacromolecules 20 (10) (2019) 3627–3640.
[117] M. Zarek, N. Mansour, S. Shapira, D. Cohn, 4D printing of shape memory-based personalized Endoluminal medical devices, Macromol. Rapid Commun. 38 (2) (2017) 1600628.
[118] A.C. Weems, M.C. Arno, W. Yu, R.T.R. Huckstepp, A.P. Dove, 4D polycarbonates via stereolithography as scaffolds for soft tissue repair, Nat. Commun. 12 (1) (2021) 3771.
[119] D. You, G. Chen, C. Liu, X. Ye, S. Wang, M. Dong, M. Sun, J. He, X. Yu, G. Ye, Q. Li, J. Wu, J. Wu, Q. Zhao, T. Xie, M. Yu, H. Wang, 4D printing of multi-responsive membrane for accelerated in vivo bone healing via remote regulation of stem cell fate, Adv. Funct. Mater. 31 (40) (2021) 2103920.
[120] Y. Yang, X. Zhao, S. Wang, Y. Zhang, A. Yang, Y. Cheng, X. Chen, Ultra-durable cell-free bioactive hydrogel with fast shape memory and on-demand drug release for cartilage regeneration, Nat. Commun. 14 (1) (2023) 7771.
[121] C. Zhang, D. Cai, P. Liao, J.-W. Su, H. Deng, B. Vardhanabhuti, B.D. Ulery, S. Y. Chen, J. Lin, 4D Printing of shape-memory polymeric scaffolds for adaptive biomedical implantation, Acta Biomater. 122 (2021) 101–110.
[122] R. Qu, D. Zhou, T. Guo, W. He, C. Cui, Y. Zhou, Y. Zhang, Z. Tang, X. Zhang, Q. Wang, T. Wang, Y. Zhang, 4D printing of shape memory inferior vena cava filters based on copolymer of poly(glycerol sebacate) acrylate-co-hydroxyethyl methacrylate (PGSA-HEMA), Mater. Des. 225 (2023) 111556.
[123] W. Zhao, H. Chen, Y. Zhang, D. Zhou, L. Liang, B. Liu, T. Xu, Adaptive multi-degree-of-freedom in situ bioprinting robot for hair-follicle-inclusive skin repair: a preliminary study conducted in mice, Bioeng. Transl. Med. 7 (3) (2022) e10303.
[124] H. Chen, X. Ma, T. Gao, W. Zhao, T. Xu, Z. Liu, Robot-assisted in situ bioprinting of gelatin methacrylate hydrogels with stem cells induces hair follicle-inclusive skin regeneration, Biomed. Pharmacother. 158 (2023) 114140.
[125] S. Chen, S. Tan, L. Zheng, M. Wang, Multilayered shape-morphing scaffolds with a hierarchical structure for uterine tissue regeneration, ACS Appl. Mater. Interfaces 16 (6) (2024) 6772–6788.
[126] S. Zu, Z. Zhang, Q. Liu, Z. Wang, Z. Song, Y. Guo, Y. Xin, S. Zhang, 4D printing of core–shell hydrogel capsules for smart controlled drug release, Bio-Design and Manufacturing 5 (2) (2022) 294–304.
[127] L.R. Khoury, M. Slawinski, D.R. Collison, I. Popa, Cation-induced shape programming and morphing in protein-based hydrogels, Sci. Adv. 6 (18) (2020) eaba6112.
[128] S.T. McLoughlin, A.R. McKenna, J.P. Fisher, 4D bioprinting via molecular network contraction for membranous tissue fabrication, Adv. Healthc. Mater. 12 (27) (2023) 2300642.
[129] J. Gong, C.C.L. Schuurmans, A.M.v. Genderen, X. Cao, W. Li, F. Cheng, J.J. He, A. López, V. Huerta, J. Manríquez, R. Li, H. Li, C. Delavaux, S. Sebastian, P. E. Capendale, H. Wang, J. Xie, M. Yu, R. Masereeuw, T. Vermonden, Y.S. Zhang, Complexation-induced resolution enhancement of 3D-printed hydrogel constructs, Nat. Commun. 11 (1) (2020) 1267.
[130] M. Champeau, D.A. Heinze, T.N. Viana, E.R. de Souza, A.C. Chinellato, S. Titotto, 4D printing of hydrogels: a review, Adv. Funct. Mater. 30 (31) (2020) 1910606.
[131] M. Jamal, S.S. Kadam, R. Xiao, F. Jivan, T.M. Onn, R. Fernandes, T.D. Nguyen, D. H. Gracias, Bio-origami hydrogel scaffolds composed of photocrosslinked PEG bilayers, Adv. Healthc. Mater. 2 (8) (2013) 1142–1150.
[132] Y.B. Lee, O. Jeon, S.J. Lee, A. Ding, D. Wells, E. Alsberg, Induction of four-dimensional Spatiotemporal geometric transformations in high cell density tissues via shape-changing hydrogels, Adv. Funct. Mater. 31 (24) (2021) 2010104.
[133] A. Ding, S.J. Lee, S. Ayyagari, R. Tang, C.T. Huynh, E. Alsberg, 4D biofabrication via instantly generated graded hydrogel scaffolds, Bioact. Mater. 7 (2022) 324–332.

[134] A. Ding, S.J. Lee, R. Tang, K.L. Gasvoda, F. He, E. Alsberg, 4D cell-condensate bioprinting, Small 18 (36) (2022) 2202196.
[135] P.J. Díaz-Payno, M. Kalogeropoulou, I. Muntz, E. Kingma, N. Kops, M. D'Este, G. H. Koenderink, L.E. Fratila-Apachitei, G.J.V.M. van Osch, A.A. Zadpoor, Swelling-dependent shape-based transformation of a human mesenchymal stromal cells-laden 4D bioprinted construct for cartilage tissue engineering, Adv. Healthc. Mater. 12 (2) (2023) 2201891.
[136] A. Roy, Z. Zhang, M.K. Eiken, A. Shi, A. Pena-Francesch, C. Loebel, Programmable tissue folding patterns in structured hydrogels, Adv. Mater. (2023) 2300017.
[137] L. Zhang, Y. Xiang, H. Zhang, L. Cheng, X. Mao, N. An, L. Zhang, J. Zhou, L. Deng, Y. Zhang, A biomimetic 3D-self-forming approach for Microvascular scaffolds, Adv. Sci. 7 (9) (2020) 1903553.
[138] Z.L. Wu, M. Moshe, J. Greener, H. Therien-Aubin, Z. Nie, E. Sharon, E. Kumacheva, Three-dimensional shape transformations of hydrogel sheets induced by small-scale modulation of internal stresses, Nat. Commun. 4 (1) (2013) 1586.
[139] Y.D. Zhao, J.H. Lai, M. Wang, 4D printing of self-folding hydrogel tubes for potential tissue engineering applications, Nano LIFE 11 (4) (2021) 2141001.
[140] M. Wang, Q. Zhao, Biomedical Composites, Reference Module in Biomedical Sciences: Encyclopedia of Biomedical Engineering, 2019.
[141] S. Liu, M. Jin, Y. Chen, H. Gao, X. Shi, W. Cheng, L. Ren, Y. Wang, High internal phase emulsions stabilised by supramolecular cellulose nanocrystals and their application as cell-adhesive macroporous hydrogel monoliths, J. Mater. Chem. B 5 (14) (2017) 2671–2678.
[142] A. Pardo, M. Gómez-Florit, S. Barbosa, P. Taboada, R.M.A. Domingues, M. E. Gomes, Magnetic Nanocomposite hydrogels for tissue engineering: design concepts and remote actuation strategies to control cell fate, ACS Nano 15 (1) (2021) 175–209.
[143] Y. Jin, C. Liu, W. Chai, A. Compaan, Y. Huang, Self-supporting nanoclay as internal scaffold material for direct printing of soft hydrogel composite structures in air, ACS Appl. Mater. Interfaces. 9 (20) (2017) 17456–17465.
[144] Q. Gao, X. Niu, L. Shao, L. Zhou, Z. Lin, A. Sun, J. Fu, Z. Chen, J. Hu, Y. Liu, Y. He, 3D printing of complex GelMA-based scaffolds with nanoclay, Biofabrication 11 (3) (2019) 035006.
[145] S. Li, X. Li, Y. Xu, C. Fan, Z.A. Li, L. Zheng, B. Luo, Z.P. Li, B. Lin, Z.G. Zha, H. T. Zhang, X. Wang, Collagen fibril-like injectable hydrogels from self-assembled nanoparticles for promoting wound healing, Bioact. Mater. 32 (2024) 149–163.
[146] J. Guo, R. Zhang, L. Zhang, X. Cao, 4D printing of robust hydrogels consisted of agarose nanofibers and polyacrylamide, ACS Macro Lett. 7 (4) (2018) 442–446.
[147] Y. Kim, X. Zhao, Magnetic soft materials and robots, Chem. Rev. 122 (5) (2022) 5317–5364.
[148] H. Wei, Q. Zhang, Y. Yao, L. Liu, Y. Liu, J. Leng, Direct-write fabrication of 4D active shape-changing structures based on a shape memory polymer and its nanocomposite, ACS Appl. Mater. Interfaces 9 (1) (2017) 876–883.
[149] C. Yue, M. Li, Y. Liu, Y. Fang, Y. Song, M. Xu, J. Li, Three-dimensional printing of cellulose nanofibers reinforced PHB/PCL/Fe3O4 magneto-responsive shape memory polymer composites with excellent mechanical properties, Addit. Manuf. 46 (2021) 102146.
[150] H. Liu, F. Wang, W. Wu, X. Dong, L. Sang, 4D printing of mechanically robust PLA/TPU/Fe3O4 magneto-responsive shape memory polymers for smart structures, Compos. B Eng. 248 (2023) 110382.
[151] H. Hwangbo, H. Lee, E.J. Roh, W. Kim, H.P. Joshi, S.Y. Kwon, U.Y. Choi, I.B. Han, G.H. Kim, Bone tissue engineering via application of a collagen/hydroxyapatite 4D-printed biomimetic scaffold for spinal fusion, Appl. Phys. Rev. 8 (2) (2021) 021403.
[152] P.T. Mather, X. Luo, I.A. Rousseau, Shape memory polymer research, Annu. Rev. Mater. Res. 39 (1) (2009) 445–471.
[153] M. Abbasi-Shirsavar, M. Baghani, M. Taghavimehr, M. Golzar, M. Nikzad, M. Ansari, D. George, An experimental–numerical study on shape memory behavior of PU/PCL/ZnO ternary blend, J. Intell. Mater. Syst. Struct. 30 (1) (2018) 116–126.
[154] M. Hosseinzadeh, M. Ghoreishi, K. Narooei, An investigation into the effect of thermal variables on the 3D printed shape memory polymer structures with different geometries, J. Intell. Mater. Syst. Struct. 33 (5) (2022) 715–726.
[155] S. Timoshenko, Analysis of bi-metal thermostats, Josa 11 (3) (1925) 233–255.
[156] A. Zolfagharian, L. Durran, S. Gharaie, B. Rolfe, A. Kaynak, M. Bodaghi, 4D printing soft robots guided by machine learning and finite element models, Sensor Actuator Phys. 328 (2021) 112774.
[157] M.O. Faruque, Y. Lee, G.J. Wyckoff, C.H. Lee, Application of 4D printing and AI to cardiovascular devices, J. Drug Deliv. Sci. Technol. 80 (2023) 104162.
[158] C.M. Hamel, D.J. Roach, K.N. Long, F. Demoly, M.L. Dunn, H.J. Qi, Machine-learning based design of active composite structures for 4D printing, Smart Mater. Struct. 28 (6) (2019) 065005.
[159] X. Sun, L. Yue, L. Yu, H. Shao, X. Peng, K. Zhou, F. Demoly, R. Zhao, H.J. Qi, Machine learning-evolutionary algorithm enabled design for 4D-printed active composite structures, Adv. Funct. Mater. 32 (10) (2022) 2109805.
[160] O. Sigmund, K. Maute, Topology optimization approaches: a comparative review, Struct. Multidiscip. Optim. 48 (6) (2013) 1031–1055.
[161] K. Maute, A. Tkachuk, J. Wu, H. Jerry Qi, Z. Ding, M.L. Dunn, Level set topology optimization of printed active composites, J. Mech. Des. 137 (11) (2015) 111402.
[162] V.S. Murphy, A. Atala, 3D bioprinting of tissues and organs, Nat. Biotechnol. 32 (8) (2014) 773.
[163] M. Hospodiuk, M. Dey, D. Sosnoski, I.T. Ozbolat, The bioink: a comprehensive review on bioprintable materials, Biotechnol. Adv. 35 (2) (2017) 217–239.
[164] H. Li, S. Liu, L. Li, Rheological study on 3D printability of alginate hydrogel and effect of graphene oxide, Int. J. Bioprinting 2 (2) (2016) 54–66.
[165] N. Paxton, W. Smolan, T. Böck, F. Melchels, J. Groll, T. Jungst, Proposal to assess printability of bioinks for extrusion-based bioprinting and evaluation of rheological properties governing bioprintability, Biofabrication 9 (4) (2017) 044107.
[166] A. Shafiee, E. Ghadiri, H. Ramesh, C. Kengla, J. Kassis, P. Calvert, D. Williams, A. Khademhosseini, R. Narayan, G. Forgacs, A. Atala, Physics of bioprinting, Appl. Phys. Rev. 6 (2) (2019) 021315.
[167] L. Ouyang, R. Yao, Y. Zhao, W. Sun, Effect of bioink properties on printability and cell viability for 3D bioplotting of embryonic stem cells, Biofabrication 8 (3) (2016) 035020.
[168] D. Jang, D. Kim, J. Moon, Influence of fluid physical properties on ink-jet printability, Langmuir 25 (5) (2009) 2629–2635.
[169] D.F. Williams, Definitions in Biomaterials: Proceedings of a Consensus Conference of the European Society for Biomaterials, Elsevier Science Limited, Chester, England, 1987. March 3-5, 1986.
[170] D.F. Williams, On the mechanisms of biocompatibility, Biomaterials 29 (20) (2008) 2941–2953.
[171] A. Ding, O. Jeon, R. Tang, Y.B. Lee, S.J. Lee, E. Alsberg, Cell-laden multiple-step and reversible 4D hydrogel actuators to mimic dynamic tissue Morphogenesis, Adv. Sci. 8 (9) (2021) 2004616.
[172] R. Lanza, R. Langer, J.P. Vacanti, A. Atala, Principles of Tissue Engineering, Academic press, 2020.
[173] C.K. Chua, W.Y. Yeong, Bioprinting: Principles and Applications, World Scientific Publishing Co Inc, 2014.
[174] S.S. Soman, S. Vijayavenkataraman, Applications of 3D bioprinted-induced pluripotent stem cells in Healthcare, Int. J. Bioprinting 6 (4) (2020) 280.
[175] A.S. Lee, C. Tang, M.S. Rao, I.L. Weissman, J.C. Wu, Tumorigenicity as a clinical hurdle for pluripotent stem cell therapies, Nat. Med. 19 (8) (2013) 998–1004.
[176] A.G. Tabriz, M.A. Hermida, N.R. Leslie, W. Shu, Three-dimensional bioprinting of complex cell laden alginate hydrogel structures, Biofabrication 7 (4) (2015) 045012.
[177] J. Lai, C. Wang, J. Liu, S. Chen, C. Liu, X. Huang, J. Wu, Y. Pan, Y. Xie, M. Wang, Low temperature hybrid 3D printing of hierarchically porous bone tissue engineering scaffolds with in situ delivery of osteogenic peptide and mesenchymal stem cells, Biofabrication 14 (4) (2022) 045006.
[178] J. Lai, X. Chen, H.H. Lu, M. Wang, 3D bioprinting of graphene oxide-incorporated hydrogels for neural tissue regeneration, 3D Print. Addit. Manuf. (2023).
[179] N.E. Fedorovich, J.R. De Wijn, A.J. Verbout, J. Alblas, W.J. Dhert, Three-dimensional fiber deposition of cell-laden, viable, patterned constructs for bone tissue printing, Tissue Eng. 14 (1) (2008) 127–133.
[180] S. Chen, Y. Wang, J. Lai, S. Tan, M. Wang, Structure and properties of gelatin methacryloyl (GelMA) Synthesized in different reaction systems, Biomacromolecules 24 (6) (2023) 2928–2941.
[181] J. He, Y. Sun, Q. Gao, C. He, K. Yao, T. Wang, M. Xie, K. Yu, J. Nie, Y. Chen, Y. He, Gelatin methacryloyl hydrogel, from Standardization, performance, to biomedical application, Adv. Healthc. Mater. 12 (23) (2023) 2300395.
[182] S. Xiang, Z. Li, M.R. Fritch, L. Li, S. Velankar, Y. Liu, J. Sohn, N. Baker, H. Lin, R. S. Tuan, Caveolin-1 mediates soft scaffold-enhanced adipogenesis of human mesenchymal stem cells, Stem Cell Res. Ther. 12 (1) (2021) 347.
[183] L. Ouyang, J.P.K. Armstrong, Y. Lin, J.P. Wojciechowski, C. Lee-Reeves, D. Hachim, K. Zhou, J.A. Burdick, M.M. Stevens, Expanding and optimizing 3D bioprinting capabilities using complementary network bioinks, Sci. Adv. 6 (38) (2020) eabc5529.
[184] Y.C. Li, Y.S. Zhang, A. Akpek, S.R. Shin, A. Khademhosseini, 4D bioprinting: the next-generation technology for biofabrication enabled by stimuli-responsive materials, Biofabrication 9 (1) (2017) 012001.
[185] J.L. Tan, J. Tien, D.M. Pirone, D.S. Gray, K. Bhadriraju, C.S. Chen, Cells lying on a bed of microneedles: an approach to isolate mechanical force, Proc. Natl. Acad. Sci. USA 100 (4) (2003) 1484–1489.
[186] K. Kuribayashi-Shigetomi, H. Onoe, S. Takeuchi, Cell origami: self-folding of three-dimensional cell-laden microstructures driven by cell traction force, PLoS One 7 (12) (2012) e51085.
[187] F. Zhou, Y. Hong, R. Liang, X. Zhang, Y. Liao, D. Jiang, J. Zhang, Z. Sheng, C. Xie, Z. Peng, X. Zhuang, V. Bunpetch, Y. Zou, W. Huang, Q. Zhang, E.V. Alakpa, S. Zhang, H. Ouyang, Rapid printing of bio-inspired 3D tissue constructs for skin regeneration, Biomaterials 258 (2020) 120287.
[188] M.S. Chaudhry, A. Czekanski, In-situ bioprinting of skin-a review, Bioprinting 31 (2023) e00271.
[189] C. Zhao, Z. Zeng, N.T. Qazvini, X. Yu, R. Zhang, S. Yan, Y. Shu, Y. Zhu, C. Duan, E. Bishop, J. Lei, W. Zhang, C. Yang, K. Wu, Y. Wu, L. An, S. Huang, X. Ji, C. Gong, C. Yuan, L. Zhang, W. Liu, B. Huang, Y. Feng, B. Zhang, Z. Dai, Y. Shen, X. Wang, W. Luo, L. Oliveira, A. Athiviraham, M.J. Lee, J.M. Wolf, G.A. Ameer, R.R. Reid, T.C. He, W. Huang, Thermoresponsive citrate-based graphene oxide scaffold enhances bone regeneration from BMP9-stimulated adipose-derived mesenchymal stem cells, ACS Biomater. Sci. Eng. 4 (8) (2018) 2943–2955.
[190] H. Ding, B. Li, Z. Liu, G. Liu, S. Pu, Y. Feng, D. Jia, Y. Zhou, Decoupled pH- and Thermo-responsive injectable chitosan/PNIPAM hydrogel via Thiol-Ene Click Chemistry for potential applications in tissue engineering, Adv. Healthc. Mater. 9 (14) (2020) 2000454.
[191] C. Wang, H. Yue, Q. Feng, B. Xu, L. Bian, P. Shi, Injectable Nanoreinforced shape-memory hydrogel system for regenerating spinal Cord tissue from Traumatic Injury, ACS Appl. Mater. Interfaces 10 (35) (2018) 29299–29307.
[192] B.P. Chan, T.Y. Hui, M.Y. Wong, K.H.K. Yip, G.C.F. Chan, Mesenchymal stem cell–encapsulated collagen Microspheres for bone tissue engineering, Tissue Eng. C Methods 16 (2) (2009) 225–235.

[193] F.C. Kung, Injectable collagen/RGD systems for bone tissue engineering applications, Bio Med. Mater. Eng. 29 (2018) 241–251.
[194] Z. Lv, T. Hu, Y. Bian, G. Wang, Z. Wu, H. Li, X. Liu, S. Yang, C. Tan, R. Liang, X. Weng, A MgFe-LDH Nanosheet-incorporated smart Thermo-responsive hydrogel with controllable growth factor releasing capability for bone regeneration, Adv. Mater. 35 (5) (2023) 2206545.
[195] L. Kuang, J. Huang, Y. Liu, X. Li, Y. Yuan, C. Liu, Injectable hydrogel with NIR light-responsive, dual-mode PTH release for osteoregeneration in osteoporosis, Adv. Funct. Mater. 31 (47) (2021) 2105383.
[196] M. Chen, H. Tan, W. Xu, Z. Wang, J. Zhang, S. Li, T. Zhou, J. li, X. Niu, A self-healing, magnetic and injectable biopolymer hydrogel generated by dual cross-linking for drug delivery and bone repair, Acta Biomater. 153 (2022) 159–177.
[197] X. Li, K. Xu, Y. He, B. Tao, K. Li, C. Lin, J. Hu, J. Wu, Y. Wu, S. Liu, P. Liu, H. Wang, K. Cai, ROS-responsive hydrogel coating modified titanium promotes vascularization and osteointegration of bone defects by orchestrating immunomodulation, Biomaterials 287 (2022) 121683.
[198] B. Duan, State-of-the-Art review of 3D bioprinting for cardiovascular tissue engineering, Ann. Biomed. Eng. 45 (1) (2017) 195–209.
[199] W. Kitana, I. Apsite, J. Hazur, A.R. Boccaccini, L. Ionov, 4D biofabrication of T-shaped vascular bifurcation, Adv. Mater. Technol. 8 (1) (2023) 2200429.
[200] R. Xie, Y. Cao, R. Sun, R. Wang, A. Morgan, J. Kim, S.J.P. Callens, K. Xie, J. Zou, J. Lin, K. Zhou, X. Lu, M.M. Stevens, Magnetically driven formation of 3D freestanding soft bioscaffolds, Sci. Adv. 10 (5) (2024) eadl1549.
[201] G. Constante, I. Apsite, H. Alkhamis, M. Dulle, M. Schwarzer, A. Caspari, A. Synytska, S. Salehi, L. Ionov, 4D biofabrication using a Combination of 3D printing and melt-electrowriting of shape-morphing polymers, ACS Appl. Mater. Interfaces 13 (11) (2021) 12767–12776.
[202] J. Uribe-Gomez, A. Posada-Murcia, A. Shukla, M. Ergin, G. Constante, I. Apsite, D. Martin, M. Schwarzer, A. Caspari, A. Synytska, S. Salehi, L. Ionov, Shape-morphing fibrous hydrogel/Elastomer bilayers fabricated by a Combination of 3D printing and melt electrowriting for muscle tissue regeneration, ACS Appl. Bio Mater. 4 (2) (2021) 1720–1730.
[203] Y. Wang, H. Cui, Y. Wang, C. Xu, T.J. Esworthy, S.Y. Hann, M. Boehm, Y.L. Shen, D. Mei, L.G. Zhang, 4D printed cardiac construct with aligned Myofibers and Adjustable curvature for myocardial regeneration, ACS Appl. Mater. Interfaces 13 (11) (2021) 12746–12758.
[204] S. Choi, K.Y. Lee, S.L. Kim, L.A. MacQueen, H. Chang, J.F. Zimmerman, Q. Jin, M. M. Peters, H.A.M. Ardoña, X. Liu, A.-C. Heiler, R. Gabardi, C. Richardson, W. T. Pu, A.R. Bausch, K.K. Parker, Fibre-infused gel scaffolds guide cardiomyocyte alignment in 3D-printed ventricles, Nat. Mater. 22 (8) (2023) 1039–1046.
[205] X. Wang, Y. Yu, C. Yang, L. Shang, Y. Zhao, X. Shen, Dynamically responsive scaffolds from microfluidic 3D printing for skin Flap regeneration, Adv. Sci. 9 (22) (2022) 2201155.
[206] T.G. Molley, T.T. Hung, K.A. Kilian, Cell-laden gradient microgel Suspensions for spatial control of differentiation during biofabrication, Adv. Healthc. Mater. 11 (24) (2022) 2201122.
[207] M. Trujillo-Miranda, I. Apsite, J.A.R. Agudo, G. Constante, L. Ionov, 4D biofabrication of mechanically stable tubular constructs using shape morphing porous bilayers for vascularization application, Macromol. Biosci. 23 (1) (2023) 2200320.
[208] G. Sossou, F. Demoly, H. Belkebir, H.J. Qi, S. Gomes, G. Montavon, Design for 4D printing: a voxel-based modeling and simulation of smart materials, Mater. Des. 175 (2019) 107798.
[209] M.L. Terpstra, J. Li, A. Mensinga, M. de Ruijter, M.H.P. van Rijen, C. Androulidakis, C. Galiotis, I. Papantoniou, M. Matsusaki, J. Malda, R. Levato, Bioink with cartilage-derived extracellular matrix microfibers enables spatial control of vascular capillary formation in bioprinted constructs, Biofabrication 14 (3) (2022) 034104.
[210] X. Yang, Y. Ma, X. Wang, S. Yuan, F. Huo, G. Yi, J. Zhang, B. Yang, W. Tian, A 3D-bioprinted functional module based on decellularized extracellular matrix bioink for Periodontal regeneration, Adv. Sci. 10 (5) (2022) 2205041.
[211] G. Yang, B.B. Rothrauff, H. Lin, R. Gottardi, P.G. Alexander, R.S. Tuan, Enhancement of tenogenic differentiation of human adipose stem cells by tendon-derived extracellular matrix, Biomaterials 34 (37) (2013) 9295–9306.
[212] G. Yang, B.B. Rothrauff, H. Lin, S. Yu, R.S. Tuan, Tendon-derived extracellular matrix enhances transforming growth factor-β3-induced tenogenic differentiation of human adipose-derived stem cells, Tissue Eng. 23 (3–4) (2016) 166–176.
[213] D. Wang, C.C.M. Pun, S. Huang, T.C.M. Tang, K.K.W. Ho, B.B. Rothrauff, P.S. H. Yung, A.M. Blocki, E.D.F. Ker, R.S. Tuan, Tendon-derived extracellular matrix induces mesenchymal stem cell tenogenesis via an integrin/transforming growth factor-β crosstalk-mediated mechanism, Faseb. J. 34 (6) (2020) 8172–8186.
[214] Y. Rao, C. Zhu, H.C. Suen, S. Huang, J. Liao, D.F.E. Ker, R.S. Tuan, D. Wang, Tenogenic induction of human adipose-derived stem cells by soluble tendon extracellular matrix: composition and transcriptomic analyses, Stem Cell Res. Ther. 13 (1) (2022) 380.
[215] B.E. Kelly, I. Bhattacharya, H. Heidari, M. Shusteff, C.M. Spadaccini, H.K. Taylor, Volumetric additive manufacturing via tomographic reconstruction, Science 363 (6431) (2019) 1075.
[216] X. Kuang, Q. Rong, S. Belal, T. Vu, A.M. López López, N. Wang, M.O. Arıcan, C. E. Garciamendez-Mijares, M. Chen, J. Yao, Y.S. Zhang, Self-enhancing sono-inks enable deep-penetration acoustic volumetric printing, Science 382 (6675) (2023) 1148–1155.
[217] M. Xie, L. Lian, X. Mu, Z. Luo, C.E. Garciamendez-Mijares, Z. Zhang, A. López, J. Manríquez, X. Kuang, J. Wu, J.K. Sahoo, F.Z. González, G. Li, G. Tang, S. Maharjan, J. Guo, D.L. Kaplan, Y.S. Zhang, Volumetric additive manufacturing of pristine silk-based (bio)inks, Nat. Commun. 14 (1) (2023) 210.
[218] S. Jing, L. Lian, Y. Hou, Z. Li, Z. Zheng, G. Li, G. Tang, G. Xie, M. Xie, Advances in volumetric bioprinting, Biofabrication 16 (1) (2023) 012004.
[219] K. Ruberu, M. Senadeera, S. Rana, S. Gupta, J. Chung, Z. Yue, S. Venkatesh, G. Wallace, Coupling machine learning with 3D bioprinting to fast track optimisation of extrusion printing, Appl. Mater. Today 22 (2021) 100914.
[220] G.D. Goh, S.L. Sing, W.Y. Yeong, A review on machine learning in 3D printing: applications, potential, and challenges, Artif. Intell. Rev. 54 (1) (2021) 63–94.
[221] T.S. Tamir, G. Xiong, Q. Fang, Y. Yang, Z. Shen, M. Zhou, J. Jiang, Machine-learning-based monitoring and optimization of processing parameters in 3D printing, Int. J. Comput. Integrated Manuf. 36 (9) (2023) 1362–1378.
[222] Z. Jin, Z. Zhang, X. Shao, G.X. Gu, Monitoring Anomalies in 3D bioprinting with deep neural networks, ACS Biomater. Sci. Eng. 9 (7) (2023) 3945–3952.
[223] T.J.K. Buchner, S. Rogler, S. Weirich, Y. Armati, B.G. Cangan, J. Ramos, S. T. Twiddy, D.M. Marini, A. Weber, D. Chen, G. Ellson, J. Jacob, W. Zengerle, D. Katalichenko, C. Keny, W. Matusik, R.K. Katzschmann, Vision-controlled jetting for composite systems and robots, Nature 623 (7987) (2023) 522–530.
[224] Z. Ren, L. Gao, S.J. Clark, K. Fezzaa, P. Shevchenko, A. Choi, W. Everhart, A. D. Rollett, L. Chen, T. Sun, Machine learning–aided real-time detection of keyhole pore generation in laser powder bed fusion, Science 379 (6627) (2023) 89–94.
[225] M. Sun, D. You, N. Zhan, C. Liu, X. Zhang, L. Lin, J. Zhang, Y. Lou, Y. Chen, C. Liu, H. Wang, Y. He, M. Yu, 4D oriented dynamic scaffold for promoting peripheral nerve regeneration and functional recovery, Adv. Funct. Mater. 34 (2) (2024) 2305827.
[226] I. Apsite, G. Constante, M. Dulle, L. Vogt, A. Caspari, A.R. Boccaccini, A. Synytska, S. Salehi, L. Ionov, 4D Biofabrication of fibrous artificial nerve graft for neuron regeneration, Biofabrication 12 (3) (2020) 035027.
[227] C. Wang, H. Yue, W. Huang, X. Lin, X. Xie, Z. He, X. He, S. Liu, L. Bai, B. Lu, Y. Wei, M. Wang, Cryogenic 3D printing of heterogeneous scaffolds with gradient mechanical strengths and spatial delivery of osteogenic peptide/TGF-β1 for osteochondral tissue regeneration, Biofabrication 12 (2) (2020) 025030.
[228] B. Duan, L.A. Hockaday, K.H. Kang, J.T. Butcher, 3D Bioprinting of heterogeneous aortic valve conduits with alginate/gelatin hydrogels, J. Biomed. Mater. Res. 101 (5) (2013) 1255–1264.
[229] A. Lee, A.R. Hudson, D.J. Shiwarski, J.W. Tashman, T.J. Hinton, S. Yerneni, J. M. Bliley, P.G. Campbell, A.W. Feinberg, 3D bioprinting of collagen to rebuild components of the human heart, Science 365 (6452) (2019) 482.
[230] N. Noor, A. Shapira, R. Edri, I. Gal, L. Wertheim, T. Dvir, 3D printing of personalized thick and perfusable cardiac patches and hearts, Adv. Sci. 6 (11) (2019) 1900344.
[231] G. Janani, S. Priya, S. Dey, B.B. Mandal, Mimicking native liver Lobule Microarchitecture in vitro with Parenchymal and non-parenchymal cells using 3D bioprinting for drug toxicity and drug screening applications, ACS Appl. Mater. Interfaces 14 (8) (2022) 10167–10186.
[232] A.M. Jorgensen, J.J. Yoo, A. Atala, Solid organ bioprinting: strategies to achieve organ function, Chem. Rev. 120 (19) (2020) 11093–11127.
[233] I. Lukin, S. Musquiz, I. Erezuma, T.H. Al-Tel, N. Golafshan, A. Dolatshahi-Pirouz, G. Orive, Can 4D bioprinting revolutionize drug development? Expet Opin. Drug Discov. 14 (10) (2019) 953–956.
[234] Z. Li, Z. Lin, S. Liu, H. Yagi, X. Zhang, L. Yocum, M. Romero-Lopez, C. Rhee, M. J. Makarcyzk, I. Yu, E.N. Li, M.R. Fritch, Q. Gao, K.B. Goh, B. O'Donnell, T. Hao, P.G. Alexander, B. Mahadik, J.P. Fisher, S.B. Goodman, B.A. Bunnell, R.S. Tuan, H. Lin, Human mesenchymal stem cell-derived miniature joint system for disease modeling and drug Testing, Adv. Sci. 9 (21) (2022) 2105909.
[235] Z.A. Li, J. Shang, S. Xiang, E.N. Li, H. Yagi, K. Riewruja, H. Lin, R.S. Tuan, Articular tissue-mimicking organoids derived from mesenchymal stem cells and induced pluripotent stem cells, Organoids (2022) 135–148.
[236] Z.A. Li, S. Sant, S.K. Cho, S.B. Goodman, B.A. Bunnell, R.S. Tuan, M.S. Gold, H. Lin, Synovial joint-on-a-chip for modeling arthritis: progress, pitfalls, and potential, Trends Biotechnol. 41 (4) (2023) 511–527.
[237] R. Xiao, J. Ye, X. Li, X. Wang, Dual size/charge-switchable and multi-responsive gelatin-based nanocluster for targeted anti-tumor therapy, Int. J. Biol. Macromol. 238 (2023) 124032.
[238] M. Samandari, A. Mostafavi, J. Quint, A. Memić, A. Tamayol, In situ bioprinting: intraoperative implementation of regenerative medicine, Trends Biotechnol. 40 (10) (2022) 1229–1247.